6-1-2008

Corona ion deposition: A novel non-contact method for drug and gene delivery to living systems

Niraj Ramachandran
University of South Florida

Corona Ion Deposition: A Novel Non-Contact Method for Drug and Gene Delivery to Living Systems

by

Niraj Ramachandran

A dissertation submitted in partial fulfillment
of the requirements for the degree of
Doctor of Philosophy
Department of Chemical & Biomedical Engineering
College of Engineering
University of South Florida

Major Professor: Mark Jaroszeski, Ph.D.
Andrew Hoff, Ph.D.
Richard Gilbert, Ph.D.
Richard Heller, Ph.D.
William Lee, Ph.D.

Date of Approval:
May 1, 2008

Keywords: Plasma Ions, Genetherapy, Electroporation, Molecular Delivery, Tumors

ACKNOWLEDGEMENTS

My dissertation has been one of the most significant writing challenges I have faced in my life and I am immensely grateful to all my committee members for helping me and guiding me throughout this process. I am deeply indebted to Dr. Mark Jaroszeski, my mentor, who has been very patient and encouraging during my work. I would also like to extend my gratitude to the center for molecular delivery, Dr. Richard Gilbert, Dr. Andrew Hoff, Dr. Loree Heller, Dr. Richard Heller and Dr. Antony Llewellyn for their help and suggestions.

I would specially like to acknowledge my friends Richard Connolly and Jose Rey who have been a source of inspiration and help to me in good and difficult times. My aunt and uncle Mr. and Mrs. Paralkar who believed in me and pushed me to get my doctorate, my parents, brother Tapan and all my family members for their support and faith in me. Last, but certainly not the least, my lovely wife Rani for standing by me and supporting me throughout my memorable scientific journey.

NOTE TO READER

The original of this document contains color pictures that might be necessary for understanding the data. The original dissertation is on file with the USF library in Tampa, Florida.

TABLE OF CONTENTS

LIST OF TABLES

LIST OF FIGURES

LIST OF ABBREVIATIONS

B16F10	Murine melanoma cells
FDA	Food and Drug Administration
ADA	Adenosine Deaminase
DNA	Deoxyribonucleic acid
RNA	Ribonucleic acid
DC	Direct current
RF	Radio frequency
GFP	Green fluorescent protein
eV	Electron volt
keV	Kiloelectron volt
GUS	β-glucuronidase
hyp	Hypophosphatemic
m	Meter
J	Joules

MV	Megavolts
kV	Kilovolts
$(H_3O)^+_n$	Conventional positive air ion
CO_3^{--}	Conventional negative air ion
µm	Micrometer
mm	Millimeter
DAQ	Data acquisition card
CPVC	Chlorinated polyvinyl chloride
µA	Microamperes
nA	Nanoamperes
v/v	Volume to volume ratio
µM	Micromolar
PBS	Phosphate buffered saline
SDS	Sodium docecyl sulfate
µl	Microliter
°C	Degree Celsius
%	Percentage

IC_{50}	Median Inhibition Concentration (concentration that reduces the effect by 50%)
M	Molar
MTT	(3-(4,5-Dimethylthiazol-2-yl)-2,5-diphenyltetrazolium bromide, a tetrazole)
hrs.	Hours
DMSO	Dimethyl sulfoxide
OD	Optical density
LUC	Luciferase
mg	Milligrams
cm	centimeter
ROI	Region of Interest
sec.	Seconds
DI	Deionized
A.U.	Arbitrary Units
µg	Micrograms
min.	Minutes
s.e.m	Standard error of the mean
CMFDA	5-chloromethylfluorescein diacetate

ECM	Extracellular Matrix
SY	SYTOX-green molecule
NU_B	Number of SYTOX-green binding sites
Pa	Pascal

LIST OF SYMBOLS

Q	Charge of a particle, coulombs
E	Electric field, $\frac{V}{m}$
Δ	Change (final-initial)
ΔKE	Increase in kinetic energy in joules
e	Charge of an electron and negative ion, coulombs
Δz	Mean free path, m
Δz_i	Mean free path traversed by an ion, m
Δz_e	Mean free path traversed by an electron, m
d	Distance in cm
ΔE_e	Total energy gain of an electron, Joules
ΔE_i	Total energy gain of an ion, Joules
$E_{breakdown}$	Breakdown field strength, $\frac{V}{m}$

≈	Approximately equal to
g	Gravitational acceleration, $\frac{m^2}{\sec.}$
×	Multiplied by
25X	Magnification 25 times
250X	Magnification 250 times
400X	Magnification 400 times
V	Volume, mm^3
π	3.1415926
SUS304	Surgical grade stainless steel
$T_{\Delta M}$	Total transmembrane potential, mV
E_s	Potential at the membrane aqueous interface, mV
E_d	Membrane Dipole potential, arising due to dipolar lipid groups and permanent water dipoles, mV
ΔE_i	Transmembrane potential difference between bulk inside and outside, mV
MDP	Membrane dipole potential

μ_0 Permeability of SYTOX-green at time zero after corona ion exposure, $\frac{m}{\sec}$

μ_1 Average effective permeability of SYTOX-green inside the cell after corona ion exposure, $\frac{m}{\sec}$

t Time, $\sec.$

T Resealing time constant, sec.

J_s Flux of SYTOX-green through the permeated cell membrane, $\frac{mol}{cm^2 \sec}$

V_o Volume of a cell, m^3

S_o Surface area of a cell, m^2

D_i Effective Diffusivity,

ϕ Partition coefficient,

x Membrane thickness, m

C_o Extracellular concentration of SYTOX-green, $\frac{mol}{m^3}$

C_i Intracellular concentration of SYTOX-green, $\frac{mol}{m^3}$

K_E Equilibrium constant for SYTOX-green binding to nucleic acids inside the cell, $\frac{m^3}{mol}$

SY_b	Amount of SYTOX-green bound per cell, $\frac{mol}{cell}$
N_o	Total number of binding sites, $\frac{mol}{cell}$

Corona Ion Deposition: A Novel Non-Contact Method for Drug and Gene Delivery to Living Systems

Niraj Ramachandran

ABSTRACT

Application of corona ions produced in air to B16F10 murine melanoma cells *in vitro* and in animal models resulted in the transport of molecular therapeutics across the cell membrane. This work presents the development of new methods for drug and gene delivery based upon similar principles as the traditional electrode driven membrane destabilization processes known as electroporation. This was achieved with non-contact corona ion deposition that temporarily increased the permeability of cell membranes.

Interaction of corona charge with biological cells was studied and their potential for molecular delivery was established. Molecular delivery was first demonstrated *in vitro* using tracer molecules followed by *in vitro* delivery of the cytotoxic drug bleomycin. Building upon these results, the delivery of bleomycin coincident with ion deposition was

shown to significantly slow the growth of very aggressive solid tumors in animal models, compared to drug alone or no treatment. Delivery of plasmid DNA to cells in the skin of animal models indicated that application of corona ions (both positive and negative) to live tissue produced a four to six fold increase in gene expression. As this is the first significant study of the interaction and impact of corona ions on the delivery of drug and plasmid DNA to biological cells, numerous fundamental investigations were performed and discussed. A charge dose dependence was observed and physical mechanistic models were proposed. A model of cell resealing time constant following corona ion exposure was developed and demonstrated a reasonable prediction of experimental findings. The foundation laid by this work may enable continued exploration and use of corona ion deposition in the future as a new and promising physical method for drug and gene delivery.

1 INTRODUCTION

1.1 Drug and Gene Delivery

Technological advancement in the areas of molecular biology and biotechnology have resulted in the development of numerous novel molecules that have potential for use as therapeutic agents. One of the primary reasons for continuous research in the area of drug delivery has been the fact that many good drug candidates are rejected because they cannot be efficiently delivered *in vivo*. A second reason is that as drug patents expire novel delivery methods provide a competitive advantage in the market. Both issues can be addressed by developing novel methods for delivering these therapeutics.

The development of new drug delivery systems requires a proper understanding of drug formulation, bioavailability of the drug and optimization of the delivery vehicle. A drug delivery engineer has to be aware of the main obstacles in these three areas. Two basic areas of innovation that can potentially improve efficacy of a therapeutic agent are, a change in the drug formulation and changes in the system used to administer the drug. Since delivering a therapeutic is the ultimate

goal of this research, discussion will be restricted to different systems and methods or routes used to administer therapeutic agents. As of January 11, 2006, the FDA of the United States recognized 111 routes of drug administration [1]. Competition among drug companies is not only very intense for drug candidates where patents have been applied for a drug with the same molecular formula but different structural formula, but also among methods used to deliver them.

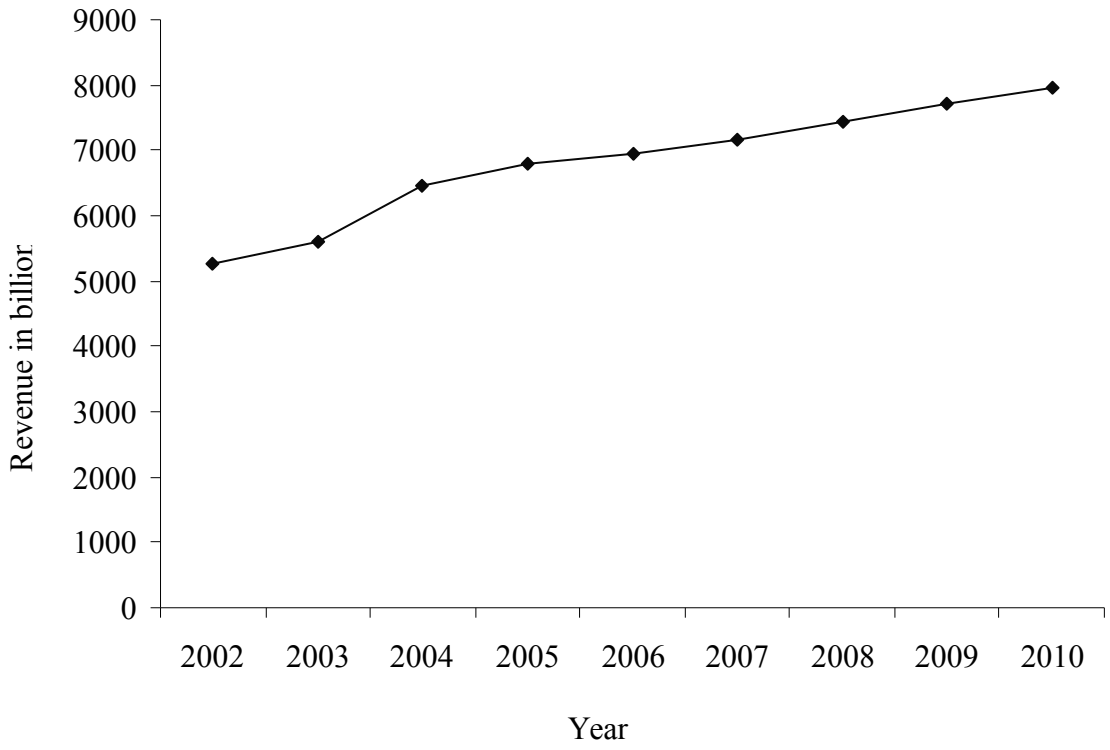

Figure 1.1: Worldwide market revenue from different drug delivery technologies [2].

Figure 1.1 shows worldwide revenues from different drug delivery technologies currently used and projected growth until the year 2010 [2]. Revenues shown above include transdermal, transmuccosal, buccal, nasal, injectables, implantables and oral drug delivery technologies. Data in the figure includes revenue earned not only from licensing a particular delivery technology but also revenue from pharmaceutical or biotechnology products that utilize that particular delivery technology. Since molecular delivery technology is an integral part of a biotech or pharmaceutical company, worldwide revenues shown above include revenues from the sales of a particular therapeutic molecule and delivery technology utilizing that molecule which by 2010 this will be a seven trillion dollar market.

Traditional administration routes for therapeutics have been parenteral, enteral and topical. Parenteral administration is carried out by injecting drugs into tissues; some examples of this route include intradermal, intramuscular, intravenous and subcutaneous injections. Direct injection into tissues avoids degradation of drugs as in the gastrointestinal tract and allows for the rapid uptake. Enteral therapeutics are administered orally or rectally to the digestive tract in the form of compressed tablets, capsules, or liquids. Topical drugs are applied as creams, lotions, or solutions directly to the site where action

is required. They avoid any effects to the surrounding tissues as they are applied only where they are needed.

Targeted delivery of drugs has been another strategy that has been the subject of many investigations in the past decade. Most strategies utilize the traditional administration routes outlined above combined with a chemical or biological component to target or localize delivery and also to reduce systemic toxicity. Targeted drug delivery can be active or passive. An example of active targeted delivery is the case of an antibody-drug conjugate for the chemotherapeutic treatment of cancerous cells [3]. Passive targeted delivery for example uses liposomes [4], polymeric micelles [5], lipid nanoparticles [6] etc. that encapsulate drug molecules and can accumulate in specific types of tissues. Despite the efficacy of all active or passive strategies, no targeting strategy has provided universal improvement. This is particularly true for the treatment of cancer. Novel anti-cancer drug candidates do not find their way to the site of action and concentrations at the tumor sites are very low to effect any action. This can be attributed to high interstitial pressure and uneven distribution of blood vessels in the tumors [7, 8].

Alternative methods of drug delivery focus on targeting specific drug and/or drug carriers with physical methods. The use of physical methods such as an energy source for delivering drugs either

systemically or locally is gaining prominence as it avoids complications with chemicals or biologicals that can arise due to systemic toxicity. The use of ultrasound [9], magnetic fields [10] and electric fields [11], as forcing functions, are a few examples of physical methods that have been developed and used for delivery of therapeutics with some degree of success.

The importance of research into new delivery methods for drugs has been highlighted above. DNA or genes are another class of molecules that have potential to be used as therapeutic agents. A gene is a physical and functional unit of hereditary, which carries information from one generation to the next. Gene delivery or gene therapy (still not approved as a therapy in humans) is another promising method to treat many diseases. Gene therapy is the insertion of a normal copy of a gene into a cell or tissue that has a defective gene to treat a disease or disorder. It is also used in cases when the normal functional gene is completely absent.

With gene therapy, it is possible to transform both somatic and germ line cells. Transforming germ line cells in humans remains very controversial; hence, most of the transformation work has been directed to somatic cells. Gene therapies can be categorized in two ways: *ex-vivo* – cells are removed from the body, modified and then transplanted back and *in vivo* – where genes are delivered to cells in-

side the body. In the *ex-vivo* technique cells are removed from the body and viral vectors are used to insert the therapeutic gene into them. The cells are then transplanted back into the body where they express the desired protein. This technique is most frequently used when the desired cells can be easily extracted from the body as in the case with blood cells [12, 13]. An example of this was the use of peripheral blood lymphocytes from two patients to transfer *ex-vivo,* the human ADA gene, into bone marrow cells and to undergo exogenous enzyme replacement therapy [13]. The *in vivo* technique was developed later and is more challenging as the genetic material has to be delivered to the cells while they are in the body. A typical example of this is the low efficiency of gene transfer *in vivo* in clinical trials for cystic fibrosis [14]. The current transfection efficiencies are probably too low to result in clinical benefit. The host innate and acquired immunity, in addition to intra and extracellular barriers are responsible for this low efficiency [14].

Biological methods were amongst the first used for gene delivery and viruses were the vehicles used as they attack host cells and deliver their genetic material into them. Viruses were prepared for gene delivery by modifying them to include a gene encoding a therapeutic molecule of interest. Retroviruses, adenoviruses and adeno-associated viruses are probably the most commonly used viruses for gene

delivery. Although viral methods generally transfer genetic material efficiently, there are drawbacks to their use. They are relatively complex to prepare, have restrictions on the size of their DNA payload and some can evoke immune responses that can seriously threaten a patient's health.

Drawbacks of viral methods have led to the development of alternative gene delivery methods that utilize physical forces to deliver DNA to target cells. These physical methods assist in the transfection of plasmid DNA. This type of construct is a circular double stranded DNA molecule that codes for a therapeutic agent of interest. Plasmids are relatively simple to prepare and do not evoke immune responses. This is an advantage relative to viruses. Some of the most common physical, or non-viral, methods for gene delivery include the use of ultrasonic irradiation [9], magnetic fields [10], pressure differentials [15] and electric fields [11].

Ultrasonic irradiation uses kilo and megahertz frequency sound waves to enhance the permeation of molecules to cells. Acoustic cavitation is thought to be the mechanism by which the plasma membranes of cells are reversibly disrupted to allow the passage of plasmid into the cells. The use of magnetic fields involves tagging DNA with iron oxide, which is biodegradable and an external magnetic field is used to drive the assembly inside the cell. This is probably a drawback

of using magnetic fields as it has to be tagged to a magnetic material. Pressure differential created by hydrostatic pressure is used to force the uptake of plasmid DNA by systemic injection of a large volume of DNA.

Exposing biological cells to electric fields for the molecular delivery of drugs and DNA is commonly known as electroporation or electropermeabilization. This type of delivery uses electric fields to affect cell membranes in a manner that temporarily increases their permeability to molecules that normally do not have access to the cytosol. This delivery method is the topic of much research and has been documented through many successes in animal models [16, 17]. Gene transfer using electroporation was first demonstrated by Neumann et al in mouse lyoma cells *in vitro* more than two decades ago [18]. Following this, the *in vivo* use of electroporation was first demonstrated by delivering the drug bleomycin to solid tumors [19, 20]. Gene transfer using electric fields first started in the early 90s [21] and has been used successfully for delivering drugs and DNA to many tissues since. Gene delivery has been reported in skin [22,23], muscle [24,25], liver [26,27] and solid tumors [28,29].

Electroporation has been noted as having the highest efficiency [30, 31] amongst the physical methods. Despite the success achieved by electroporation as a physical method for drug and gene delivery

there remain some drawbacks. The first and foremost issue with electroporation is the use of electrodes that directly penetrate/contact the tumors or target tissue. This results in the administration of high power and current to the patient. In animal studies and clinical trials focused on treating tumors and other tissues, this has shown the potential to result in muscle contraction, pain, or tissue damage [32, 33]. In addition treating large volumes of tissue can also be a problem. Hence one goal of this research was to develop a treatment system that is non-invasive and does not produce any discomfort and tissue damage.

Corona ions have the potential to be applied to living systems in a manner similar to the electric fields used during electroporation while avoiding problems associated with electrode stimulated delivery. Corona discharge, a kind of plasma generated in air, is one such physical method that can avoid contact with the target tissue. These ions can be applied using a low current to potentially avoid complications related to tissue damage due to high power that is typically used in electroporation. Therefore, coronal ions were investigated in this study as a novel non-contact means for the delivery of drugs and genes. Detailed definitions of corona ions and how they are generated are described in the sections that follow.

1.2 Review of Plasma Applications in Biomedical Engineering

Plasma is the state of matter that was first identified by Sir William Crookes in 1879 and is a gas in its ionized state. This energetic gas phase state results when electrons in the outer shell have been stripped from the atom resulting in a collection of ions and electrons separated from each other. Plasma is a unique and distinct state of matter and its unique properties are due to the presence of electrons and ions which act as free charge carriers. These free charges make the plasma conductive and when acted upon by an external electric field will be accelerated to constitute a current.

Plasmas can be generated by heating, using laser beams, ultra violet radiation, electric fields etc. Irrespective of their generation mechanism, plasmas can be categorized as thermal or nonthermal based on the relative temperatures of the ions, electrons and the neutrals. Ionized gases consist of ions, electrons and uncharged particles such as atoms, molecules and radicals. Atoms, molecules and radicals (atoms with unpaired electrons) are collectively known as neutrals. Temperature of plasma is the thermal energy per charged particle and it is measured in electron volts or Kelvins [34]. Once ionization of a gas takes place it is the difference in temperature of the electrons and ions that determines if a plasma is hot or cold.

A common method of generating plasmas used in biological applications is by an electrical discharge or ionization of the surrounding medium. Application of high voltage to a conductor can lead to the ionization of a surrounding medium due to the high value of the electric field around it. Ions and electrons generated in the process drift under the influence of the electric field and can be used to affect a target at a distance. Corona discharge is a specific sub-type of plasma generated by the ionization of air molecules at atmospheric pressure. Plasmas generated by an electrical discharge can be categorized into the following different types [34].

- Direct current discharges
- Pulsed DC discharges
- Radio Frequency (RF) discharges
    - Inductively coupled
    - Capacitively coupled
- Microwave discharges

Most electrically generated plasmas used in biomedical applications are generated by RF discharges. More information about plasmas generated by RF discharges can be obtained in work done by Kieft et al [35]. Since most plasmas used in biomedical engineering

are non-thermal; discussion will be restricted to non-thermal plasmas. In non-thermal plasmas the ions and neutrals are at a much lower temperature than the electrons. The electrons can come back to thermodynamic equilibrium much faster with each other than they do with ions and neutrals due to difference in their masses. Hence the ion temperature, which is the most important parameter in biomedical applications, is far lower than the electron temperature [36]. Ionization of a gas is necessary for plasma to exist and the extent to which a gas is ionized (degree of ionization) which is the number of atoms or molecules that have gained or lost an electron is directly proportional to the temperature. For example a plasma is considered hot if it is fully ionized and cold if only a very small fraction of the gas is ionized.

Non-thermal plasmas have been used in surface processing [37, 38], bacterial decontamination of medical equipment and air [39, 40]. One of the main uses of plasma in biomedicine is the coating of implants with biocompatible layers [41] and the surface modification of substrates for cell culture [42]. Discharge plasmas have also been used in chemical micro patterning of cell culture substrates to induce cellular attachment [43]. More recently, corona discharge, a kind of plasma, has been investigated for its possible use in sterilizing wine [44] and heat sensitive materials [45]. Corona ion exposure has also

been investigated for eliminating dust mites and allergens [46] and for the modification of polymers used in biomedical applications [47, 48].

Plasmas generated using radio frequency excitation in inert gases have been used for manipulating mammalian cells [49-51]. The primary goal of these studies with RF plasmas was to develop a pain free system to treat skin diseases, for electrosurgery and the cleansing of dental cavities. Increases in cell detachment, apoptosis and bacterial inactivation were some of the effects observed. These RF plasmas were not generated in stationary gases but were assisted by a flowing gas which also served as a kinetic energy source to the ions.

Of the plasma applications in biomedical engineering discussed above, none have focused on drug and gene delivery. There are only few applications investigating the use of plasmas for the purposes of drug and gene delivery. A discharge plasma has been developed for *in vitro* gene transfection of primary neuronal cells from cerebral cortices of rats [52]. The atmospheric pressure plasma used by Ogawa and colleagues for this study was originally used for surface treatment of non-biological materials. The study only made visual observation of samples transfected with the GFP gene after 24 hours of treatment. Fluorescent micrographs of cells transfected with GFP appeared to show an increase in fluorescence as compared to controls, but no quantitative gene expression data was presented. More recently

Palankar and colleagues used a discharge plasma to transfect genes into the retina of rabbits *in vivo*. A 100μm electrode was used to produce the electric discharge. An electrical probe was developed with the microelectrode on it so it could be inserted behind the sclera in the rabbit eye. Application of a high voltage to the microelectrode led to the rapid vaporization of the surrounding conductive media. The resulting mechanical stress and electric current generated by the plasma were concluded as being responsible for the transfection of the gene to the retinal epithelium [53]. Higher gene expression was demonstrated over established physical methods like electroporation and ultrasound using this plasma source in the retina.

Yamada et al [54] have used water generated negative air ions to inhibit carcinogenesis in mice and also to activate natural killer cells of the immune system. Water generated negative ions were created by ionizing water using the Lenard effect [55]. The Lenard effect first studied by the German physicist P. Lenard is the separation of electric charges accompanying the aerodynamic breakup of water drops generated by passing steam. This study demonstrated delivery of the drug methylcolanthrene to established tumors in mice. Even though complete destruction of tumors was not achieved, the rate of tumor growth was slowed down for three weeks [54].

Low energy ion induced gene transfer into biological cells is another novel method that has been investigated in the recent past [56]. These ions commonly referred to as low energy ions are generated by an ion source and are accelerated under the influence of an electrostatic field to gain a certain amount of energy. The process of ion generation is very similar to that used in etching or surface sputtering and is carried out in a vacuum at reduced pressures of around 10^{-4} Pa. Cells were exposed to these low energy ions (10-15 keV) to induce gene transfer. Gene expression was only demonstrated though microscopic observations and not quantified. One study was designed to examine the effects of low energy (30 keV) electric fields [57] on cells for possible application in breeding. Plasmids carrying the GUS, hyp (hygromycin phosphotransferase) and chitinase genes were successfully delivered using this ion beam source. Mature embryos of rice, wheat and tobacco were successfully transected to create a new generation of transgenic plants.

1.3 Corona Ion Basics

As mentioned above, corona discharge is a type of plasma generated in air at atmospheric pressure and temperature. Since most biomedical applications of plasmas employ an electrical source for driving ionization, the process of generating charged particles with

electric fields in air will be described first. Air like most gases at atmospheric pressure and temperature is a good insulator. If heated to high temperatures or exposed to ultraviolet radiation, ionization of air occurs and charged particles are produced. If an external electric field is applied, these charges will be accelerated and can constitute a current. As the magnitude of electric field increases a self sustained discharge results. An increase in the electric field beyond a certain threshold can then result in electrical breakdown of air. The electrical breakdown/ionization process also depends on factors like temperature, relative humidity and pressure.

A corona discharge is the phenomenon of creating charged particles by ionizing air using a high electric field at atmospheric temperature and pressure. It is generally a silent electric discharge that occurs from very sharp or pointed objects when the electric field attains a very high value at these sharp edges. Corona discharge can also become an audible discharge, depending on the conditions of the discharge electrode; temperature, humidity and accumulation of dirt or dust. Application of a very high value of electric field close to breakdown voltage can also lead to an audible discharge. Two electrodes are typically used to produce a coronal discharge. One electrode is highly curved with a very small diameter wire or the tip of a pointed electrode through which high voltage is passed and the other

electrode is flat or blunt. The flat or blunt electrode is normally grounded to prevent arcing to the substrate. A point to be noted is that a corona discharge can also occur with only one curved or pointed electrode and the grounded electrode is not always needed.

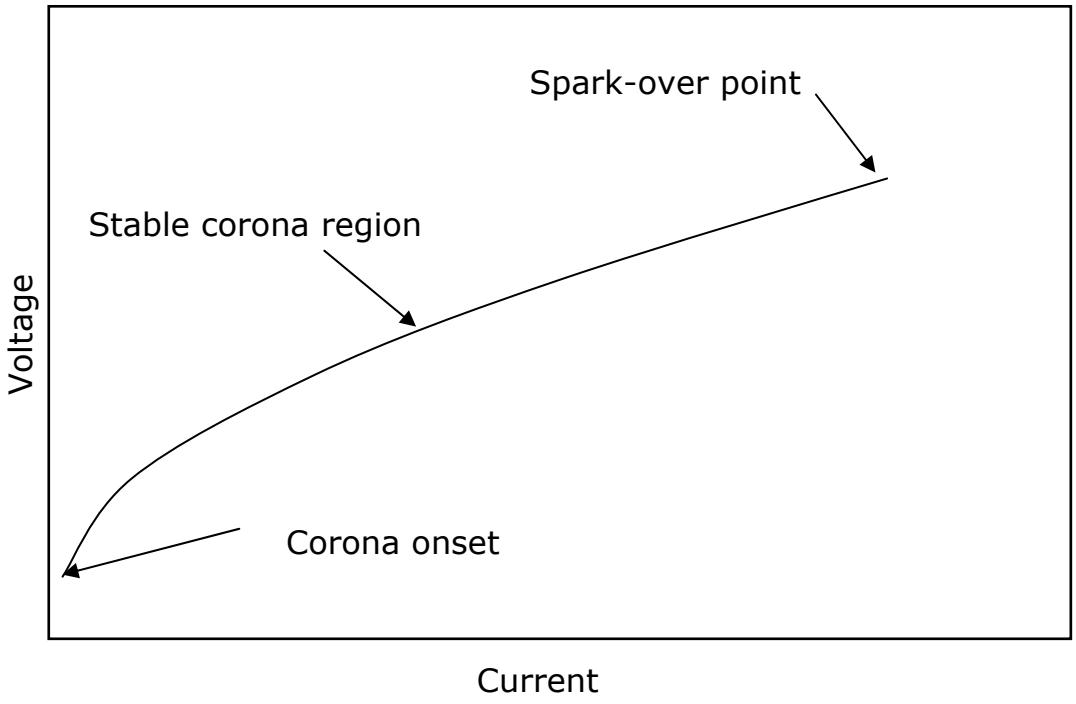

Figure 1.2: Typical voltage-current curve for a DC corona discharge [58].

Figure 1.2 shows a typical voltage-current curve for a DC corona discharge showing the corona onset voltage, which is the voltage at which current is first detected from a particular discharge electrode at a particular distance from it. The corona onset region is followed by the stable corona region. In this region of the curve, the amount of current produced is related to the voltage applied to the discharge

electrode. The spark over point is the voltage at which complete breakdown of air takes place. The stable corona region is where most corona generating devices are operated as there is predictable behavior. Corona discharges can be detected in numerous ways. The easiest method is by a weak bluish or violet glow of visible light that is produced near the discharge electrode. It can also be detected by using charge collecting and measuring devices. When a corona discharge first starts it appears as a weak and faint glow. As the voltage is increased the glow eventually spreads into streamers [59]. Streamers look like rays of light that propagate out from the discharge electrode like a spray. This happens only with particular electrode geometries and at specific applied voltages [59]

To explain the phenomenon of corona ion generation first a distinction must be established between ionization and complete breakdown or arcing. An electrical breakdown is the complete ionization of air between two electrodes. Electrical breakdown is often assumed to be associated only with high voltages, but contrary to this belief it is also possible to have a breakdown at very low voltages. The key for electrical breakdown is the electric field strength. This situation can be explained when a comparison is made between the breakdown field strength and the breakdown voltage. Consider air sandwiched in between two parallel flat plate electrodes as shown in

Figure 1.3. It is known that atmospheric air has a few naturally occurring ions and free electrons which constantly undergo random thermal collisions with other molecules. The energy of these particles is too low for them to cause ionization (i.e. stripping out an electron from an air molecule). Now if a voltage is applied to the flat plate electrode present in air, these charged particles gain energy from the field and will be accelerated. If a particle having a charge Q is accelerated by the electric field of strength E through a distance of Δz, then its kinetic energy increase (ΔKE) would equal

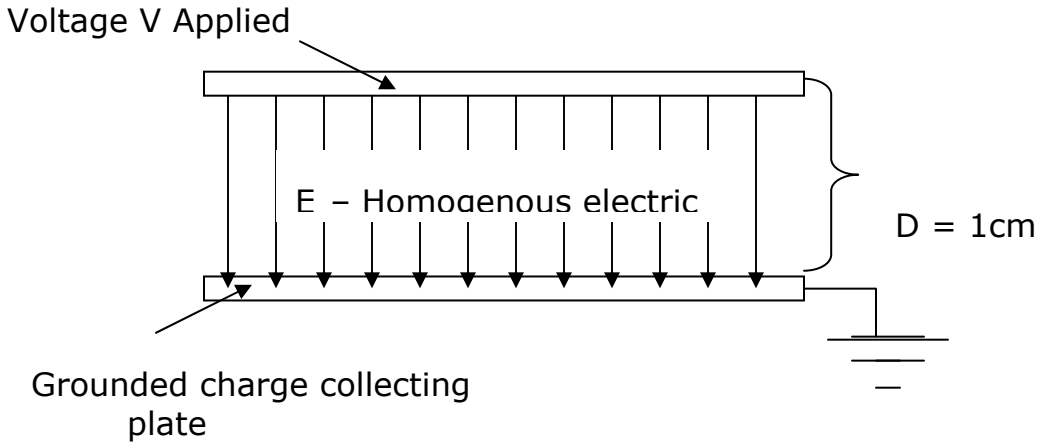

Figure 1.3: Homogenous electric field established between two parallel flat plates.

(1.1) $$\Delta KE = Q \times E \times \Delta z$$ for ions

Or

(1.2) $$\Delta KE = e \times E \times \Delta z$$ for electrons

For an electron with charge e the increase in kinetic energy is given by equation (1.2). This expression is valid only if the particle does not collide with any other particle over this distance Δz (in vacuum). An electron and negative ion have the same elementary charge e but they will move different distances even after gaining the same amount of energy due to difference in their masses. The total mean distance that an electron or an ion travels between collisions is known as their mean free path. Hence the maximum total energy expressions for an electron and ion are given by

(1.3) $$\Delta E_e = e \times E \times z_e$$

(1.4) $$\Delta E_i = e \times E \times z_i$$

Where z_e and z_i are mean free paths for electron and ion respectively, ΔE_i and ΔE_e are total energy expressions for ion and electron given by equations (1.3) and (1.4) respectively and E is the applied electric field. Now the mean free path traversed by an ion will be much smaller than an electron due to the difference in size. The mean free path of an electron is ≈ 10^{-5} m and that for an ion is ≈10^{-7} m [60], hence an electron would reach its maximum total energy ΔE_e at the breakdown field strength of air which is about 100 fold lower based on the mean free paths. If it takes energy ΔE_i to strip an electron from an air molecule to ionize it into an electron and ion pair, it is

known from the literature that $\Delta E_i \approx 5 \times 10^{-18}$ J or 30 eV [60]. For atmospheric air we can substitute this value in equation (1.4) and obtain the value for the breakdown field strength for air.

(1.5) $$\Delta E_i = E_{breakdown} \times e \times z_i$$

(1.6) $$E_{breakdown} = \frac{\Delta E_i}{e \times z_i}$$

$$= \frac{5 \times 10^{-18}}{1.6 \times 10^{-19} \times 10^{-5}}$$

(1.7) $$\therefore E_{breakdown} = 3.125 \times 10^{6}\, V/m$$

These calculations are valid only for the situation where the value of the electric field is homogenous like that established between two parallel flat plate electrodes as shown in Figure 1.3. The field strength in the space between the two plates is given by $E = V/d$. V is the applied voltage difference and d is the distance between the plates. If we substitute the value of E as $3.125\, MV/m$ and the distance d as 1 cm we obtain a value of 31,250 V. This voltage is the breakdown value or the voltage that would have to be applied in order to have complete breakdown or spark in the situation shown in Figure 1.3.

Now consider a needle with a very sharp tip as shown in Figure 1.4. If a voltage is applied to the needle, the electric field around the

needle tip will be inhomogeneous. This situation is different and more complicated as compared to the parallel flat plate situation shown in Figure 1.3. This difference in geometry results in a higher breakdown field strength and subsequently a lower breakdown voltage at the tip of the needle. The reason for this is due to the decreasing value of the electric field as the distance from the electrode is increased. The electric field will be the highest at the tip of the electrode and this is where ionization or discharge begins.

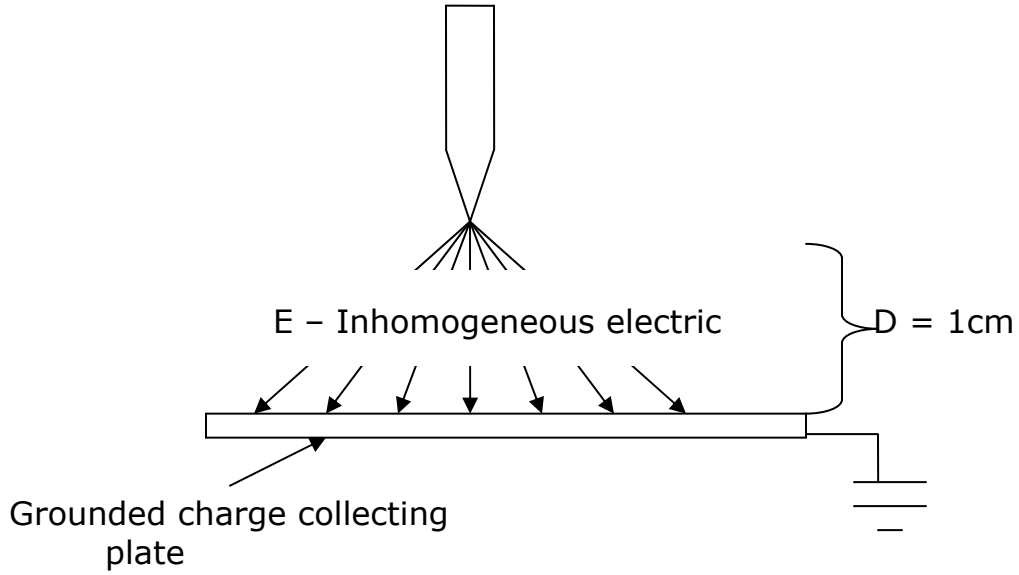

Figure 1.4: Inhomogeneous electric field established between a sharp pointed electrode and a flat plate electrode.

If a voltage is applied to the electrodes shown in Figure 1.3 and 1.4 until a current on the charge collecting plate is first detected, the voltage applied to the needle electrode will be much lower. In case of a parallel plate the breakdown field strength is exceeded at all points

and the discharge may start at any point the first free electron is available. Complete ionization will take place along this path connecting the two electrodes resulting in a spark. In case of the needle electrode the breakdown field strength is exceeded only in the small volume at the tip of the electrode resulting in the generation of ions. If the polarity of the applied voltage is positive, positive ions will drift [61] under the influence of the electric field and the negative ions and electrons will move towards the discharge electrode where they will be neutralized. This process is called a corona discharge and the ions that drift out are called corona ions.

Corona ions can be generated in air by applying a potential of approximately ± 3-7 kV to a pointed electrode or small radius wire. The majority of charged ionic species obtained are $^{+}H(H_2O)_n$ when the applied polarity is positive and $^{-}CO_3$ when the applied polarity is negative [62]. This is the conventional method of representing these ions, merely by a positive or negative sign on the left hand superscript indicating if the ion is positive or negative. The ions represented here are the classical small ions of atmospheric electricity that have around 10 to 15 polarizable water molecules attached to ions generated by ionization of air molecules. These generated ions undergo many collisions per second (on the order of a million) with other air molecules at atmospheric pressure and therefore quickly lose any excess energy that

they might have gained from the ionization process. The corona ions produced at the source electrode move under the influence of the electric field surrounding the same electrode and can be deposited onto a substrate below [61]. These ions can be directed through air to target cells *in vitro* and *in vivo*. Thus, corona ions may be applied to target cells/tissue without direct contact with an electrical source. Although there has been a significant amount of research performed on the interaction of high energy electric fields like those used in electroporation with biological cells no studies have been performed to evaluate possible effects of corona ions to biological cells for the purpose of molecular delivery. The successful use of corona ions for drug and gene delivery would address a number of issues associated with direct contact electroporation. These issues include the placement of electrodes into the target tissues, high voltage applied directly to the tissue and patient discomfort.

2 HYPOTHESIS AND SPECIFIC AIMS

2.1 Hypothesis

It is clear from the relevant literature that novel methods for delivering both drugs and genes are a significant part of biomedical research. It is also evident from the literature that delivery technologies that allow therapeutic agents access to the cytosol can result in improved therapies for many diseases. Therefore, there is a need for investigations into discovering novel methods for drug and gene delivery.

In recent history research into novel delivery methods has been focused on exploiting chemicals, biologicals, or physical forces. One successfully used physical force for molecular delivery is electric fields. The use of electric fields to deliver drugs and DNA is a well researched and established physical delivery method. It is accepted that properly applied electric fields create temporary pores or defects in cell membranes that allow the passage of impermeant molecules to the cytosol [18-29, 63-67]. This method known as electroporation or electropermeabilization has many documented successes in animal

models and in the clinic [68-72]. However, this method is not without drawbacks. Tissue damage has been a problem in animal studies and clinical trials focused on treating tumors and other tissues. In addition, electroporation has resulted in muscle contraction and pain. The reasons for this are that high voltages are used which result in correspondingly high currents [73, 74]. Also, electrode used for electroporation must be in contact with (or penetrate) the target tissue.

Thus, this research was designed to investigate corona ions as an electrical method for delivering therapeutic agents. Corona charge was selected for investigation because application does not require the direct contact between tissue and electrodes used to generate the ions and the associated current is also very low. Based on the needs and rationale presented above, this study was designed to test the following hypothesis: corona ions can be applied to living systems to deliver drugs and DNA in cell culture and in tissues.

2.2 Specific Aims

The aims of the study were established to systematically investigate the hypothesis. They were also designed to move from creating a novel corona generating system, to *in vitro* work, to tissue applications. The specific aims of this study are presented below.

2.2.1 Specific Aim 1: To Design, Construct and Characterize a Corona Generating System Suitable for Application in Living Systems

A corona ion generator was designed that produced more charge than those that were commercially available in order to facilitate experimental work. This design was characterized using a collection of instruments that were used to control corona charge generation.

2.2.2 Specific Aim 2: To Test the Capability of Corona Ions for Delivering Dyes and Tracer Molecules *In Vitro*

This aim was designed to perform basic *in vitro* testing of the corona ion generating device developed in Specific Aim 1. Molecular delivery was tested using calcein and SYTOX-green nucleic acid probe in a murine melanoma cell line. Short term viability of the cells exposed to positive and negative corona ions was also investigated.

2.2.3 Specific Aim 3: To Investigate the Use of Corona Ions for Delivering Bleomycin *In Vitro* and to Established Tumors in an Animal Model

This aim was designed to determine if corona ions could be used to deliver a cytotoxic drug to murine B16F10 tumor cells. Bleomycin was delivered to the cell line *in vitro*. Experimental work then focused on delivering bleomycin to established solid tumors using the same cell line in the flanks of a murine model.

2.2.4 Specific Aim 4: To Evaluate the Use of Corona Ions for Delivering Plasmid DNA to Cells in the Skin of a Murine Model

Experiments for this aim incorporated plasmid DNA and murine skin as a model. The reporter gene luciferase was delivered using corona charge to demonstrate the utility of this method for obtaining the expression of foreign DNA.

2.2.5 Specific Aim 5: To Investigate the Mechanism of Interaction of Corona Ions with Biological Cells

The mechanism of interaction of corona ions with biological cells was investigated. Experiments were carried out to elucidate a possible mechanism of the uptake of extracellular molecules that do not normally permeate the cell membrane. Uptake rates for a fluorescent tracer molecule were also determined.

3 MATERIALS AND METHODS

This section describes in detail all the materials and methods used to carry out experiments mentioned in the five specific aims of the study. The materials and corresponding methods used are categorized according to each specific aim. The overarching theme of this work was to demonstrate the first implementation of non-contact delivery of impermeant molecules to the cytosol of cells *in vitro* and *in vivo*. To accomplish this, a new ionic charge delivery apparatus was constructed and characterized, statistical methods were applied to explore the parameter space of the delivery methods and new protocols were developed for experiments that explored the application space of ion driven delivery to tissues.

3.1 Specific Aim 1: To Design, Construct and Characterize a Corona Generating System Suitable for Application in Living Systems

3.1.1 Corona Discharge Apparatus

Corona ions were produced using two different ion generators. The first ion generator was a commercially available product that consisted of two 150μm diameter platinum coated stainless steel wires to

which high voltage was applied. This ion generator, diagrammatically shown in Figure 3.1, included a rectangular ground plate on either side of the wires. The distance between the wires and the ground plates was 6 mm. To generate ions, the platinum coated wires were maintained at either a positive or negative potential with respect to the grounded steel bars on either side of the wires as shown in Figure 3.1. This generator (Semiconductor Diagnostic, Inc.; Tampa, FL) was originally designed to charge semiconductor substrates for electronic materials characterization.

The second corona generator, designed and implemented as part of this work, was an array of nine 28 gauge stainless steel acupuncture needles (NA2840, Suzhou Gusu Acupuncture & Moxitustion Appliance Co. Ltd.). The needles were fixed within a circular Teflon rod, machined to 26 mm high by 38 mm outside diameter as shown in Figure 3.2 a) and b).

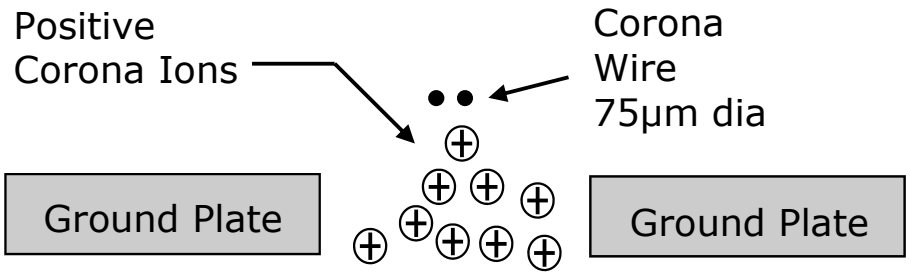

Figure 3.1: Schematic of the two wire corona generator.

The circular array was formed in this generator by inserting the needles through holes, drilled in the Teflon rod, such that the tapered tips protruded below the lower polymer surface. One needle was located at the center and the remaining eight needles were equally spaced around an 11 mm diameter circle. The needles were connected together at the top to facilitate connection to a high voltage power supply. An annular stainless steel plate, Figure 3.2 b), was affixed to the bottom of the Teflon rod and was connected to the ground of the power supply to prevent arcing from the high potential needles to either the media solution for *in vitro* work or to tissue for *in vivo* experiments. The inside diameter of the ground plate was 28 mm. The needle tips were located in the plane of the top of the ground plate. Figure 3.2 c) and d) show close up the needles used for corona ion generation. The entire corona ion generating apparatus was mounted on a micromanipulator so that it could be positioned 7 mm from cultured cells.

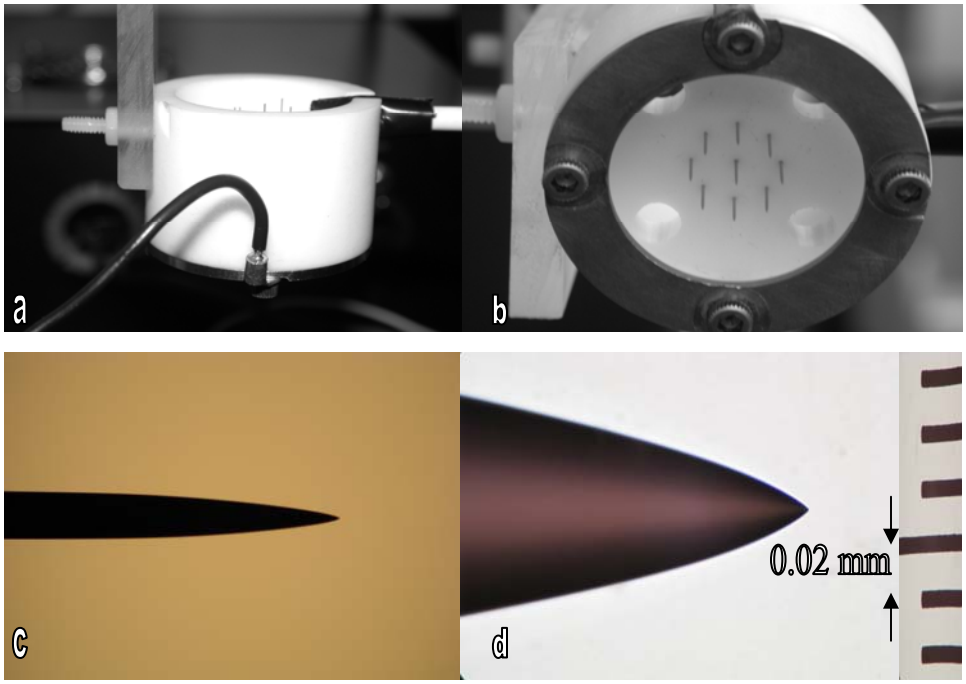

Figure 3.2: a) Side view and b) bottom view of the nine needle corona generator c) and d) magnified views of the needle tips 25X and 400X, respectively. The tip radius was approximately 2μm.

High voltage was provided to the corona generators used in this work by a programmable DC power supply (CZE 2000, Spellman High Voltage Electronics, Hauppauge, NY). A data acquisition card (DAQ) and LabView program (PCI 6036 E and LabView 8, National Instruments, Austin, TX) controlled the high voltage output from the power supply to facilitate the associated corona ion generation. The software allowed the user to control the applied voltage and time a particular sample was exposed to corona ions for. The virtual interface of the LabView program is shown in Figure 3.3 and the source code of each of its components are shown in Figures 3.4, 3.5 and 3.6.

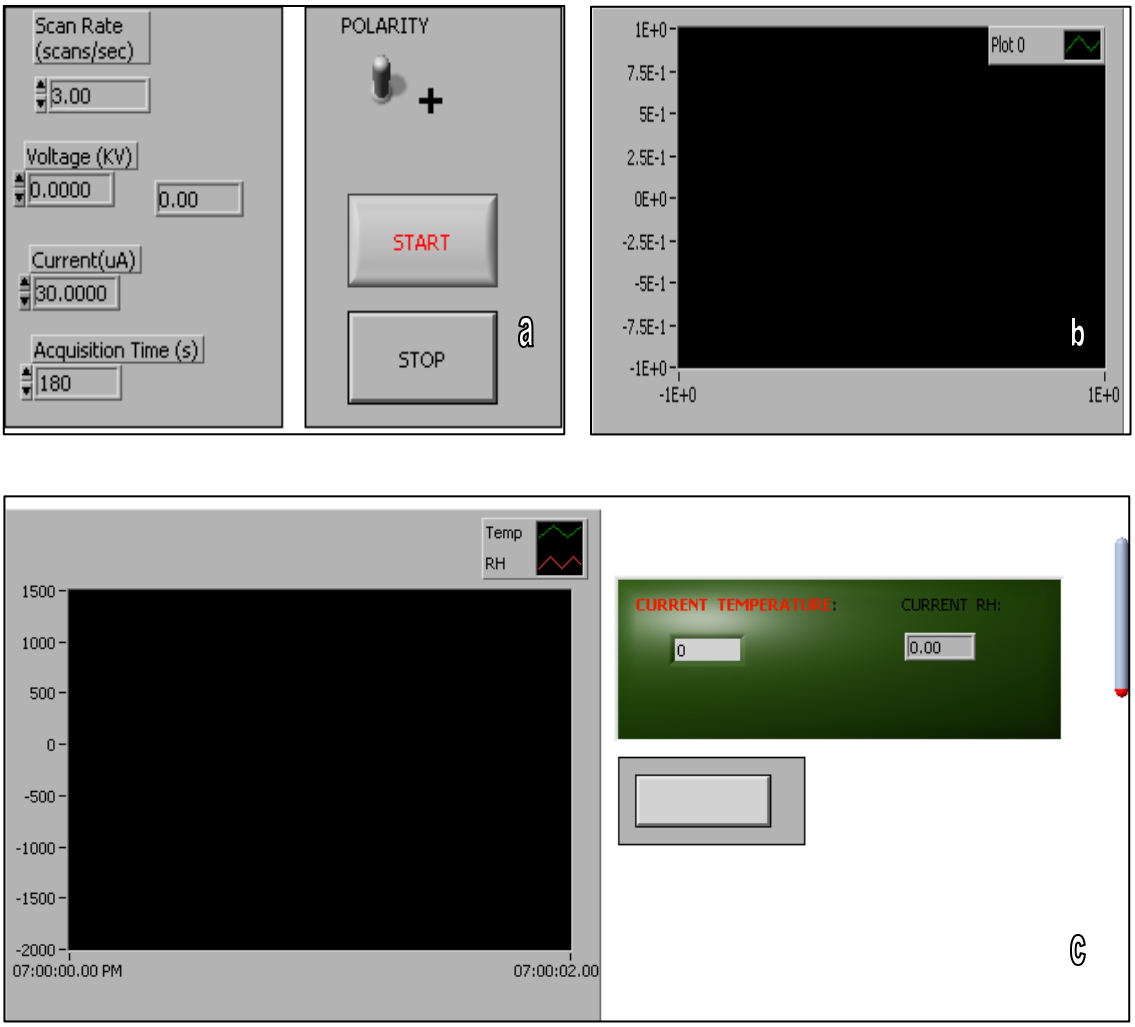

Figure 3.3: Virtual Interface of the LabView program version 8.0. a) part of the virtual interface where user inputs voltage and time for corona ion exposure b) corona current monitor c) temperature and humidity monitor.

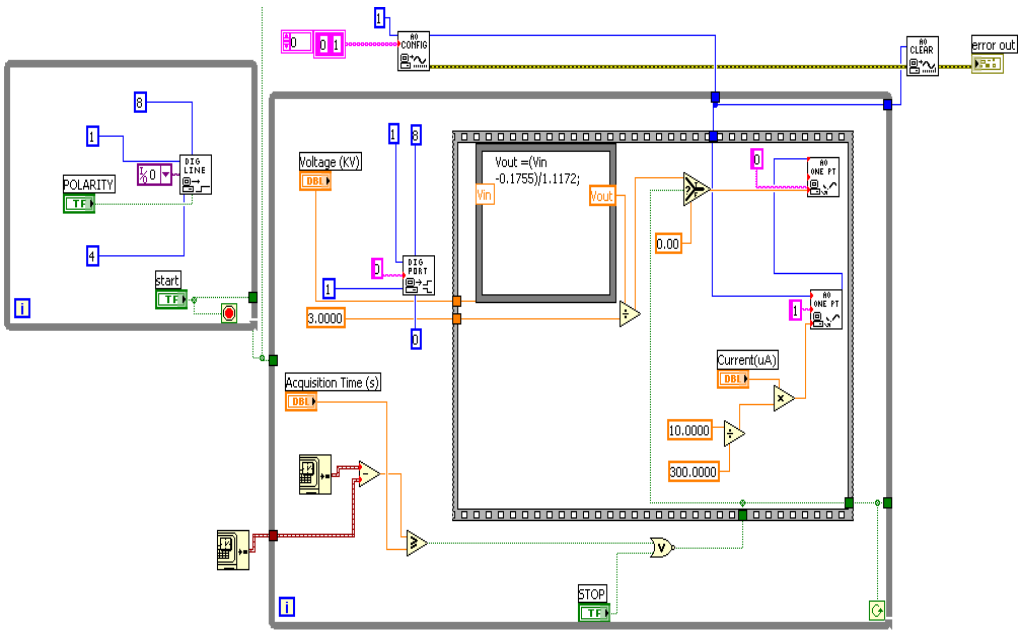

Figure 3.4: Source code of part a) of the Virtual Interface in Figure 3.3.

Figure 3.4 shows the code of the part of the virtual interface where the user inputs values for voltage and time of corona ion exposure. Once these variables have been input, a signal is sent to the programmable power supply with these parameters. The virtual interface communicates to the DAQ through a unique device ID and channel numbers. Figure 3.5 shows the source code for the corona current monitor. Current generated throughout the process was recorded and written to a text file. Figure 3.6 displays the source for monitoring the temperature and humidity during the experiment. Actual temperature and humidity values are also displayed in the main virtual interface.

This enabled monitoring the effect of temperature and humidity on the corona current.

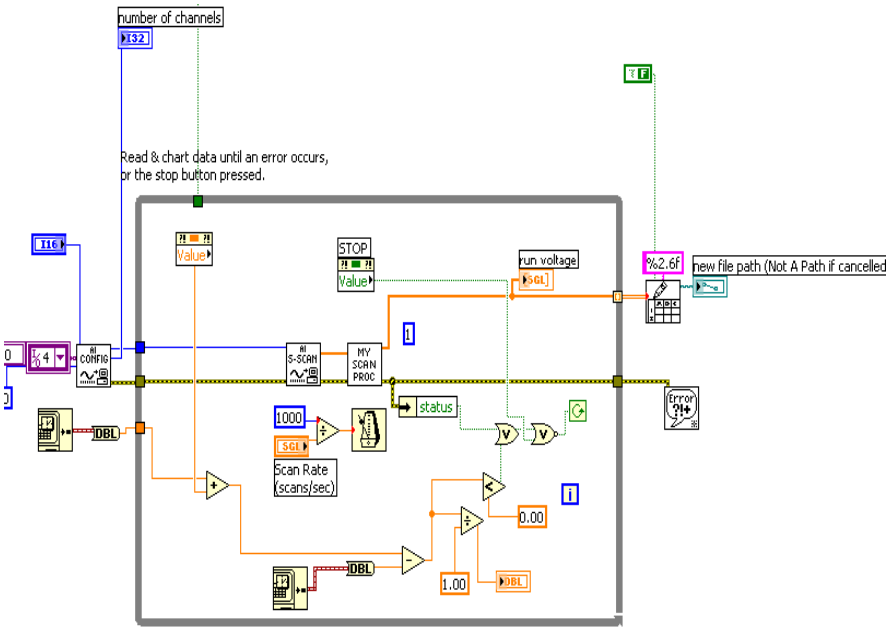

Figure 3.5: Source code for current monitor part b) in Figure 3.3.

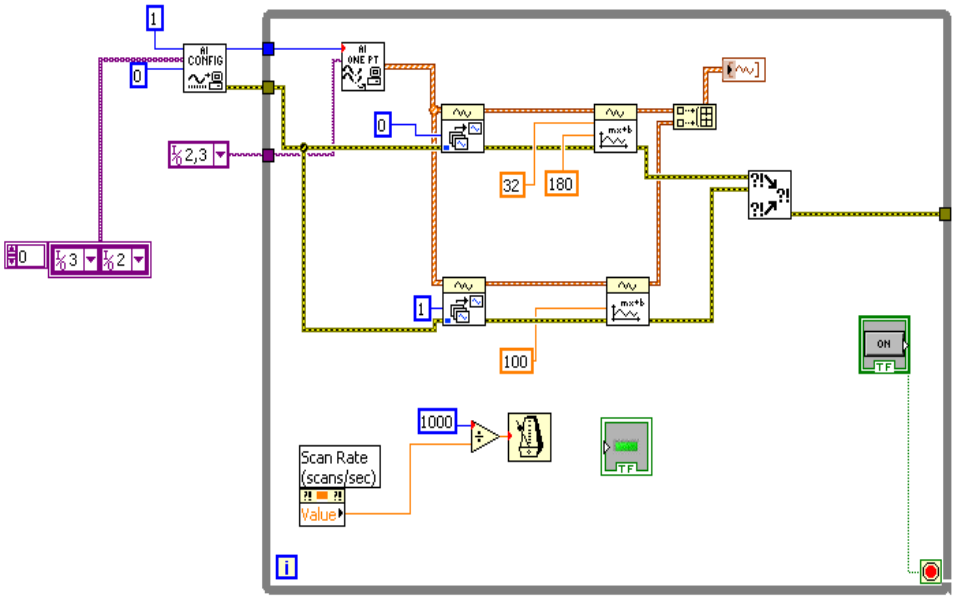

.

Figure 3.6: Source code for temperature and humidity monitor part c) in Figure 3.3.

The complete instrument system is shown in Figure 3.7 including the programmable power supply and the connector block that communicated between the DAQ card and the programmable power supply through a unique ID and channel numbers. The figure also shows the nine needle corona ion generator mounted on a micromanipulator so that the ions source may be positioned accurately relative to samples being treated.

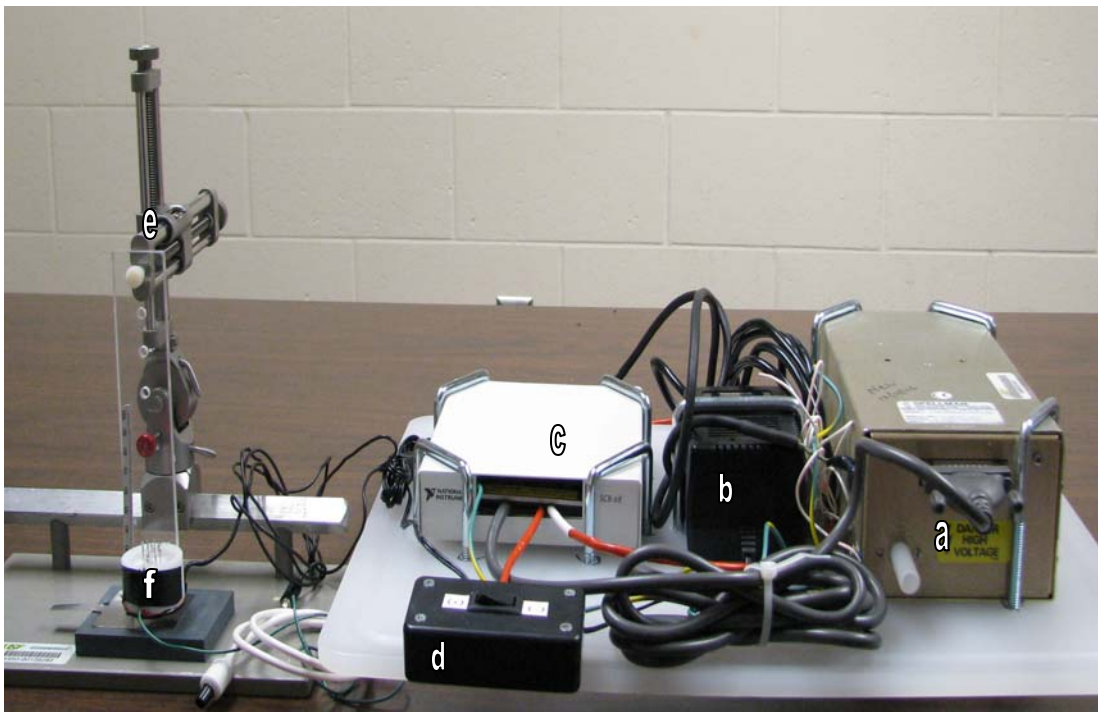

Figure 3.7: New corona ion generating system with programmable power supply and new nine needle generator. a) Programmable power supply b) 24 volts DC power supply for programmable power supply c) 68-pin connector block d) switch to reverse polarity of voltage applied to corona generator e) micromanipulator and f) corona generator.

3.1.2 Corona Discharge Characterization

To ensure that consistent ion density was provided by any corona system, ionic current from the two wire or nine needle corona ion generators was determined prior to each experiment using an electrometer (Keithley 6517A, Keithley Instruments Inc. Cleveland OH) and a stainless steel charge collecting plate located 7 mm below the bottom of the generator. A photograph of the electrometer with the charge collecting plate is shown in Figure 3.8. One end of the input cable from the electrometer terminated to a protection circuit. The other end of the cable had two alligator clips as shown in the Figure 3.8. The input high of the electrometer was connected to the metal collecting plate while the input low was connected to the ground.

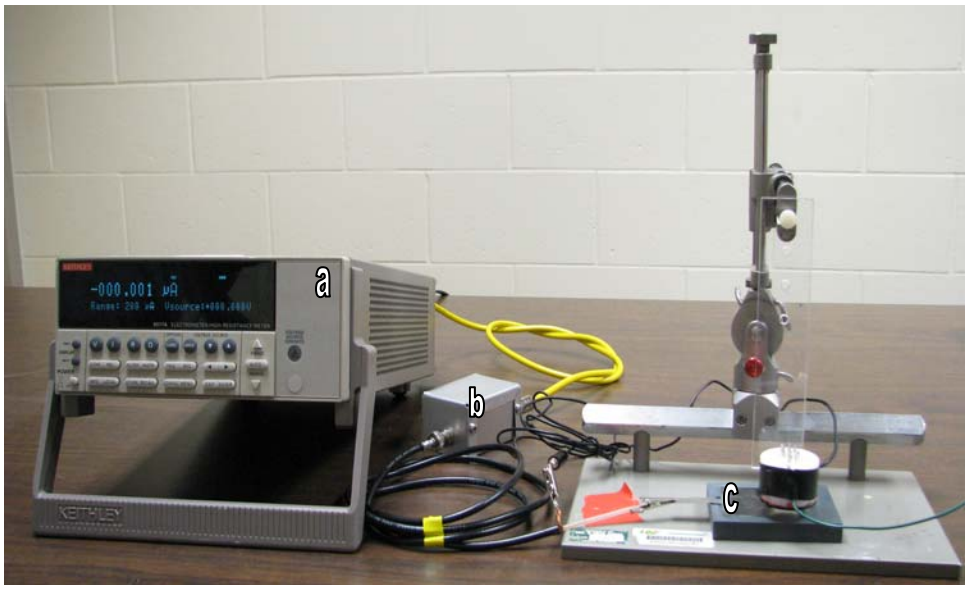

Figure 3.8: Charge collecting plate, attached to a block of CPVC, used to characterize corona ion generators. a) electrometer b) male triax connector c) charge collecting plate.

Charge deposited on the plate by the respective generators was determined for a particular applied voltage and polarity used. Typical current values for the two wire corona device were 3 μA when +6 kV was applied to the corona generating wires. The nine needle device produced +30 μA at an applied potential of +6 kV and -85 μA for -6 kV. Note that for a given potential, a higher negative current was always observed relative to positive ion current, independent of the type of the corona generator used.

3.2 Specific Aim 2: To Test the Capability of Corona Ions for Delivering Dyes and Tracer Molecules *In Vitro*

The materials and methods for this aim utilized the corona generating instrument system described in Section 3.1.1. In addition, both the corona generators described in Section 3.1.1 were also utilized. The procedure for characterizing the corona discharge was identical to the procedure presented in Section 3.1.2.

3.2.1 Cell Culture

B16F10 (ATCC CRL-6475) murine melanoma cells were grown in cell culture flasks (Costar 3000; Corning Inc., Corning, NY) in a standard 37 °C incubator in a humidified atmosphere that contained 5% CO_2. Cells were cultured in McCoy's 5A medium (MediaTech Inc., Herndon, VA) supplemented with 10% (v/v) fetal bovine serum (MediaTech Inc) and 50 µg/ml gentamicin sulfate (MediaTech Inc.). B16F10 cells were subcultured 1:12 using standard methods that included the use of trypsin (0.25% trypsin in HBSS without calcium and magnesium, MediaTech Inc.) to release the adherent cell line.

Batches of B16F10 cells were prepared for experiments by first determining their viability using trypan blue (MediaTech, Inc). All batches of cells used for this study were 95% viable or greater. Quantities of 5×10^5 cells were plated or seeded into organ culture dishes

(Falcon 353037, Becton Dickinson, Franklin Lakes, NJ). These dishes had an 18 mm diameter surface for cell growth. Dishes were seeded 12-18 hours prior to treatment with corona ions to allow for complete attachment of the cells to the growth surface.

3.2.2 Tracer Molecules

Calcein (C0875, Sigma, St. Louis, MO) and SYTOX-green (S7020, Molecular Probes) were used for this study. Calcein is an auto fluorescing tracer molecule that has a charge of -4 in solution whereas SYTOX-green is a nucleic acid stain that is an unsymmetrical cyanine dye with three positive charges. When SYTOX-green is bound to nucleic acid there is a large increase in the fluorescence emission with the greatest emission occurring when it is bound to double stranded DNA [75,76]. Both these molecules used were cell membrane impermeant making them suitable for use as indicators of intracellular molecular delivery.

3.2.3 Procedure for Molecular Delivery

Calcein was delivered to cultured B16F10 cells using the commercially available wire corona generator. The protocol included first aspirating the growth media from seeded organ culture dishes and replacing it with 250 µl of 20 µM calcein in phosphate buffered saline (PBS) over the cells in the dishes. Next, the corona generating system

was immediately lowered over the dish to expose the cells to positive corona ions, as in Figure 3.9, for either six or ten minutes at an ambient temperature of 22 °C. After ion exposure, the cells were incubated at 37 °C for ten minutes prior to fluorometric analysis. Control samples were treated by aspirating growth media and then exposing B16F10 cells to either PBS or calcein only without the influence of corona charge. These control samples were then left on the counter top for ten minutes at 22 °C and then ten minutes at 37 °C in order to match the protocol used for the samples that were exposed to corona charge.

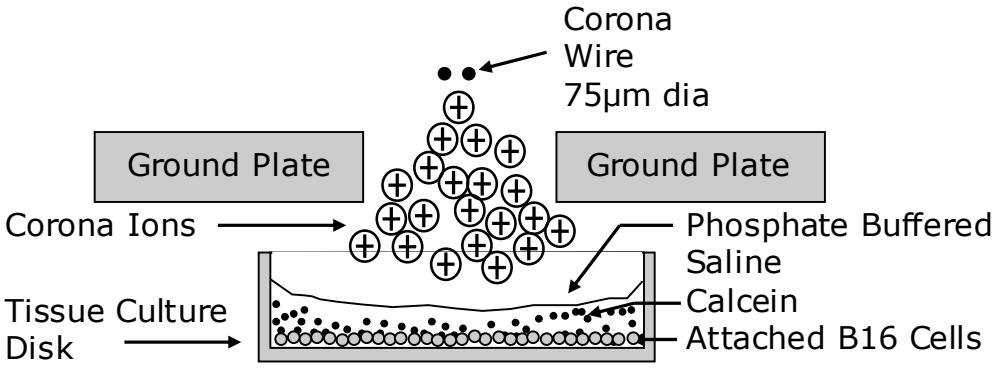

Figure 3.9: Schematic representation of the two wire corona generator treating B16F10 cells cultured on the bottom of a culture dish.

SYTOX-green was delivered to cultured B16F10 cells using the nine needle corona generator. After aspirating the growth media, 250 µl of PBS was added to the sample and either positive or negative corona charge was applied for ten minutes. Following the completion of the corona treatment, 250 µl of 1 µM SYTOX-green was added to each

culture dish. Samples were then incubated at 37 °C for ten minutes prior to fluorometric analysis. Control samples that were not scheduled to receive corona treatment were simply incubated with SYTOX-green for ten minutes at 37 °C prior to fluorometric analysis.

3.2.4 Fluorometric Analysis

Fluorometric analysis was performed on all samples following the ten minute incubation at 37 °C. The analytic procedure for calcein, included aspirating all the liquid from each culture dish, gently washing the growth surface three times with 1 ml aliquots of PBS and adding a final 1 ml volume of PBS. The cells were then lysed by adding 1 ml of 0.4% sodium docecyl sulfate (SDS) solution to each dish to release intracellular calcein. The resulting solutions were centrifuged at 225 $\times$ g for five minutes to remove cellular debris. The supernatants were then analyzed fluorometrically (LS-3B, Perkin-Elmer, Waltham, MA) using an excitation of 481 nm and an emission of 515 nm.

The procedure for fluorometric analysis of SYTOX-green was different. After the ten minute incubation of cells and SYTOX-green, the stain and PBS bathing the cells was aspirated and replaced with 250 µl trypsin to detach the cells. Ten minutes later, 1 ml of PBS was added to each dish to suspend the cells. Finally, the resulting suspensions

were analyzed using an excitation of 505 nm and an emission of 525 nm (LS-3B, Perkin-Elmer, Waltham, MA).

3.2.5 Viability Testing After Corona Charge Treatment

Viability was determined using the trypan blue dye exclusion test [77]. Cell samples with no tracer molecules present were exposed to positive or negative corona ions using the nine needle corona generator for ten minutes. Cells were exposed to +30μA or -85μA using ± 6 kV applied to the corona generator. Control samples were not treated with ions. Samples were returned to the incubator after exposure to corona ions. The circular dish was then divided into four quadrants by drawing lines corresponding to two orthogonal diameters on the bottom of the dish. All media was aspirated and replaced with 150 μl of PBS and 50 μl of trypan blue. Three fields of view were randomly chosen in each quadrant and viewed at 250X. The numbers of viable and nonviable cells were enumerated in each field and data for all four quadrants in each sample were summed. Observations were made on different samples at 30 minutes, 6 hours and 12 hours following corona ion treatment. Control samples, not treated with corona ions, were also analyzed in an identical manner at the same time points.

3.2.6 Statistical Analysis

Mean fluorometric data from samples were compared using a one tailed t-test. A one tailed t-test was used to establish that the mean fluorescence of groups that received corona ion exposure were higher than the controls. A 95% level of significance was chosen. If the p values obtained when comparing the two sets of means using the one tailed t-test were less than or equal to 0.05 ($p \leq 0.05$), then the differences were considered statistically significant and the null hypothesis that the two means are not different was rejected in favor of the alternate.

3.3 Specific Aim 3: To Investigate the Use of Corona Ions for Delivering Bleomycin *In Vitro* and to Established Tumors in an Animal Model

The instrument system used to drive corona generation was the same as described in Section 3.1.1. The nine needle corona ion generator was used for all the experiments in this aim. B16F10 cells used for *in vitro* and *in vivo* experiments were cultured as described in section 3.2.1.

3.3.1 Corona Discharge Characterization

The corona ions were generated using the protocol as described in Section 3.1.2. The system was characterized by determining the

quantity of charge collected on a stainless steel plate located 7 mm below the generator. This distance was identical to the distance between the generator and cultured cells during treatment. In experiments carried out in this aim, the quantity of charge that the cells were exposed to was increased by increasing the input voltage to the corona generator. The nine needle device generated +45μA at an applied potential of +6.5 kV and -95μA when the polarity was reversed to -6.5 kV.

3.3.2 Procedure for Molecular Delivery of Bleomycin *In Vitro*

Bleomycin is a commonly used cytotoxic drug that causes nicks in double and single stranded DNA. It was known from previously published work [78] that IC_{50} for bleomycin in B16F10 cells is 1×10^{-4} M and that concentrations lower than 1×10^{-5} M have little or no effect on the growth of B16F10 cells in culture. Bleomycin is a well known chemotherapeutic agent, however, its use has been hindered by the fact that it does not readily cross the cell membrane [79, 80]. Bleomycin has been successfully delivered using electroporation and very little drug is required to achieve a response (cell death).

In vitro experiments included six different combinations of bleomycin (NDC 0703-3155-01, Sicor Pharmaceuticals Inc., Irvine, CA) treatment and corona exposures. The treatment conditions were: no

treatment, corona exposure only for ten minutes, bleomycin exposure only and bleomycin exposure combined with corona exposure for two, five and ten minutes. Triplicate samples were used for each treatment condition. The protocol included aspirating the growth media from culture dishes, seeded with 1 x 10^5 cells as described in Section 3.2.1 and replacing it with 250 µl of 1 x10^{-5} M bleomycin in PBS. The corona generating system was lowered over the dish to expose the cells to corona ions of positive or negative polarity for the times mentioned above at ambient temperature (22°C). After a ten minute incubation period, growth media was added to each dish to make the final volume 3 ml. The culture dishes were then returned to incubator for further analysis.

3.3.3 MTT Survival Assay for Cultured Cells

Forty eight hours after treatment the samples were analyzed using a standard MTT (Thiazolyl Blue) survival assay [78]. This assay included exposing the plated cells to 1 mg/ml MTT reagent for two hours at 37°C in growth media. After two hours the media containing the MTT was aspirated and 400 µL of DMSO (D587needle, Sigma, St. Louis, MO) was added to each culture dish to dissolve the cells and the resulting intracellular purple crystalline product which is the basis of this colorimetric assay. Four 100 µL aliquots from each treated dish

were analyzed for optical density (OD) using a microplate reader (EL340, BioTek Instruments Inc., Winooski, VT) with the reference filter set at 630 nm and the test filter set at 570 nm. The resulting OD data from samples with like treatment groups were combined to obtain a mean OD for each treatment group.

3.3.4 Tumor Induction

B16F10 cells were removed from culture using the method described in Section 3.2.1 and washed three times in phosphate buffered saline by centrifugation (225 $\times$ g). The washed cells were suspended in normal saline and enumerated using a hemacytometer. Cells were used only if the viability of the enumerated culture was above 95%. Prepared cells were injected into the shaved left flank of female 6-8 week old C57Bl/6 mice. Each animal received a subcutaneous injection containing 1 x 10^6 cells in 50 µl saline. Tumors were allowed to grow for approximately ten days which resulted in tumors that were approximately 80 mm^3. Tumor volumes were determined by measuring three mutually orthogonal diameters using digital Vernier calipers. Measurements where converted to volumes using the formula $V = a \times b \times c \times \pi/6$ were V was the volume and a, b and c were the three measured dimensions (mm).

3.3.5 Procedure for *In Vivo* Delivery of Bleomycin to Tumors

Tumor bearing mice were randomized into different treatment groups. Each group received a different treatment consisting of bleomycin injection only, corona exposure only, exposure to both corona ions and bleomycin or no treatment (controls). In addition, some groups received the same treatment on three successive days. Details of the treatment scheme are shown in Table 3.1. The treatment protocol included anesthetizing each mouse with isoflurane (Isothesia, Abbott Laboratories, IL) using a calibrated vaporizer. Anesthesia was maintained using 1.5% isoflurane. All mice remained in an anesthetized state until treatment was complete. Animals scheduled to receive bleomycin were injected with a volume of the drug that was equivalent to 50% of the tumor volume (measured immediately prior to treatment). The concentration of the drug was 4 units/ml in sterile injectable saline and a single point injection was made directly into the center of the tumor. All other animals received an injection of saline equivalent to the 50% of their tumor volumes. Mice that had corona ions as all or part of their treatment were exposed to either positive or negative corona charge for 20 minutes as indicated in Table 3.1. This was achieved by lowering the corona ion generator towards each animal to position the center needle of the generator 5 mm from the center of the tumor.

Table 3.1: Treatment conditions for *in vivo* delivery of bleomycin

No Treatment
Bleomycin only once
20 min. Negative Corona only
20 min. Positive Corona only
Bleomycin + 20 min. Positive Corona once
Bleomycin + 20 min. Negative Corona once
Bleomycin only on three successive days
20 min. Positive Corona only on three successive days
20 min. Negative Corona only on three successive days
Bleomycin + 20 min. Positive Corona on three successive days
Bleomycin + 20 min. Negative Corona on three successive days

Corona treatment was started two minutes after bleomycin injection. A saline injection was substituted for bleomycin for tumors not scheduled to receive the drug. The two minute delay time between injection and start of corona ion exposure was determined to be sufficient to allow the drug to distribute within the tumor [79]. Post treatment follow-up consisted of measuring the volume of each individual tumor at periodic intervals as described in section 3.3.4. These volumes were normalized to the day zero (day of treatment) tumor volume for each individual animal. Normalized tumor volumes were

expressed as percentage increase or decrease over day zero and mean data was computed for animals in the same treatment group on the same follow-up day. Animals were humanely euthanatized when their tumor volumes reached 1000 mm^3.

3.3.6 Statistical Analysis

In vitro data analysis was conducted by comparing the means from the MTT survival assay using a one tailed t-test. The means of the controls and treatment groups were compared to see if the treatment set had a lower mean absorbance. Sets of two means were compared at a significance level of 95% as described in section 3.2.6. *In vivo* data analysis was performed in a similar manner by comparing mean normalized tumor volumes for each group on a particular day post treatment to test for differences at a 95% significance level. This data was also examined using a one tailed t-test.

3.4 Specific Aim 4: To Evaluate the Use of Corona Ions for Delivering Plasmid DNA to Cells in the Skin of a Murine Model

The corona ion generation apparatus for Specific Aim 4 was the same as used in Specific Aim 3 and the same procedure was used to calibrate the instrument system. The only difference in Specific Aim 4 was that more current was desired relative to earlier work and so an applied potential of +/-7.5 kV was employed to generate, respectively,

55 μA or 165 μA of corona ions. Hence, the same nine needle corona ion generator was used and instead of 6.5 kV, the voltage applied was 7.5 kV. The higher current was chosen in accord with analysis of data from experiments in Specific Aim 3 that focused on delivering bleomycin to tumors *in vivo*. It was hypothesized that an increase in current would be necessary to drive DNA, which is a bigger molecule. Female C57Bl/6 mice were used as the animal model. The procedure for delivery of genes, including the experimental conditions and post treatment analysis which were different from the tumor work are described below.

3.4.1 Procedure for *In Vivo* Delivery of Reporter Plasmid Coding for Luciferase

The capability of corona charge to facilitate *in vivo* uptake of plasmid DNA was examined using the skin of C57Bl/6 mice (female, 6-7 weeks old). A reporter plasmid that coded for the enzyme luciferase (gWiz^{TM} Luciferase, Aldevron, Fargo, ND) was used. The target tissue was a shaved area of skin on the left flank. Mice were randomly divided into treatment groups as shown in Table 3.2. Each group received a different treatment consisting of plasmid injection only, corona exposure only, exposure to both corona ions and plasmid for 10 or 30 minutes and no treatment. In addition, two groups received treatments of plasmid and positive or negative corona exposure with a

grounded counter electrode inserted subcutaneously below the site of injection. The counter electrode was a 28 gauge stainless steel acupuncture needle and the part of the electrode that was outside the body was covered with insulation so that the charges would not drift directly to the grounded electrode.

Each mouse was first anesthetized using isofluorane, as described in section 3.3.5 and remained in this state until treatment was complete. All animals scheduled to receive the plasmid got an intradermal injection of 50 µl saline that contained 2 mg/ml of the reporter plasmid. All other animals received a 50 µl injection of saline only. After plasmid injection, the corona ion generator was lowered toward each animal to position the center needle of the generator 1 cm from the center of the bubble formed in the skin due to injection. Mice that received exposure to corona ions as all or part of their treatment were exposed to either positive or negative corona charge for the amount of time indicated in Table 3.2.

Table 3.2: Treatment conditions for *in vivo* delivery of reporter plasmid coding for luciferase (LUC)

No Treatment
50µl of LUC Plasmid only
30 min. of Positive Corona only
30 min. of Negative Corona only
50µl of LUC Plasmid + 10 min. Positive Corona
50µl of LUC Plasmid + 30 min. Positive Corona
50µl of LUC Plasmid + Counter Electrode+ 10 min. Positive Corona
50µl of LUC Plasmid + 10 min. Negative Corona
50µl of LUC Plasmid + 30 min. Negative Corona
50µl of LUC Plasmid + Counter Electrode+ 10 min. Negative Corona

3.4.2 Analysis of Delivered Reporter Plasmid Coding for Luciferase

Luciferase is an enzyme commonly found in nature that participates in a bioluminescent reaction when allowed to react with an appropriate substrate. This reaction takes place in many bioluminescent organisms. The injected plasmid if delivered inside the cell would be acted upon by the cell machinery and the enzyme luciferase would be produced. The analysis was performed to examine the expression of luciferase by the cells. Light is emitted when luciferase catalyses the oxidation of a chemical substrate called luciferin. The oxidation of luci-

ferin by luciferase, in the presence of ATP, is a very energy efficient reaction and the subsequent photon emission can be detected with a sensitive CCD camera. Therefore, all mice were intraperitonealy injected with 150 mg/kg of luciferin at prescribed time points after the plasmid was delivered. Luciferin was allowed to distribute for about 15 minutes and the mice were then anaesthetized and imaged using an IVIS 200 imaging system (Xenogen, Hopkinton, MA). The images were then analyzed by proprietary software from Xenogen (Living Image 2.6). A region of interest (ROI) was selected; this was the region over which the expressed luciferase protein was detected. The average photon flux in photons/cm^2/sec over the ROI was recorded. The same procedure was followed for all animals.

3.4.3 Statistical Analysis

In vivo data analysis was conducted by comparing the mean photon fluxes from all the groups at specific time points after DNA delivery. A one tailed t-test was used to determine if the mean photon flux of the groups that received exposure to both the plasmid and either type of corona ions were greater than the controls. The groups which received plasmid only or corona ions exposure only were designated as controls. A one tailed t-test was performed on each day the photon flux was measured and the two sets of means were compared

to check for differences at a significance level of 95% as described in section 3.2.6.

3.5 Specific Aim 5: To Investigate the Mechanism of Interaction of Corona Ions with Biological Cells

In addition to using B16F10 murine melanoma cells, fibroblasts [ATCC -CRL-2522-BJ] were also used for one part of this study. Same cell culture protocol used for B16F10 cells was used for the fibroblasts. All protocols and materials were same as used in Specific aims 1 and 2. Cells were grown on culture dishes as described previously, the corona ion generator was lowered on the top of the dish and ions were deposited on the surface of the media covering the cells. The nine needle corona generator was used for this specific aim and produced 45 µA at an applied potential of +6.5 kV and – 95 µA when the polarity was reversed.

3.5.1 Cell Culture

The procedure for growing B16F10 cells was same as mentioned in 3.2.1. Fibroblasts [ATCC -CRL-2522-BJ] cells used in addition for this study were grown in similar cell culture flasks in a standard 37 °C incubator in a humidified atmosphere which contained 5% CO_2. Cells were cultured in DMEM (MediaTech Inc., Herndon, VA) supplemented with 10% (v/v) fetal bovine serum (MediaTech Inc.) and 50 µg/ml

gentamicin sulfate (MediaTech Inc.). Fibroblasts were also subcultured 1:12 using standard methods that included the use of trypsin (0.25% trypsin in HBSS without calcium and magnesium, MediaTech Inc.) to release the adherent cell line. Batches of fibroblasts were prepared for experiments by first determining their viability using trypan blue (MediaTech, Inc). All batches of cells used for this study were 95% viable or greater. 5×10^5 cells of both kinds were plated into organ culture dishes used in section 3.2.1 prior to treatment.

3.5.2 Interaction of Deposited Corona Ions with the Media *In Vitro*

Experiments were performed in order to elucidate some details of the interaction of corona ions with the media surrounding the cells. B16F10 cells used were exposed to corona ions of either polarity and experimental observations were performed. Observations were made on cells exposed to corona ions for ten minutes followed by SYTOX-green exposure to delineate the area which had maximum delivery of SYTOX-green. Also a visual model was developed to depict the interaction of the ions deposited on the surface of the media.

3.5.3 Mechanism of *In Vitro* Delivery Based on Experimental Observation

Experiments were designed and performed to investigate physical parameters as a cause for molecular delivery. Temperature and pH

were first measured to determine if a change in any of these two could cause molecular delivery. Following this, effect of corona ion deposition on transmembrane potential and cell adhesion was observed.

3.5.3.1 Temperature and pH Measurements

Temperature change of the media exposed to corona ions was studied in this section. B16F10 cells were grown at the bottom of culture dishes and the media surrounding the cells was exposed to either ten minutes of positive or negative corona and the temperature was measured with an infra red thermometer (Fluke #62, WA) and a Fischer scientific alcohol thermometer. Following this, pH measurements were made separately using a PHR-146 microelectrode (LAZAR Research Laboratories Inc., Los Angeles, CA). Both temperature and pH measurements of the media surrounding the cells were performed before and after corona ion exposure. Six temperature and pH measurement experiments were performed in triplicate on different days. Hence the mean temperature and pH from six different experiments performed on six different days was measured to see if there was a change.

3.5.3.2 Effect of Corona Ions on Transmembrane Potential

The effect of corona ion exposure on the resting membrane potential of cells was studied using the voltage sensitive dye Di-8-

ANEPPS (Molecular Probes, Eugene, OR). Di-8-ANEPPS is an amphiphilic dye with a hydrophilic head and a hydrocarbon chain [81]. Due its structure the dye intercalates in the lipid bilayer and orients itself perpendicular to the membrane/aqueous interface. The dye increases in fluorescence, due to change in its electronic structure when there is a change in the packing of the lipids in the plasma membrane [82]. Hence an increase in fluorescence after corona ion exposure would confirm a change in resting membrane potential as well as a change in the structure of the lipid bilayer. Di-8-ANEPPS has a very fast response time and the increase in fluorescence due to the dye is only about 10-25% [83]. B16F10 and fibroblast cells used for this aim were stained with 1μM dye for 20 minutes in an incubator at 37 °C in a humidified atmosphere that contained 5% CO_2. Following the staining the cells were treated with either positive or negative corona ions for five minutes. The treatment was carried out on an inverted microscope which had the excitation source at the bottom. This arrangement was used so that the images could be captured instantly after the corona exposure ceased and there would be no time lost in adjusting or moving the treated sample. Fluorescence images were captured with the inverted microscope (Leica 520804, Germany) to see the visual effect following the ion exposure. The microscope had a digital camera (#15.264MP, Diagnostic Instruments Inc., MI) mounted on top

and the images were captured using proprietary software (SPOT 4.5, Diagnostic Instruments Inc., MI). The captured images were then analyzed and the mean light intensity of each image was calculated using Daime (Free Software by Holger Daime).

3.5.3.3 Effect of Corona Ion Exposure on Cell Adhesion

B16F10 cells were used for this study and were stained with a fluorescent dye CMFDA (Invitrogen. Eugene, OR). CMFDA belongs to the family of fluorescent chloromethyl derivatives that freely permeate the membranes of live cells. They react with intracellular components to produce cells that are both fluorescent and viable for at least 24 hours after loading. CMFDA has a relatively low acid dissociation constant (pKa), due to which bright green fluorescence in the cytoplasm will be detected at all physiological pH levels [84]. Half a million cells seeded in culture dishes, as described in section 3.2.1, were stained with CMFDA for two hours. Following staining, the cells were exposed to either positive or negative corona ions for ten minutes. Images of cells were captured at 0, 5, 10 and 15 minute intervals after the start of corona ion exposure. Fluorescent images were captured with an inverted microscope (Leica 520804, Germany) that had a digital camera (#15.264MP, Diagnostic Instruments Inc., MI) mounted on the top and images were captured using proprietary software (SPOT 4.5, Diagnos-

tic Instruments Inc., MI). An image was captured at time zero and the excitation source was turned off until the next time when the image had to be captured. This was done in order to protect the cells from continuous exposure to the excitation source.

3.5.4 Rate of Uptake of SYTOX-Green

Rate of uptake of the nucleic acid probe SYTOX-green was carried out to facilitate the development of a model to describe the time dependence of molecular transport into corona ion treated cells. A quantity of 5×10^5 B16F10 cells were grown in 12 well plates (Falcon 353047, Becton Dickinson, Franklin Lakes, NJ) similar to the procedure explained in 3.2.1. Uptake of the dye was followed starting immediately after corona charge treatment ceased. The procedure for measuring the uptake of SYTOX-green was carried out using a fluorometer (FLx800, BioTech Instruments Inc., Winoski, VT). The fluorometer was programmed to read every 15 seconds throughout a 35 minute follow-up period. Each fluorescence reading performed was an average of 10 different spots read on the cell growth surface of a particular sample.

3.6 Corona Ions: Safety Concerns

As described in the section 1.3 on generation of corona ions at atmospheric pressure, a high voltage around ± X kV (3-8KV) was re-

quired for ionization of air. With the use of input voltages reaching a few kilovolts the fields can reach as high as 9×10^{6} V·m^{-1} very close to the discharge electrode as shown in Figure 4.15. Proximity of such high value electric fields close to biological subjects could be a concern. Two examples of phenomena in daily life where discharges are encountered but are not fatal are a discharge to a door knob after walking on a carpet and charging of hair and body. The reason for these discharges not being as dangerous is that the power dissipated in these applications is very low. In the case of ions generated by the system used in this research the power dissipated is also very low due to low input current (100 μA) hence there is a very remote possibility of damage to tissues or biological cells. In addition to this the target tissue or cells are at a distance 7 mm away from the discharge electrode. The field near the electrode decreased with distance away from it.

The values of the electric fields used in typical electroporation experiments are generally in the range of 10^{5} to 10^{8} V·m^{-1} [110-113]. The associated current in these electroporation experiments is in milliamperes [90, 114] to amperes [115, 116] making the power dissipated in the range of tens of thousands to gigawatts [116]. In animal studies and clinical trials focused on treating tumors and other tissues, direct contact has resulted in muscle contraction, pain, or tissue dam-

age [32, 33, 73 and 74]. The values of electric fields during corona ion generation that cells would be exposed were modeled to be around 2×10^5 $V\cdot m^{-1}$ which is close to values used in electroporation experiment. The difference between the two is the power dissipated which is around 0.7 watts (input voltage times the input current). Hence any concerns that can arise due to high values of exposed electric fields can be put to rest. Visual observations on mice did not reveal any irritation or damage to the skin as compared to the untreated controls.

Corona discharge has been used in the past to kill dust mites, allergens and for biological decontamination. The main mechanism of destruction was attributed to the charged species generated and not due the ozone that was generated as a by-product [44]. It has also been determined from a previous study that the ozone generated in this kind of a corona discharge is well below the safety limit recommended by the EPA [117]. Correlation between the ozone generated and the input power used was investigated. There was found to be a direct relation between the power input to the system and the ozone generated. The input power in the system used in the current study is 0.7 watts which much lower than the one carried out in the study by Yehia. Hence the ozone generated is also subsequently lower and any concern of ozone generated as a by product of corona ion generation effecting the cells is very remote. Another concern with atmospheric

plasmas is exposure of biological cells to UV radiation. Most non-equilibrium plasmas operating at atmospheric pressure are poor sources of UV and hence this should not be a concern either [118].

4 RESULTS

4.1 Specific Aim 1: To Design, Construct and Characterize a Corona Generating System Suitable for Application in Living Systems

Determining the quantity of corona charge generated versus applied voltage was the primary means of characterizing the corona generating system, hence this experiment was carried out first. The commercially available corona generator that was used to test the initial delivery experiments was used for the corona charge characterization. Figure 4.1 shows results plotted with the independent axis vertical and the dependent axis horizontal. The charge emitted from the commercial corona generator was roughly a linear function of the applied voltage as shown in the figure and was similar to the relationship shown in Figure 1.2. The experiments carried out to obtain results in Figure 4.1 were for a fixed distance of 5 mm between the bottom of the ground plate and the charge collecting plate. This distance was an approximation to the distance that would be used in subsequent *in vitro* and *in vivo* delivery experiments. The maximum current that could be generated for a positive applied potential was about 6.5 μA and 10 μA for negative applied voltage. Attempts to generate more current

for both cases by increasing the applied voltage resulted in arcing or sparkover.

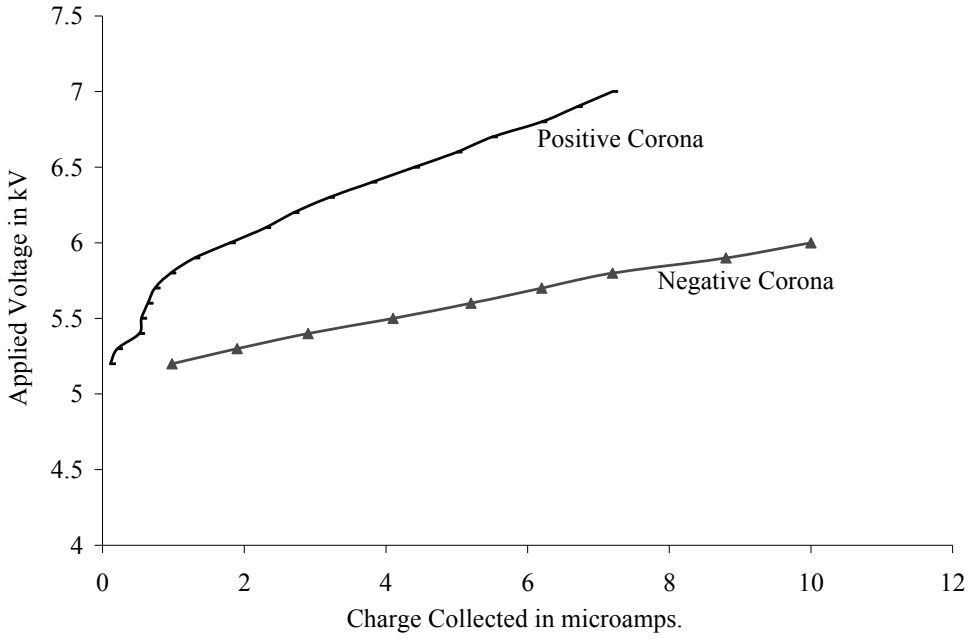

Figure 4.1: Voltage applied (kV) to the commercial corona ion generator versus charge collected (μA).

A fixed distance of 5 mm was used for initial characterization of the corona generator. A second experiment was performed to see changes in the quantity of charge collected by varying the distance between the charge collecting plate and the corona generator. Distance was varied from 1 mm to 7 mm and the results from this experiment are shown in Figure 4.2. A positive voltage of 5.5 kV was applied to the corona generating elements. As the distance from the bottom of the ground plate to the charge collecting plate was increased, the

charge collected decreased exponentially as shown in Figure 4.2. It can be observed that the last point in the graph is 6.74 mm; this was the approximate distance between the generator ground plate to the bottom of the cell growth surface for *in vitro* experiments performed in Specific Aim 2.

The third characterization experiment was designed to maximize the amount of charge that could be generated with the commercial corona generating element without reducing the distance between the ion generating source and the charge collecting plate. The strategy to maximize current generated involved, isolating/confining the generated corona ions in the space between the generator and ground plate using plexi-glass tubes with different diameters and heights.

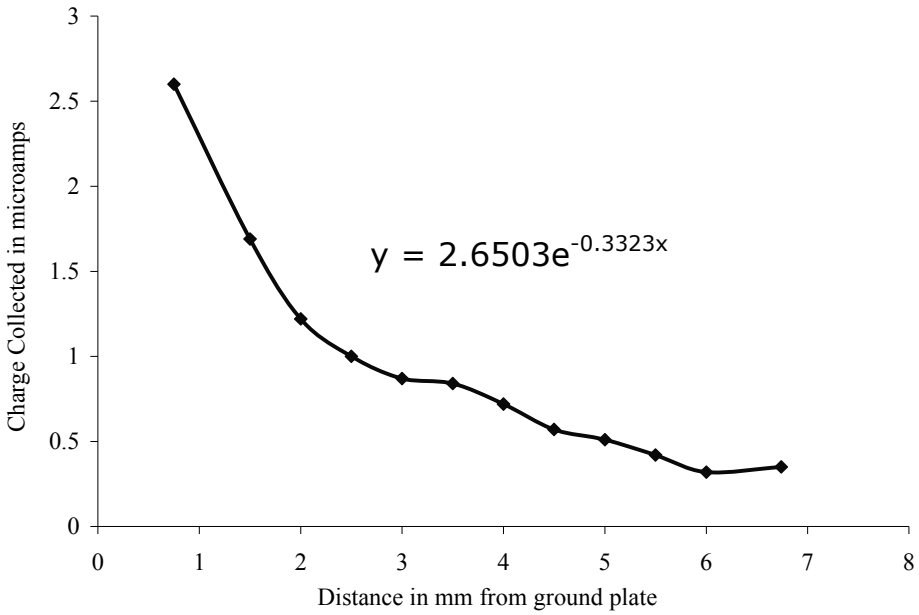

Figure 4.2: Charge collected (μA) from the commercial corona generator as a function of distance from the bottom of the charge collecting plate. A positive voltage of 5.5 kV was applied to the corona generator.

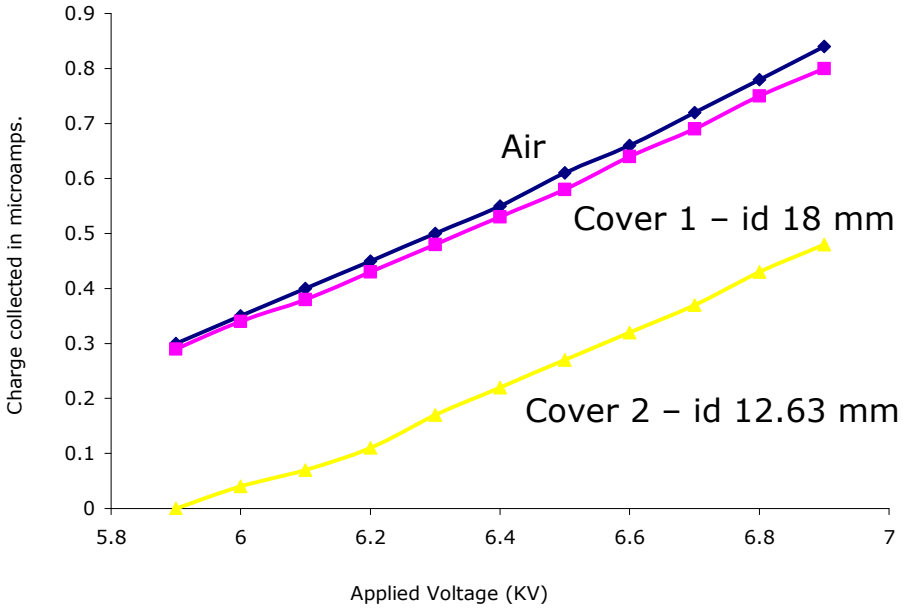

Figure 4.3: Corona charge collected (μA) versus positive applied voltage (kV) with different plexi-glass cylinders.

Figure 4.3 shows the results of experiments with the different plexi-glass cylinders. As indicated in the figure, cylinders with two different diameters were utilized along with an ambient condition that was used as a control. Cover 1 was a plexi-glass cylinder with an inner diameter of 18 mm, which is the same inner diameter of the culture dishes that were planned for *in vitro* experiments. Cover 2 was a cylinder with inner diameter that was same as the diameter of the hole in the bottom of the ground plate (about 12.64 mm). The height of both cylinders, cover 1 and cover 2, was 7 mm, which was the distance between the bottom of the ground plate and the culture dish used in subsequent experiments. The polarity of the applied voltage was positive. Results from Figure 4.3 clearly indicated corona ion generation in open air resulted in the highest current relative to each cylinder.

The current generated under the conditions shown in Figure 4.3 was lower compared to that shown in Figure 4.1 due the difference in the distance between the corona generator and the charge collecting plate. A distance of 5 mm was used to generate results in Figure 4.1 whereas a distance of 7 mm was used to generate results in Figure 4.3. Results of these experiments with the commercially available ion generator motivated the design of a new corona ion generator capable of producing more charge because it was hypothesized that better de-

livery results would be obtained using more charge. The commercial corona generator used for characterization experiments had a linear corona generating electrode while the culture dishes that were planned to be used for *in vitro* experiments were circular. Hence to better fit the circular geometry of the tissue culture dishes and solid tumors that would be treated in subsequent experiments, a circular geometry was chosen for the new corona generator.

4.1.1 Design of a New Corona Generator

After attempts to increase the amount of charge from the existing instrument system (commercial corona generator) were unsuccessful, a second generation corona generator was designed. It was hypothesized that with this new design there would be an increase in corona charge and also it would better match the geometry of the circular culture dishes used for delivery experiments. A needle electrode geometry was chosen as compared to thin wires as in the commercial generator as multiple needle emitters were thought to give more current. As described in the Section 1.3 the key to the generation of corona ions is the thickness of the tip of the ion generating electrode, hence experiments were first carried out to determine what needle thickness and electrode configuration would maximize current output with this new geometry. Needle diameters of 0.35, 0.6, 0.7, 0.8 and

0.9 mm were used to test which needle configuration would generate maximum amount of corona ions. All needles had tapered tips.

The new corona generator was custom made such that the needles would form an array within a circular Teflon rod, 38 mm by 26 mm, diameter to height; details of the instrument system are described in Section 3.1.1. Experiments were first carried out with 0.35 mm diameter needles. Four different needle configurations were chosen; first nine needles were inserted through holes in the Teflon rod such that the tapered tips just protruded below the lower polymer surface. One needle was located at the center and the remaining eight needles were equally spaced around a 11 mm diameter circle as shown in Figure 4.4. Three other configurations with eight needles, five needles and four needles inserted in the Teflon rod were also investigated. To achieve the eight needle configuration, only the central needle was removed from the nine needle configuration while measuring charge. The five needle configuration consisted of the central needle and four needles inserted on two orthogonal diameters.

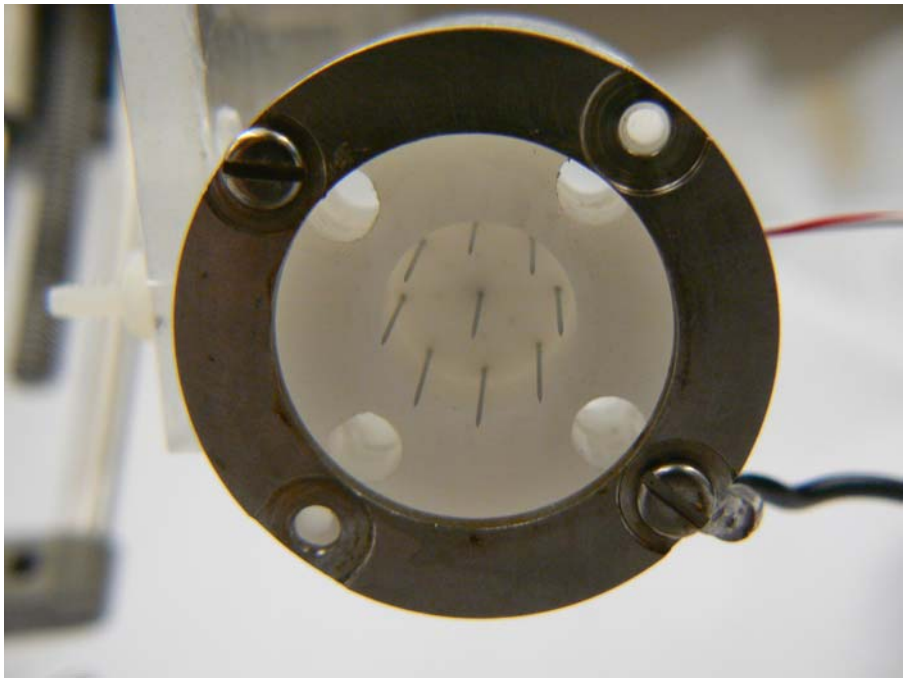

Figure 4.4: Corona generator showing the nine needle configuration.

The four needle configuration had only four needles at opposite ends of two perpendicular diameters. The needles were connected together at the top to facilitate connection to the high voltage power supply. An annular stainless steel ground plate was affixed to the bottom of the Teflon rod and was connected to the ground of the power supply. The inside diameter of the ground plate was 28 mm. The needle tips were located in the plane of the top of the ground plate. Figures 4.5 and 4.6 show results of charge generated in different configurations for the 0.35 mm thickness needles for positive and negative polarities. Similar experiments were carried out with the other needle sizes and different needle configurations. The results of these

remaining experiments are shown in Figures 4.7-4.14. In conclusion, the nine needle configuration with 0.35 mm diameter was judged to be the best option for delivery experiments. Even though results presented below indicated that some other needle configurations and needle thickness gave more charge, the needle size chosen was 0.35 mm based on the availability of these needles and also the fact that microscopic observations revealed that they had a uniform tip size as compared to the other needle sizes. Also the 0.35 mm needles were made of a surgical grade of stainless steel [SUS304] that was different from the other needles used and hence had the potential to last longer as compared to all other needles.

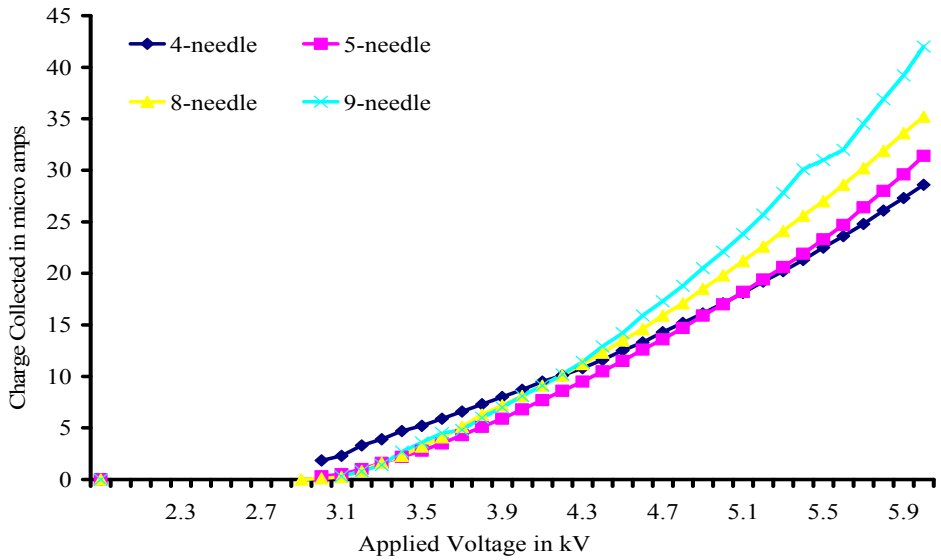

Figure 4.5: Corona charge collected (μA) versus applied voltage (kV) for a needle thickness of 0.35 mm and the applied polarity was positive.

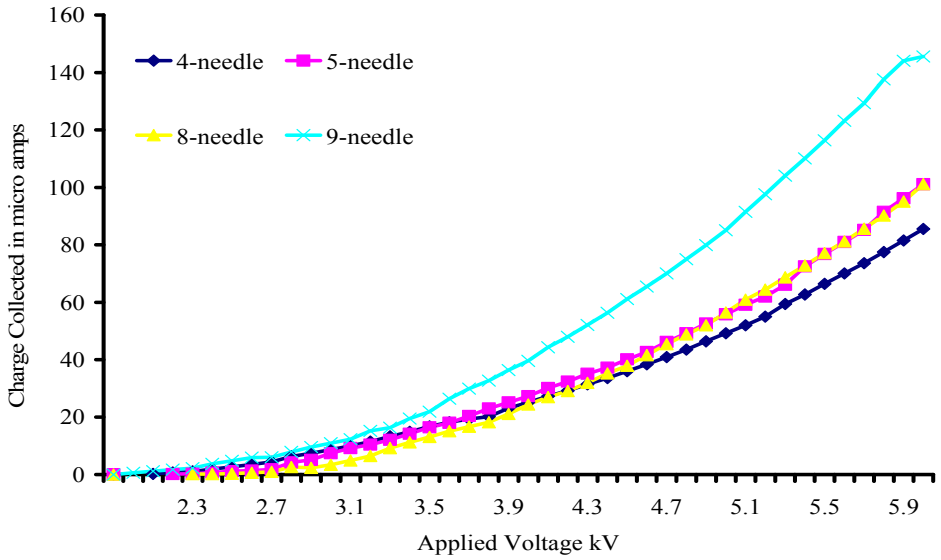

Figure 4.6: Corona charge collected (μA) versus applied voltage (kV) for a needle thickness of 0.35 mm and the applied polarity was negative.

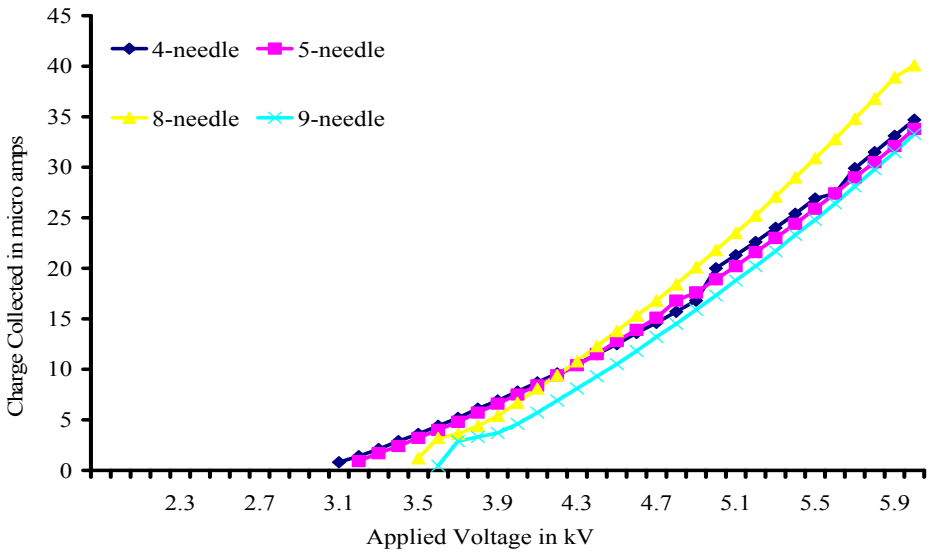

Figure 4.7: Corona charge collected (μA) versus applied voltage (kV) for a needle thickness of 0.6 mm and the applied polarity was positive.

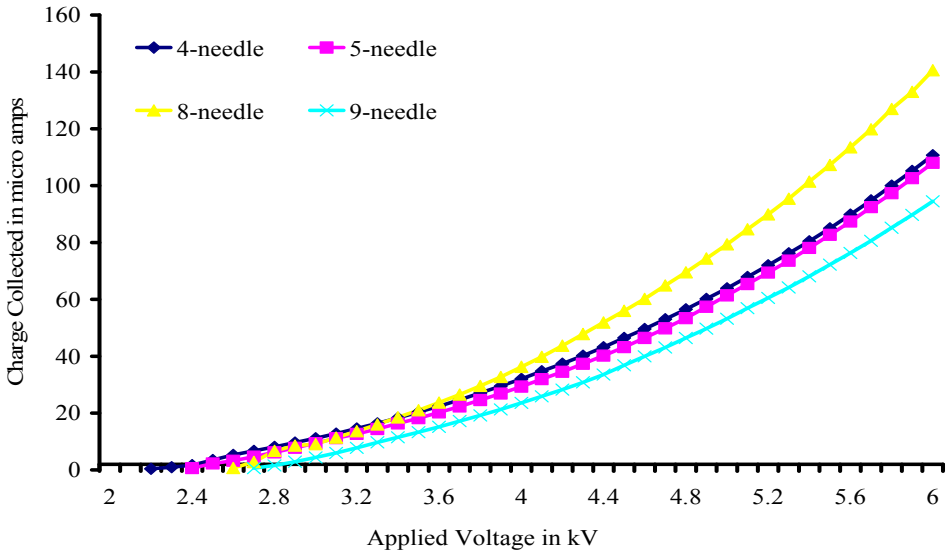

Figure 4.8: Corona charge collected (μA) versus applied voltage (kV) for a needle thickness of 0.6 mm and the applied polarity was negative.

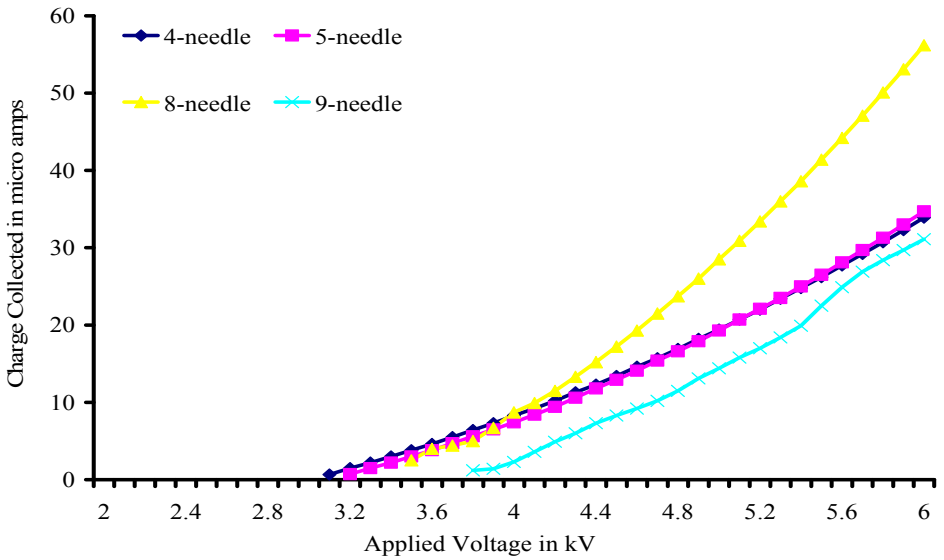

Figure 4.9: Corona charge collected (μA) versus applied voltage (kV) for a needle thickness of 0.7 mm and the applied polarity was positive.

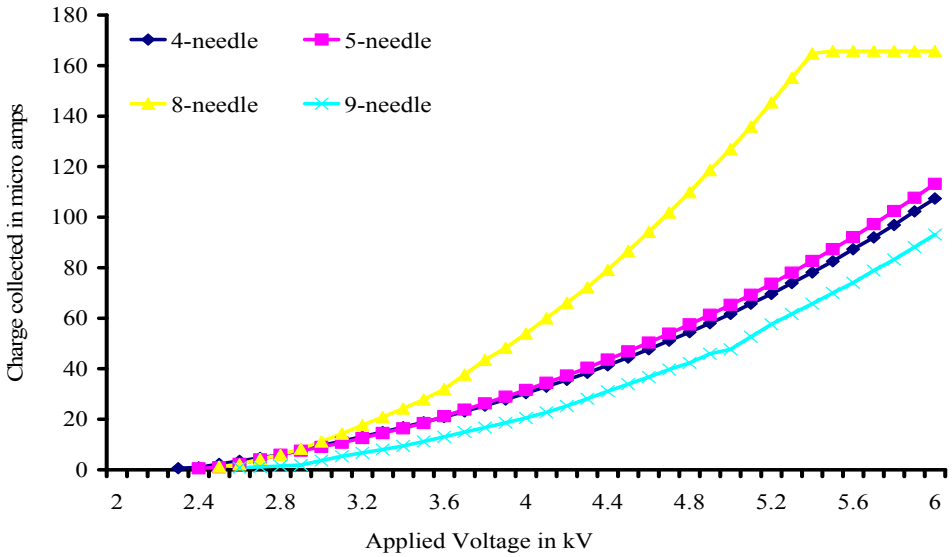

Figure 4.10: Corona charge collected (μA) versus applied voltage (kV) for a needle thickness of 0.7 mm and the applied polarity was negative.

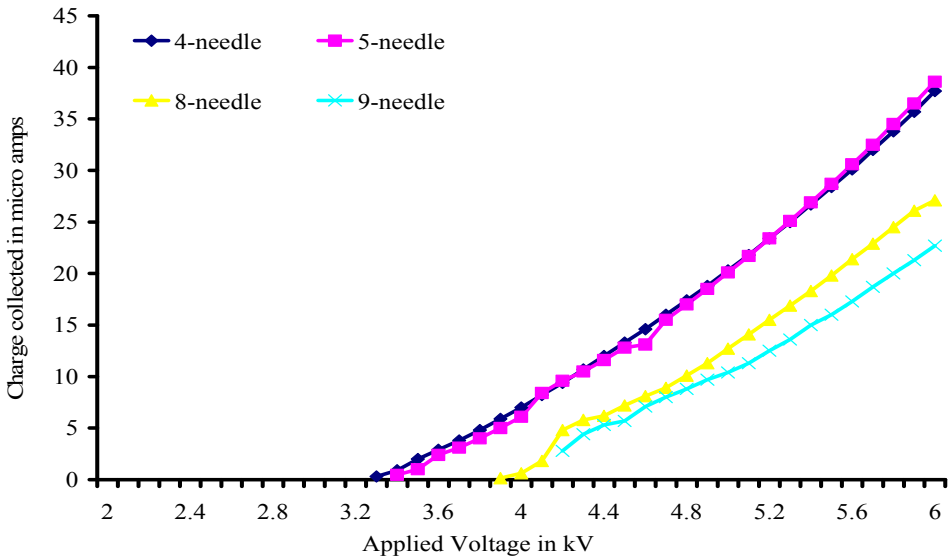

Figure 4.11: Corona charge collected (μA) versus applied voltage (kV) for a needle thickness of 0.8 mm and the applied polarity was positive.

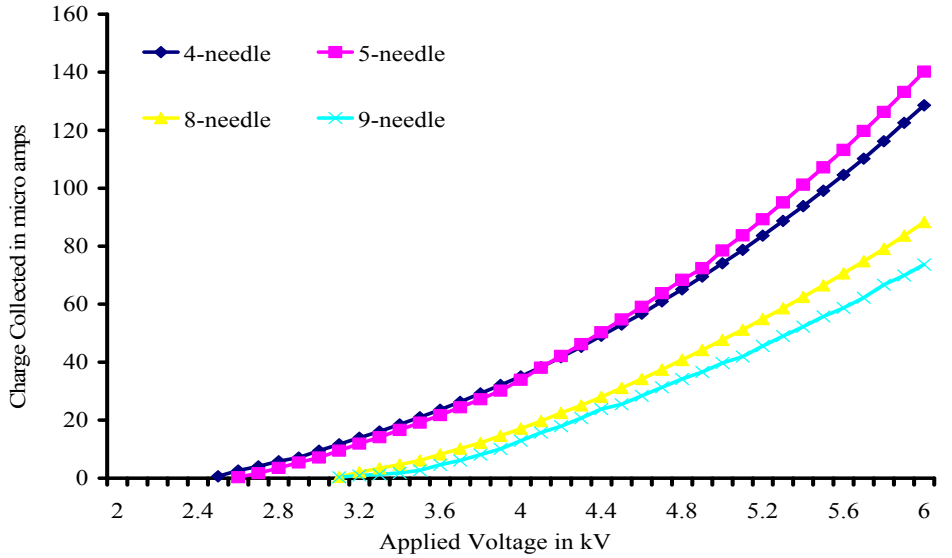

Figure 4.12: Corona charge collected (μA) versus applied voltage (kV) for a needle thickness of 0.8 mm and the applied polarity was negative.

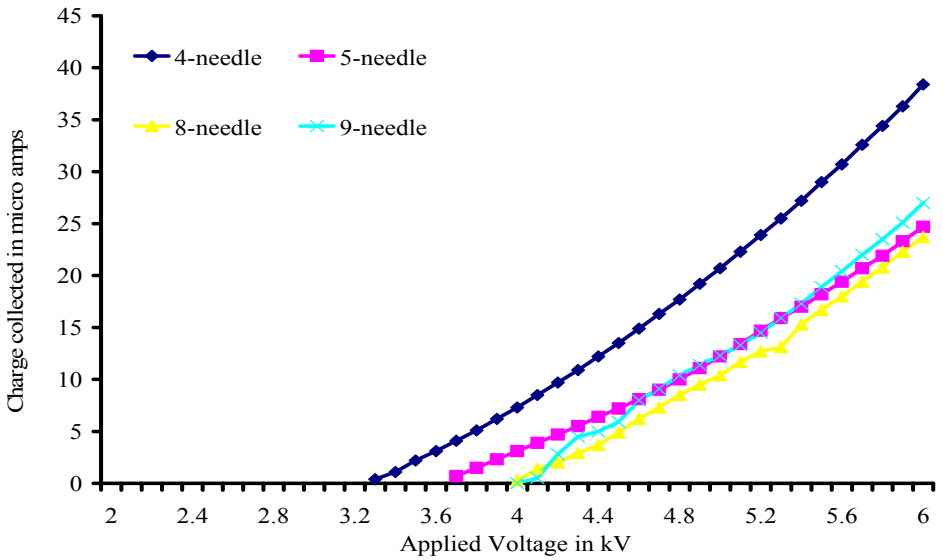

Figure 4.13: Corona charge collected (μA) versus applied voltage (kV) for a needle thickness of 0.9 mm and the applied polarity was positive.

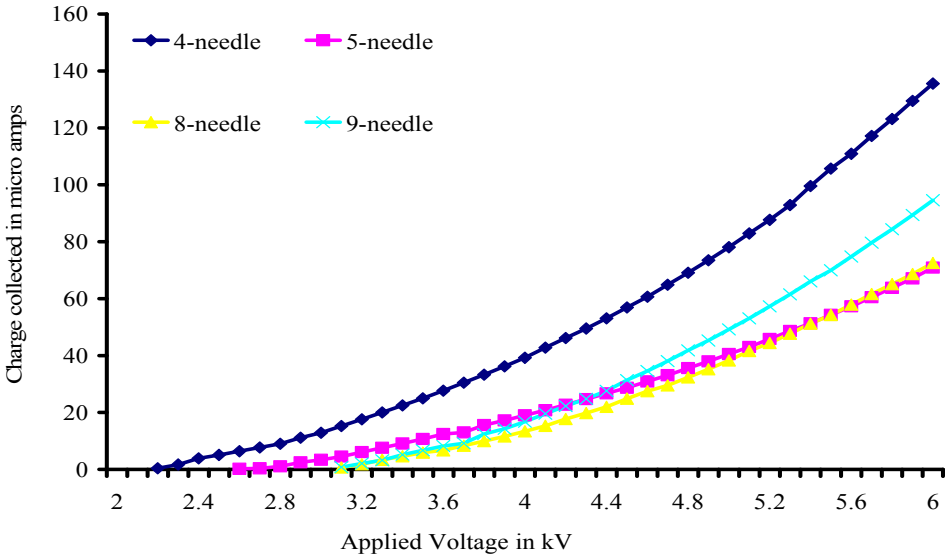

Figure 4.14: Corona charge collected (μA) versus applied voltage (kV) for a needle thickness of 0.9 mm and the applied polarity was negative.

Electric field intensities around one needle and around the complete array of nine needles were simulated using software packages Maxwell 2D [Ansoft Inc., PA] and COMSOL Multiphysics [COMSOL Inc., MA]. The electrostatic model in COMSOL Multiphysics and Ansoft Maxwell were used to estimate the electric field values produced by the corona ion generator. The value of the electric field is the negative gradient of the potential $E = -\nabla V$ and is estimated using the Laplace equation $\nabla^2 V = 0$. The Laplacian of the scalar field V is also the divergence of the gradient of V. Solving of the Laplace equation helped determine whether the electric field values were due to a source or a sink [85].

Since the needle size chosen from the experiments above was 0.35 mm the simulations used this needle size. Figure 4.15 shows the values of electric fields generated around one needle for positive applied voltage and Figure 4.16 simulates the complete *in vitro* situation. As shown in Figure 4.15 the highest value of electric field was close to the needle tip for an applied voltage of 7 kV and was above 9.0 MV/m. Section 1.3 showed that the breakdown field strength of air is around 3.25 MV/m; hence even though the highest value at the tip of the needle is much more than the breakdown value of air we still do not get a breakdown at this voltage. This is due to the needle electrode geometry which has a non-uniform electric field around the tip similar

to the one shown in Figure 1.4. The highest value of the electric field is only very close to the tip and not over an extended distance hence even if there is a breakdown due to voltage; it is likely confined and does not form arcs to surrounding grounded objects. Figure 4.16 depicts the *in vitro* situation with all the nine needles. For *in vitro* experiments the corona ion generator is lowered to the top of the culture dish and simulation in COMSOL estimated the values of the electric field that the cells would be exposed to.

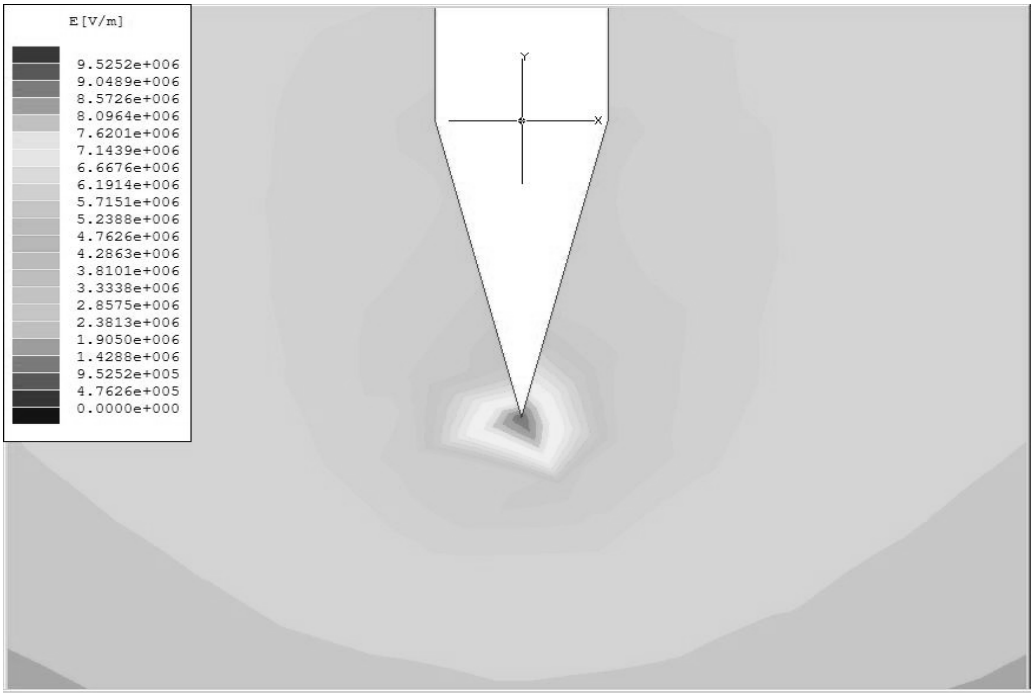

Figure 4.15: Simulation of electric field values around one needle for an applied voltage of 7 kV using Maxwell 2D.

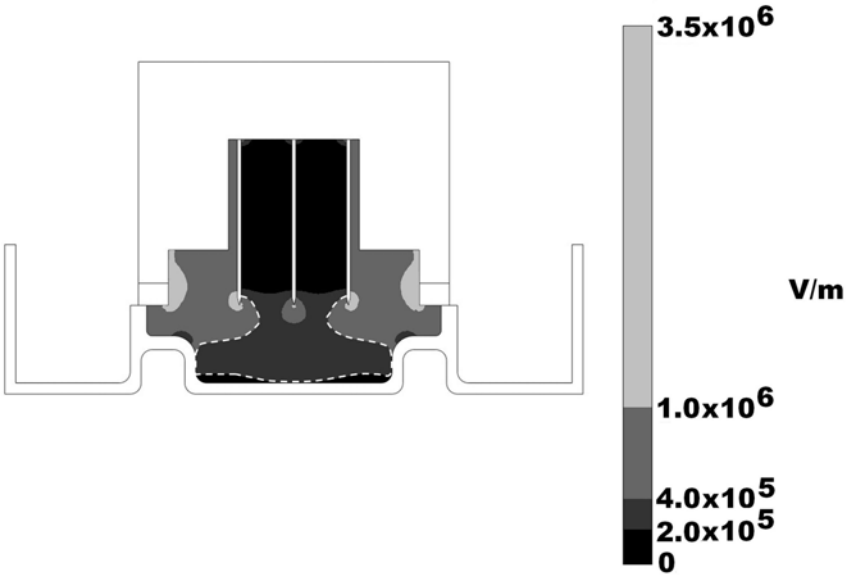

Figure 4.16: Simulation of electric field values with the nine needle corona generator using COMSOL.

4.1.2 Effect of Liquid Volume on Charge Collected

It was clear from the results obtained in Figure 4.2 above that the distance between the corona generator and the charge collecting plate had a very strong influence on the quantity of charge collected. Planned experiments for this study included depositing corona charge on the surface of media and measuring the charge collected with the stainless steel plate at the bottom of a culture dish covered in an isotonic solution such as PBS or growth media. In this situation, the effects of corona charge would need to traverse some air space and some liquid before reaching the charge collecting plate located at the

bottom of the dish. This is in contrast to all of the corona charge characterization experiments performed above where the only media between the charge collecting plate and the corona generator was air. It was envisioned that the presence of liquid media in the planned experiments involving cultured cells would influence the amount of current detected on the cell growth surface of the culture dishes. It was also envisioned that the height of liquid in the dishes would influence the quantity of corona charge collected. Therefore experiments were designed to determine the effect of liquid volume on the charge collected.

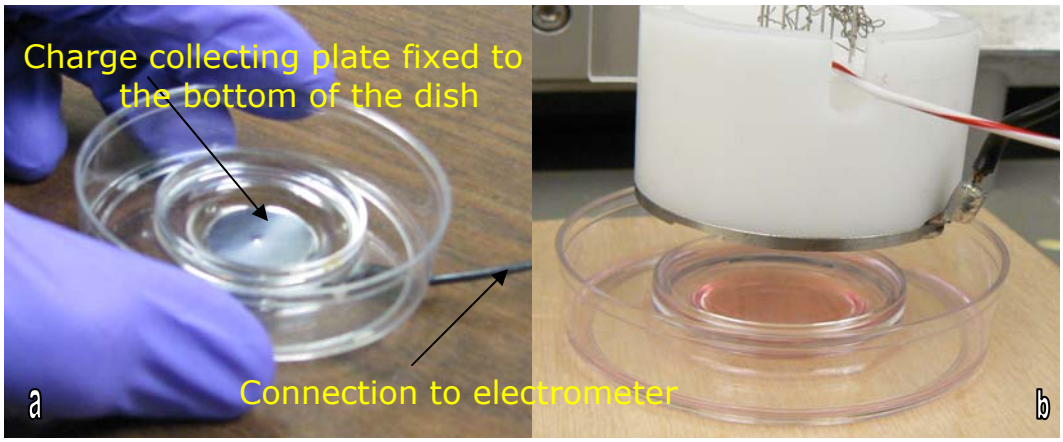

Figure 4.17: a) Stainless steel plate fixed at the bottom of the culture dish to measure the charge collected b) media was added on top of the charge collecting plate shown in a), the corona generator was lowered and charge collected measured.

A small stainless steel charge colleting plate fixed to the bottom of the central culture dish, shown in Figure 4.17, that the cells were

normally grown on for *in vitro* experiments. However, no cells were used in this experiment. Different volumes (250, 500, 750 and 1000 µl) of phosphate buffered saline were added to the central well of the dish. The corona generator was positioned on top of the dish and the charge generated was measured for these different volumes. A small hole was made in the bottom of the dish to facilitate connection to the stainless steel plate. A simple copper wire was used to make this connection and the other end of the wire was connected to the electrometer shown in Figure 4.8 to measure the charge collected. The results indicated that the charge collected increased linearly as the liquid volume was increased as shown in Figure 4.18. For example with a liquid volume of 250 µl the charge collected was 41 µA, while a liquid volume of 500 µl measured approximately 75 µA for negative polarity. These experiments were carried out at 4 kV.

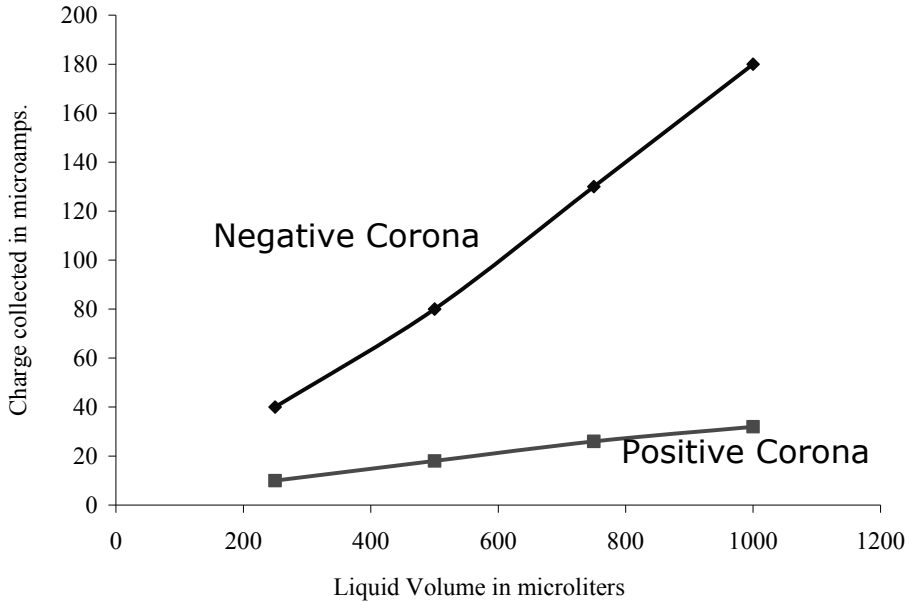

Figure 4.18: Charge collected (μA) as a function of liquid volume. A voltage of 4 kV was applied for both polarities.

Applying voltages above 5 kV and liquid volume above 750 μl resulted in a spark to the liquid. Since voltages higher than 6 kV would be used for experiments 750 μl was chosen as an upper limit. Volumes below 250 μl for any applied voltage and an exposure time of ten minutes resulted in a dry spot in the center of the dish. Hence, 250 μl was chosen as the lower limit. An experiment was also performed to check whether using different liquids had any effect on the charge collected. Cell growth media, phosphate buffered saline, saline and DI water were used to test the amount of charge collected. Data indicated that the type of liquid had no effect on the charge collected. Hence for 250 μl, of any kind of liquid used, the charge collecting plate

measured exactly the same amount of charge. For a liquid volume of 250 µl and positive applied polarity, the charge collected was 10 µA, for 500 µl it was 18 µA and so on.

4.2 Specific Aim 2: To Test the Capability of Corona Ions for Delivering Dyes and Tracer Molecules *In Vitro*

Molecular delivery experiments were carried out with tracer molecules in this specific aim to test if corona ions could indeed be used as a novel method to facilitate molecular delivery *in vitro*. Calcein was first used to test molecular delivery with the commercially available two wire corona generator. Characterization of the corona ion generators in the previous aim demonstrated the effect of liquid volume in the culture dishes on the charge collected by a metal plate fixed at the bottom of the dishes. A part of the experimental work in Specific Aim 2 was to determine if liquid volume had any effect on molecular delivery. After determining an appropriate liquid volume, the nucleic acid probe SYTOX-green was used as tracer molecules to examine the effects of corona ion deposition on molecular delivery. None of these tracer molecules transit the cell membrane and gain access to cytosol on their own. The materials and methods used to perform these experiments were described in Chapter 3.

Calcein delivery experiments were performed using the commercially available wire corona generator. This device generated 3 µA of

current that was deposited on the culture surface emitted in two lines of charge across the culture plates. This source was used to demonstrate delivery of calcein to B16F10 cells. Following the demonstrated success with the wire corona source, the nine needle corona generator, developed as mentioned above in Section 4.1, was implemented in experiments to study the delivery of SYTOX-green to cultured B16F10 cells. The custom made nine needle generator was better suited for the experiments because its circular geometry matched the shape of the culture dishes and it also provided two to three orders of magnitude higher ion density than the two wire source.

4.2.1 Delivery of Calcein

Figure 3.9 in Section 3.2.3 shows the experimental setup for treatment of cultured B16F10 cells with the commercially available corona generator. Positive corona ions were applied directly to the surface of the PBS-calcein mixture that surrounded the adherent cells. Corona ions were deposited on the culture media for either six or ten minutes. The resulting fluorometric data, shown in Figure 4.19, from samples that were washed and then lysed clearly indicate that the B16F10 cells exposed to calcein and corona charge had increased fluorescence relative to cells that were exposed to calcein alone. The six minute exposure time samples exhibited a three fold higher fluores-

cence than control samples that were exposed to calcein alone. This increase was statistically significant ($p \leq 0.05$, $p = 0.007$). Ten minutes of corona exposure produced a response five fold higher than control samples. These samples exhibited a mean increase that was also significant ($p \leq 0.05$, $p = 0.001$) relative to control.

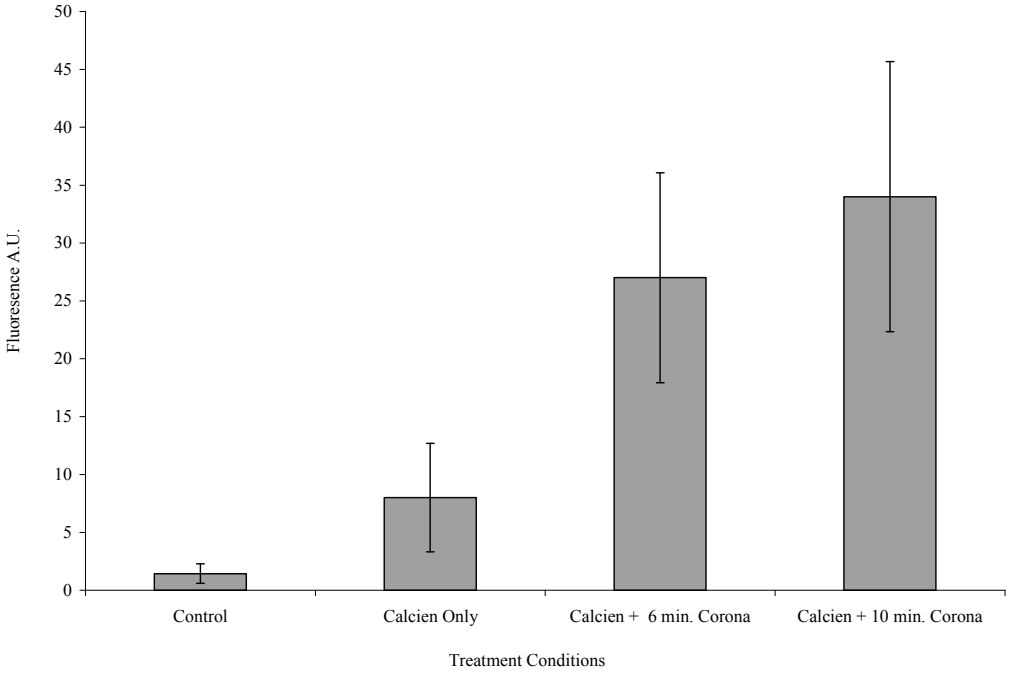

Figure 4.19: Fluorometric data for positive corona ion mediated delivery of calcein to B16F10 cells *in vitro,* expressed in arbitrary units (A.U.). Each bar represents the mean fluorescence ± s.e.m. Each bar also represents data from triplicate experiments with three identically treated samples per treatment condition for each experiment.

4.2.2 Effect of Liquid Volume on Molecular Delivery

Delivery experiments performed previously with calcein in section 4.2.1 used a liquid volume of 250 µl. Since the end goal of these experiments was molecular delivery, an experiment was designed to determine the effect that the liquid volume on molecular delivery. The liquid volume was varied from 250 µl to 1000 µl. The nucleic acid probe SYTOX-green was used as a tracer molecule. The protocol followed was the same as described in section 3.2.3. Analysis consisted of measuring the fluorescence, in A.U., for the different treatment groups.

Each treatment group for a particular liquid volume was compared to its control and the difference in fluorescence intensity was noted. For example the corona treated group with 250 µl of liquid volume during treatment was compared with 250 µl control and the difference in fluorescence between the two noted. Three such experiments were performed with triplicate samples in each treatment condition. The difference between the controls and their respective treatment groups for a particular liquid volume is plotted in Figure 4.20. An expected curve is also shown along with the actual experimental curve. Previous results had indicated that the charge collected increased as the liquid volume in the dish was increased, hence this expected curve represented fluorescence increase if molecular delivery

were directly proportional to the charge generated. Results from Figure 4.20 clearly indicate that delivery is independent of the liquid volume. A liquid volume of 250 µl covering the cells while being exposed to corona ions was chosen for further *in vitro* experiments. A liquid volume of 250 µl would also maximize the distance of the cells from the ion generating electrode without compromising on molecular delivery.

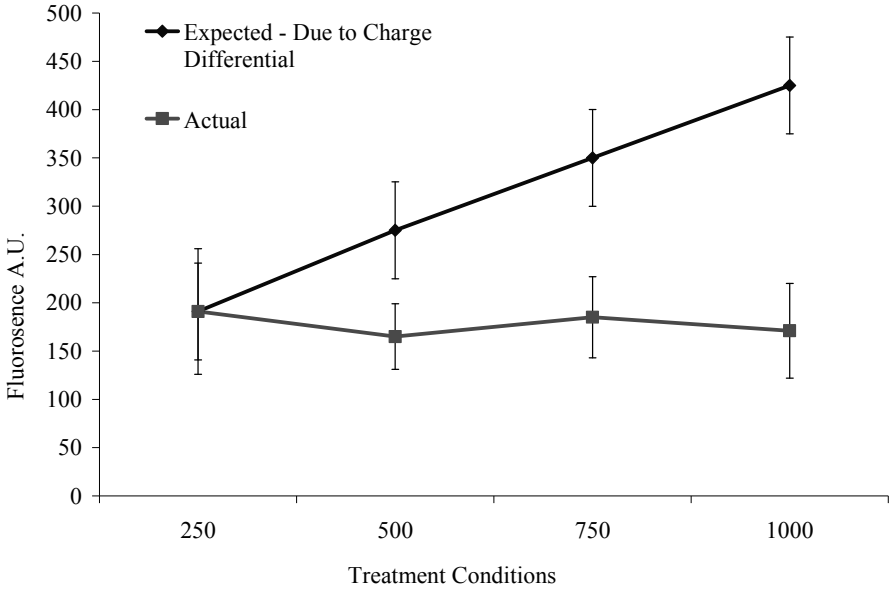

Figure 4.20: Fluorescence (A.U.) of B16F10 cells treated with corona charge to deliver SYTOX-green using different liquid volumes.

4.2.3 Delivery of SYTOX-Green

Following results from the delivery of calcein (Figure 4.19) which clearly indicated fluorescence increase after corona ion exposure, an exposure time of ten minutes was chosen. Negative corona ion exposure was also included in this treatment protocol to see if it could also affect molecular delivery. To better match the geometry of circular dishes the new nine needle corona generator was used which generated more charge. The characterized nine needle corona generator was used to deliver SYTOX-green to cultured B16F10 cells.

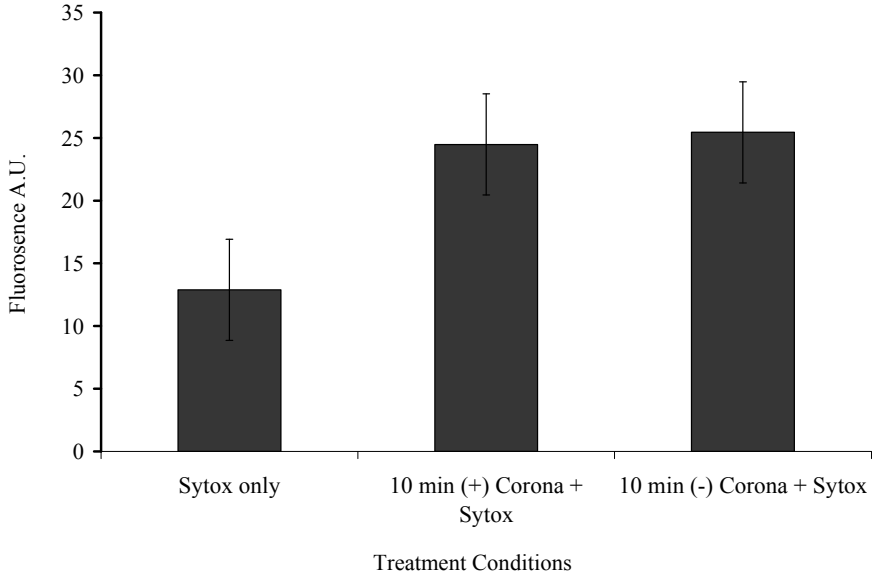

Figure 4.21: Positive and negative corona ion mediated delivery of SYTOX-green to B16F10 cells *in vitro*. Mean data ± the s.e.m. for each treatment condition is expressed in arbitrary units (A.U.). Each mean is the combined data from six identical experiments. Three samples were treated for each set of conditions in each of the six experiments.

Fluorometric data for the molecular delivery of SYTOX-green is shown in Figure 4.21. Samples that received exposure to both corona ions and SYTOX-green were about two fold higher than the control samples that were exposed only to SYTOX-green. This data indicated that treatment with either positive or negative corona ions resulted in about the same increase in delivered SYTOX-green. The difference in means between the control and the positive and negative treatment groups were both significant ($p= 0.003$ and 0.00001, respectively).

Microscopic observations were made on all samples prior to performing the fluorometric assays. An interesting and important observation was that dye uptake occurred only in the central area of the dishes. The total area available for cell growth was 225 mm^2, while the treatment was effective only in an area of approximately 95 mm^2 in the center. This central region was equivalent to 40% of the total growth area and corresponded to the circular arrangement of needles in the corona generator. This observation could also be due the fact that the intensity of the ions was highest over the center of the dish as is typically observed with ions emanating from this kind of a needle source [59].

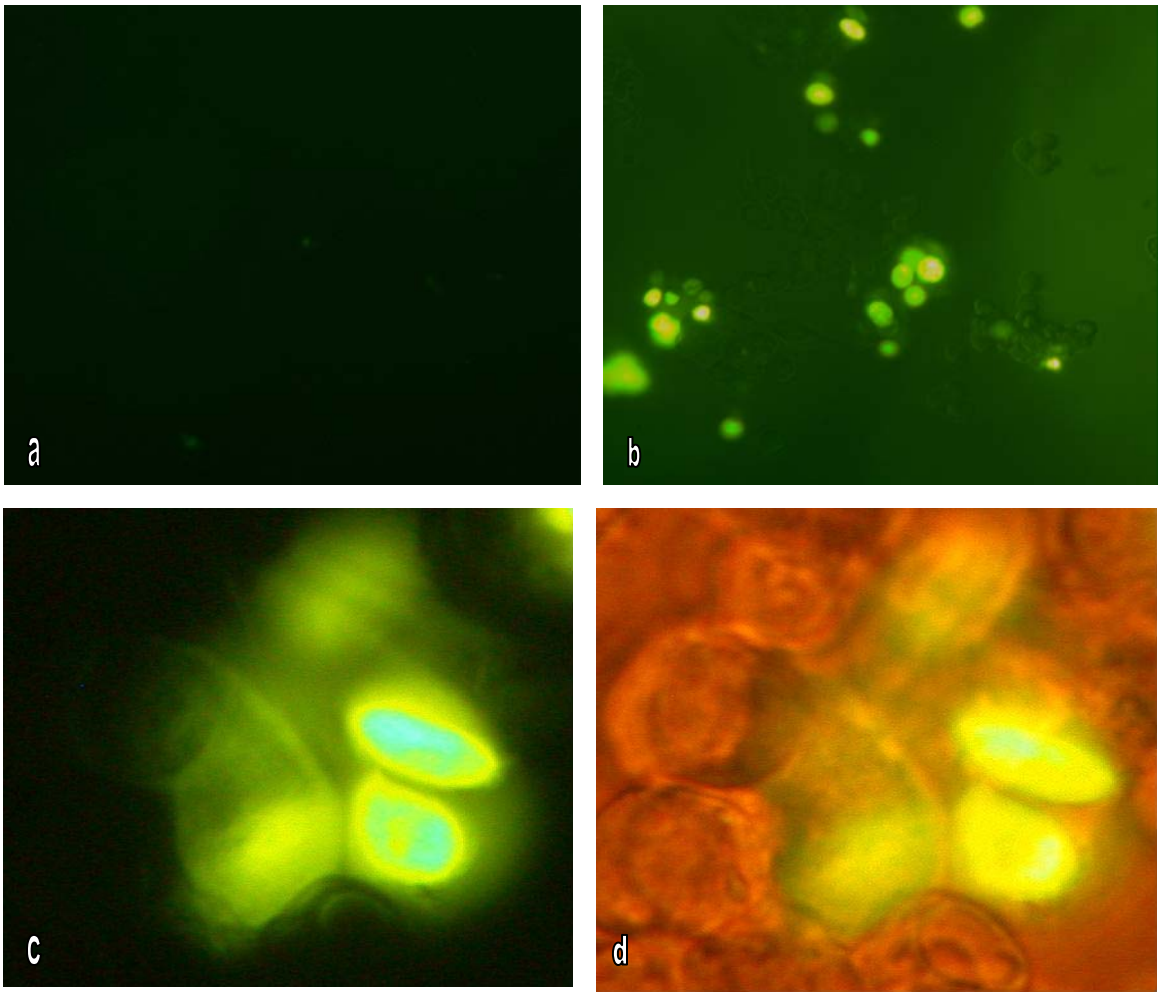

Figure 4.22: SYTOX-green delivered to cultured B16F10 cells 15 minutes after treatment with positive corona charge. a) Control cells treated with SYTOX-green (250X) alone b) cells treated with positive corona ions for 10 minutes followed by exposure to 1 μM SYTOX-green (250X) c) fluorescent and d) white light views of b) at higher magnification (400X). Images b) – d) were taken from the central region of the culture dishes where delivery occurred. Similar observations were made for samples treated with negative corona charge (not shown).

Dye uptake was typically observed in 40-50% of the cells in the central area of the corresponding to 95 mm^2. Delivery was also inho-

mogeneous when either positive or negative corona charge was used for delivery based upon the observed weak fluorescence of some cells and the very bright fluorescence of other cells. Another observation was that partial detachment of a fraction of the cells occurred within the treated 95 mm^2 area. These cells reattached back to the culture dish in about thirty minutes and continued to grow normally in supplemented growth media.

Fluorescent cells were rare in samples that were exposed only to SYTOX-green, as seen in Figure 4.22 a) and likely correspond to the small fraction of cells with compromised membranes. However, cells exhibiting high levels of green fluorescence were quite common in cultures that were exposed to corona ions and then to SYTOX-green as seen in Figures 4.22 b), c) & d). These qualitative observations support the fluorometric data shown in Figure 4.21 and suggest that corona ions of both polarities may be used to facilitate the introduction of non-permeant molecules to the cytosol of living cells.

4.2.4 Viability After Corona Charge Treatment

Cell viability was assessed by the trypan blue test following either positive or negative corona ion treatment for ten minutes. Cells with compromised or damaged membranes appear blue as a result of this test and healthy cells absorb no color. Cells were assessed at three time intervals (30 minutes, 6 and 12 hours) following corona ion exposure to determine if there were any immediate adverse effects. Control samples that were not exposed to corona charge were assessed at the same times. Viability was determined by this test to range from 96-99% in the control samples and 96-99% for positive corona treatment at the same three times. Negative corona treatment resulted in viabilities that ranged from 96-98%. There did not appear to be a pattern with respect to time for positive corona, negative corona, or no treatment. This indicated that corona charge exposure for ten minutes did not affect the short term viability of cells. In addition, cultures treated with either positive or negative corona charge were visually indistinguishable, as demonstrated in Figure 4.23, from the no treatment samples at any time point with respect to confluence, or cell growth.

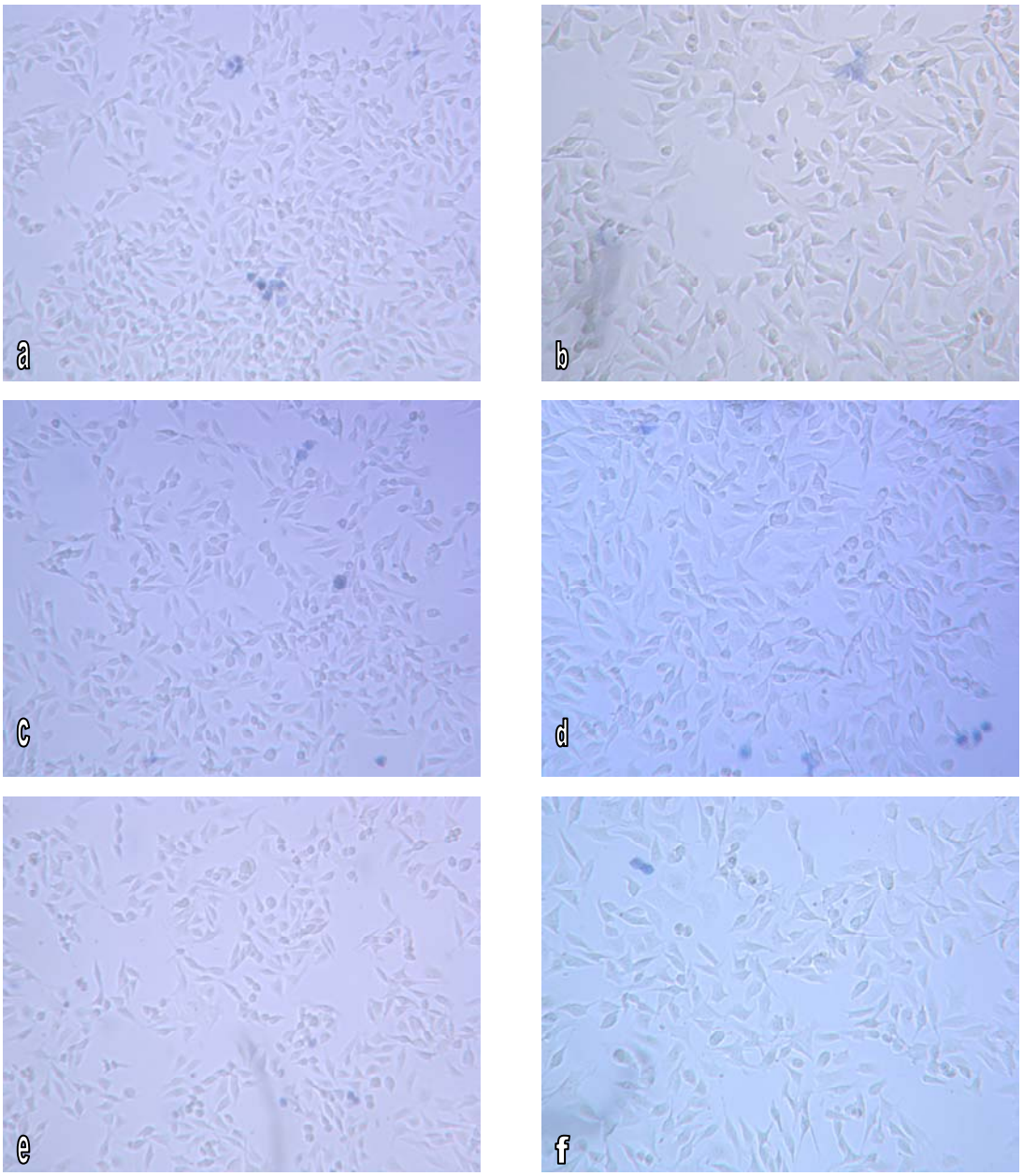

Figure 4.23: Viability of B16 cells treated with 10 minutes positive corona charge and untreated control samples. All cultures contained trypan blue. Panels a), c) and e) show representative fields of view for positive corona treated cells at 30 minutes, 6 and 12 hours after treatment, respectively. Panels b), d) and f) show untreated control B16F10 cultures analyzed at the same time points.

These studies demonstrated that corona ions deposited on the surface of media containing cultured cells facilitate the transport of non-permeant molecules to the interior of the cells. Calcein delivery using positive ions to drive the process resulted in statistically significant increases in florescence relative to controls. However, there was still a possibility that some of the tracer molecules were nonspecifically bound to the membrane and not in the cytoplasm even after washing. To address this uncertainty, work was performed with SYTOX-green as a tracer molecule. As mentioned earlier, this molecule exhibits fluorescence only after it has bound to nucleic acids which are located inside the cells. The statistically significant results obtained in these experiments are offered as conclusive evidence that the SYTOX-green molecules were delivered to the cell interiors using the application of either positive or negative ions to the culture media.

4.3 Specific Aim 3: To Investigate the Use of Corona Ions for Delivering Bleomycin *In Vitro* and to Established Tumors in an Animal Model

After successfully delivering dyes and tracer molecules *in vitro*, the experimental focus was shifted to the delivery of the drug bleomycin. The drug was delivered to cultured B16F10 cells *in vitro* and to solid tumors induced in the left flanks of female C57Bl/6 mice. Both types of experiments utilized the nine needle corona generator with 0.35 mm diameter needles.

4.3.1 Delivery of Bleomycin *In Vitro*

Bleomycin causes double and single stranded DNA nicks which ultimately results in cell death. Therefore, access to the cell interior is necessary for the drug to be cytotoxic. The drug bleomycin also does not penetrate cells with intact membranes [80] and this characteristic makes it an excellent drug for developing delivery methods because cell death is an indicator of delivery to the cell interior. Corona ions were deposited onto the surface of liquid in a culture dish that contained B16F10 cells in 250 µl of 1 x 10^{-5} M bleomycin in phosphate buffered saline solution. Deposition of corona ions on the medium was carried out for two, five or ten minutes. The results from MTT assays for either positive or negative corona exposure are shown in Figure 4.24 as percent survival forty eight hours after delivery. The no treatment group that had cells only was used forced to 100% survival. Results from test samples were normalized to this reference value.

The data indicate that positive corona ion exposure alone resulted in a modest decrease in survival; approximately 92% of the cells survived. Optimized electroporation protocols typically use electrical conditions that result in 90% survival; therefore, survival from corona exposure alone was very similar. Survival from bleomycin exposure alone did not differ significantly from the corona exposure only or no treatment.

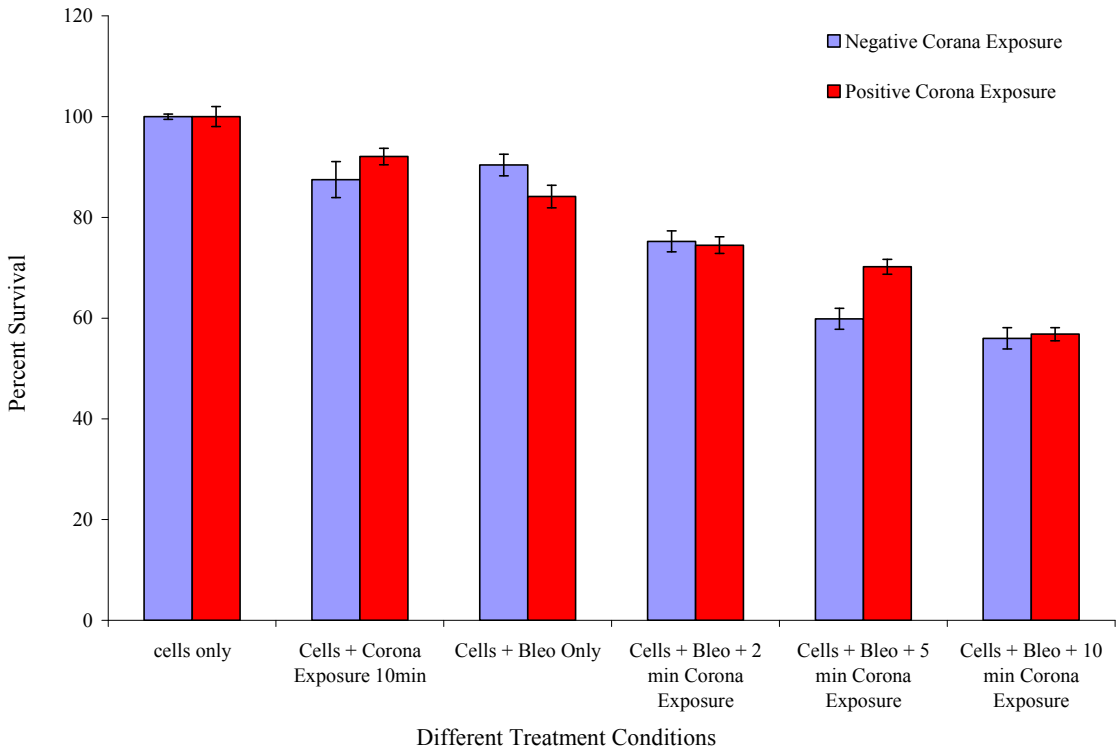

Figure 4.24: MTT survival data for the *in vitro* delivery investigation including either positive or negative corona ion mediated delivery of bleomycin to B16F10 cells. Each solid bar represents the mean survival percentage ± s.e.m (n = 9 samples per bar).

However samples that were exposed to bleomycin and then exposed to positive corona charge for ten minutes had about 60% survival. These differences were significant ($p \leq 0.05$) with the samples that received corona exposure alone, bleomycin alone, or no treatment. The two minute and five minute positive corona exposure groups were not significantly different from any of the treatment conditions used as controls.

The results of the negative corona exposure were similar to that of the positive corona. The negative corona exposure alone resulted in a decrease of 13% while the bleomycin treatment alone led to a decrease of 10%; both were not significantly different from the no treatment control. In samples exposed to bleomycin and five minutes of negative corona, 60% of the cells survived. Similarly, 55% survival resulted from exposure to ten minutes of negative corona and bleomycin. Both these cases were significantly different ($p \leq 0.05$) from the corona exposure only, bleomycin only and no treatment. The two minute corona exposure samples were not significantly different from the controls.

Microscopic observation made for both the positive and negative corona charge treated cells 48 hours after bleomycin delivery revealed that most of the cell death (or absence of growth) was in the center of the dish. In fact, the area of effected cells was a circle approximately 95 mm^2 area in the center of the dish. For the samples treated with bleomycin followed by ten minutes of corona charge (positive and negative) this region was largely void of cells. A similar area was observed above, resulting from *in vitro* SYTOX-green delivery experiments. Each culture dish had a total area of 225 mm^2 available for cell growth and failure to achieve molecular delivery throughout the entire growth surface could be due to the inverted cone shape [59] of the co-

rona fields that are emitted from point sources such as the needles of the generator. Analysis of the treated area showed that the net result of this survival data in Figure 4.24 was obtained while treating only about 37% of the growth area that was seeded with cells. Survival rates resulting from delivered bleomycin would have undoubtedly been much lower if the entire cell growth surface was treated. This survival data strongly suggests that the chemotherapeutic drug bleomycin can be delivered to cells *in vitro* using corona ions as a driving force.

4.3.2 Delivery of Bleomycin *In Vivo*

No treatment protocols existed for treatment of cancerous tissue *in vivo* using corona ions. Hence either an intelligent guess or *in vitro* results had to be used as basis for choosing a treatment protocol. During *in vitro* treatment, the cells were grown on the surface of insulating culture dishes and the ions were deposited on the surface of the media surrounding them. In that particular instance charge would be contained by the walls of the dish, however charge would probably distribute over a much larger area when treating mice as there was no insulating material around the tumors. Based upon this difference the ten minute corona charge exposure time used for the *in vitro* experiments was increased to 20 minutes for *in vivo* experiments. Figures 4.25 and 4.26 show the anti-tumor effect resulting from delivering

bleomycin to established B16F10 tumors for a single treatment and treatment on the three successive days at the beginning of the experiment.

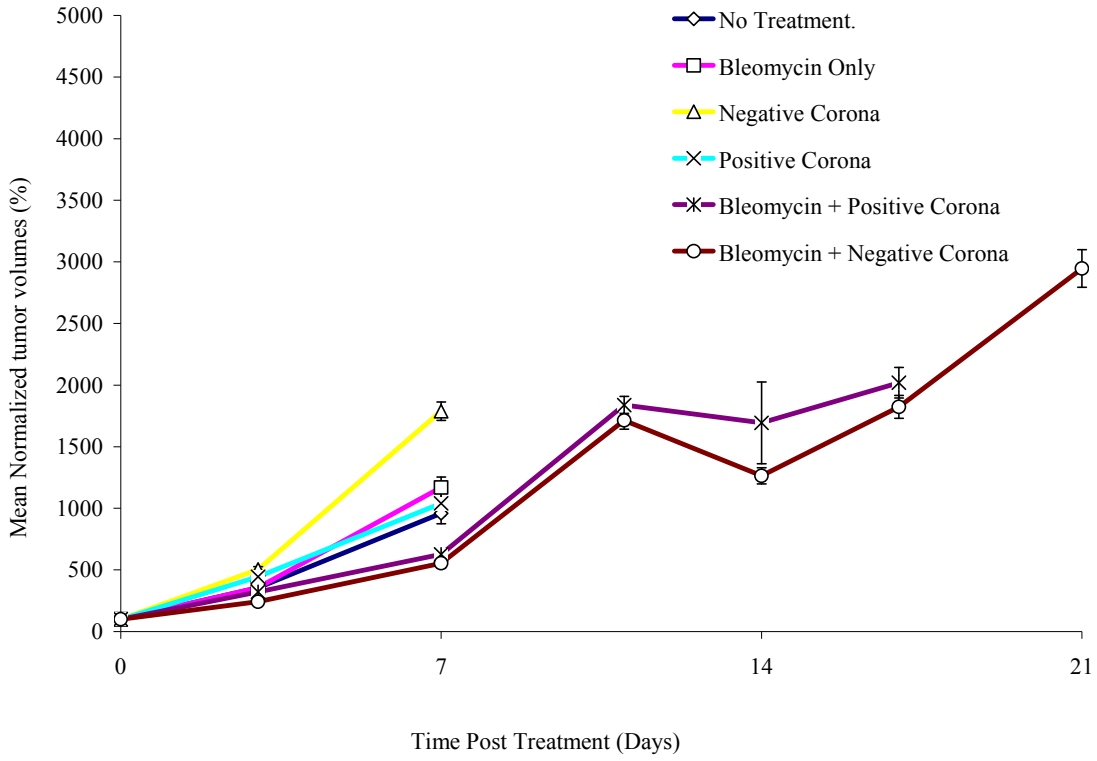

Figure 4.25: Mean normalized tumor volumes post treatment as specified in Table 3.1 for a single treatment with bleomycin and either positive or negative corona ions for 20 minutes. Each data point represents a mean normalized tumor volume ± s.e.m. (n = 7 animals per group).

The single treatment data in Figure 4.25 clearly shows that the treatment groups that received both bleomycin and corona treatment had the lowest mean tumor volumes over time. The results for delivery with negative corona ions were very similar to the results obtained

with positive corona ion exposure. Thus, delivery with corona ions of both polarities was successful in slowing down the rate of tumor growth, compared to the no treatment group and the group that received drug alone. However, none of the animals in the two groups that had bleomycin delivered achieved complete responses (complete destruction or regression of the tumor). It was hypothesized that multiple treatments might improve upon this response.

The anti-tumor effects resulting from a series of three treatments on days 0, 1 and 2 are shown in Figure 4.26. The mean tumor volume profiles indicated that there was a significant difference ($p < 0.05$) between the group that received exposure to both bleomycin and positive corona for three successive days and the no treatment (control) group on all days post treatment. Also there were significant differences between the group exposed to the drug alone and that exposed to both drug and positive corona on all days post treatment. Results for negative corona exposure were similar to that of positive corona, with significant differences between no treatment control and the group that received exposure to both the drug and negative corona ions on three successive days. The treatment groups that were exposed to the drug alone and those that were exposed to both the drug and negative ions were also significantly different on all days post treatment.

An important observation was that by day 11 all animals in the groups that received no treatment, positive corona treatment only and negative corona treatment only had to be euthanized as their tumor volumes had reached the 1000 mm^3 threshold. None of the animals in the treatment groups that received ion exposures of either kind and bleomycin and the group that received the drug alone had to be euthanatized by day 11. However, by day 14, 60% of the animals in the bleomycin only group had to be excluded from the study as their tumors were greater than 1000 mm^3. No animals were excluded from the groups that received exposure to either kind of ions and drug until day 24 (complete data not shown). Comparison of results from both Figures 4.25 and 4.26 show that by day ten the groups that received exposure to both bleomycin and one time 20 minute of corona exposure had an increase of about 1700% over their day zero tumor volume, whereas the treatment with drug and corona ions on three successive days the increase in tumor volume was only around 1200% by day 14. Even though the three successive day treatment was better in terms of slowing down the growth rate of the tumors as compared to the one time treatment, complete responses (complete tumor destruction) were not achieved.

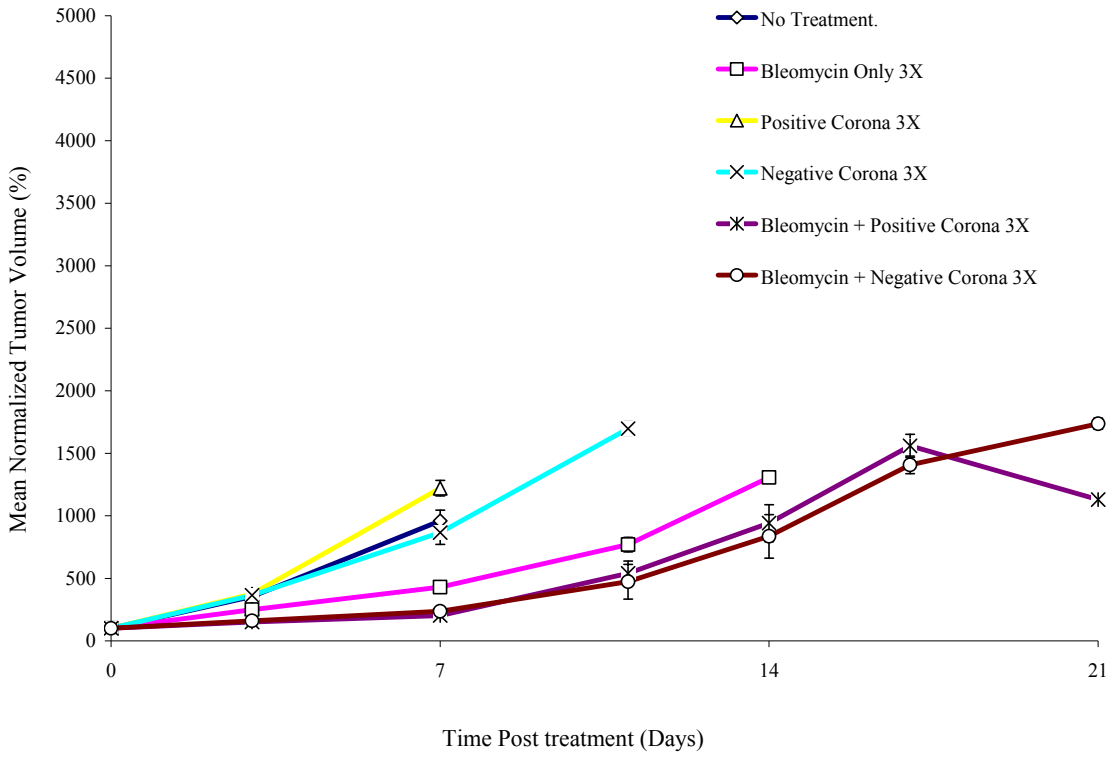

Figure 4.26: Mean normalized tumor volumes post treatment as described in Table 3.1 for three day treatments with bleomycin and either positive or negative corona ions for 20 minutes. Treatments were administered on three successive days (0, 1 and 2). Each data point represents a mean normalized tumor volume ± s.e.m. (n = 7 animals per group).

One conclusion could be that a 20 minute delivery procedure on three successive days affected only the topmost layer of the tumor closest to the corona ion source. Viable tumor cells at the base of the tumors might continue to grow in this circumstance. Nevertheless, slowing down the growth rate of this very aggressive skin tumor with the combined use of a drug and corona charge can be considered very significant. B16F10 tumors are considered to be poorly immunogenic

and mice that develop them find it difficult to trigger an adequate immune response to destroy them [86]. This is attributed to the lack of expression of MHC class I and II molecules and its tumor associated antigens [87, 88]. B16F10 tumors once developed are very difficult to treat and any kind of therapeutic effect that results in slowing down the growth rate of this kind of tumor can be considered highly positive. Another unique feature of this treatment method was that tumor growth rates were slowed without contact with the animal model. Visual observations made on animals in the corona ion treated groups did not reveal any tissue damage or burn or involuntary muscle stimulation.

4.4 Specific Aim 4: To Evaluate the Use of Corona Ions for Delivering Plasmid DNA to Cells in the Skin of a Murine Model

In this study, corona ions had been investigated as a novel forcing function for molecular delivery to cells in culture using dyes/tracers and bleomycin. In addition, they were used to deliver bleomycin to solid tumors in C57Bl/6 mice. To complete the investigation of the utility of corona ions, delivery of plasmid DNA to cells in the skin was investigated. Skin was used as a normal tissue model because it is easily accessible. 100 µg (50 µl at a concentration of 2 mg/ml) of reporter plasmid coding for the enzyme luciferase was injected intradermally into the shaved left flanks of the mice and corona charge was

applied with the nine needle generator. Details of the treatment were shown in Table 3.2. The procedure for post-treatment analysis included injecting all the mice intraperitonealy with luciferin and then imaging the resulting bioluminescence using an IVIS 200 imaging system (Xenogen, Hopkinton, MA).

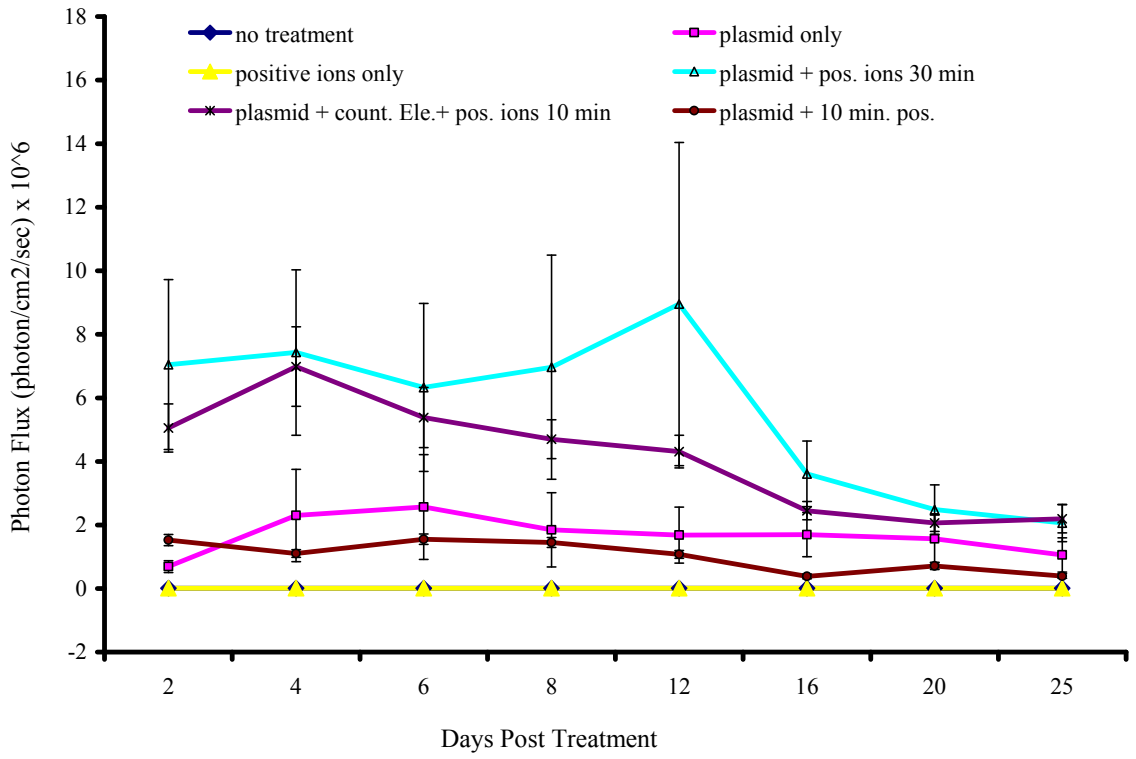

Figure 4.27: Results of *in vivo* data analysis for positive corona ion exposure. The mean photon fluxes in photons/sec/cm^2 for each group on a particular day post treatment were compared to check for differences at 95% significance level. Results indicate that the group that received treatment with both plasmid and positive corona ions for 30 minutes had an average of 5-fold increase in the 10 day period that it was it was significantly higher than the plasmid only group. The group with a counter electrode had a 7-fold increase only on day 2. Each data point represents a mean photon flux in photons/sec/cm^2 ± s.e.m. (n = 12).

The images were then analyzed to determine an average photon flux (photons/sec./cm^2) in a region of interest (entire treated area). Figures 4.27 and 4.28 show the mean photon flux measured periodically over the 25 day follow up period for positive and negative corona

ion exposure, respectively. A total of 12 animals were treated in each group.

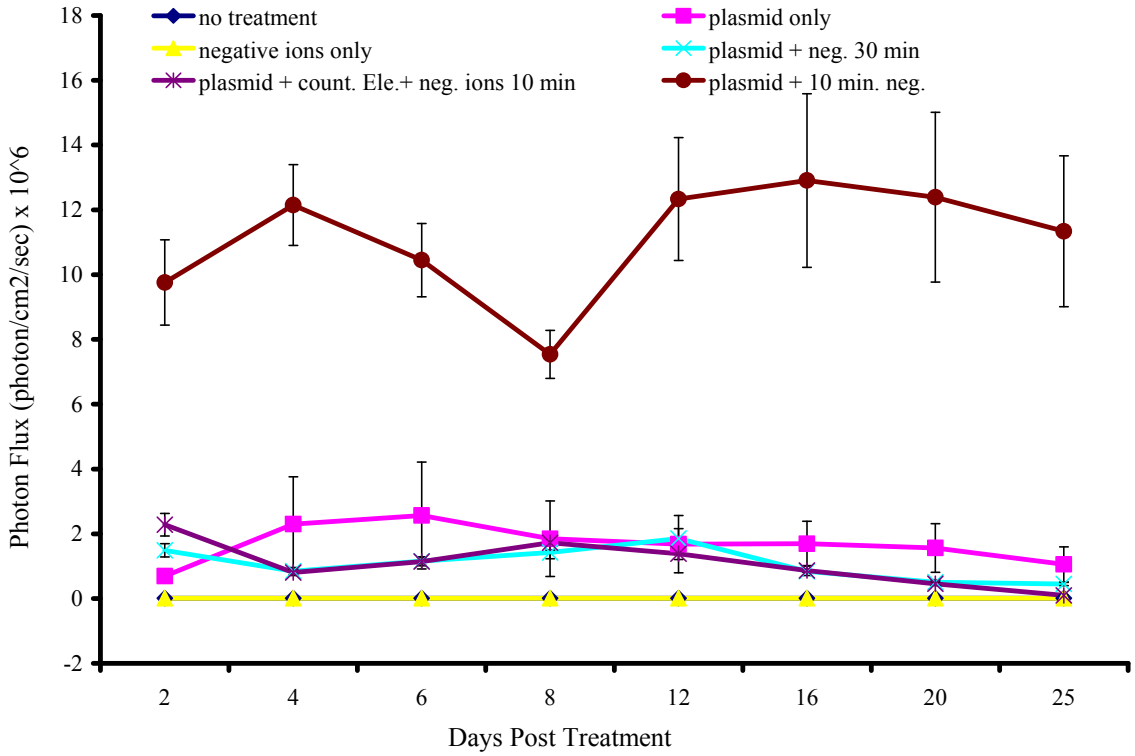

Figure 4.28: Results of *in vivo* data analysis for negative corona ion exposure. The mean photon fluxes in photons/sec/cm^2 for each group on a particular day post treatment were compared to check for differences at 95% significance level. Results indicate that the group that received plasmid injection followed by 10 minutes of negative corona was significantly higher than the group that received the plasmid only with an average of 6-8 fold increase during the time period it was significantly higher. None of the other treatment groups were significantly different with the plasmid only group. Each data point represents a mean photon flux in photons/sec/cm^2 ± s.e.m. (n = 12).

Results of positive corona ion exposure, Figure 4.27, show that the group that received plasmid and 30 minutes of positive corona ion exposure was significantly higher than the group the received plasmid only until the 16^{th} day at a 95% level of significance (for $p \leq 0.05$). The level of expression in this group corresponded to about ten fold higher expression on day two relative to the group that received a plasmid injection only. The expression reached a minimum of two fold on day six after which it peaked again to about five fold on day 12. The expression fell to about two fold again on day 16 after which it was not significantly different from the other groups. The other group that had expression levels that were significantly higher than the plasmid only group was the group that had a counter electrode inserted subcutaneously below the spot of plasmid injection. This group had a grounded electrode inserted subcutaneously below the site of plasmid injection and then received exposure with positive corona ions for ten minutes after plasmid injection. The increase over the controls was about seven fold on day two the only day that it was significantly higher than the controls.

Expression results for negative corona ion exposure, Figure 4.28, indicated that only the group that had plasmid followed with ten minutes of negative ion exposure had luciferase levels that were significantly higher (for $p \leq 0.05$) than the plasmid only group. The in-

tradermal injection of plasmid followed by ten minute exposure to negative corona ions resulted in a 14-fold increase on day two over the plasmid only group which was the peak. These two groups were significantly different until the 16^{th} day with the values peaking at day two, falling to a minimum of about four fold on day eight and again rising to about seven fold until day 16. All these differences were significant at a 95% level of significance. Figure 4.29 shows representative images of the plasmid only group and groups with plasmid injection followed by 30 minutes of positive corona and the plasmid injection followed by ten minutes of negative corona ions on days 0, 2, 4, 8, 16 and 25 post-treatment.

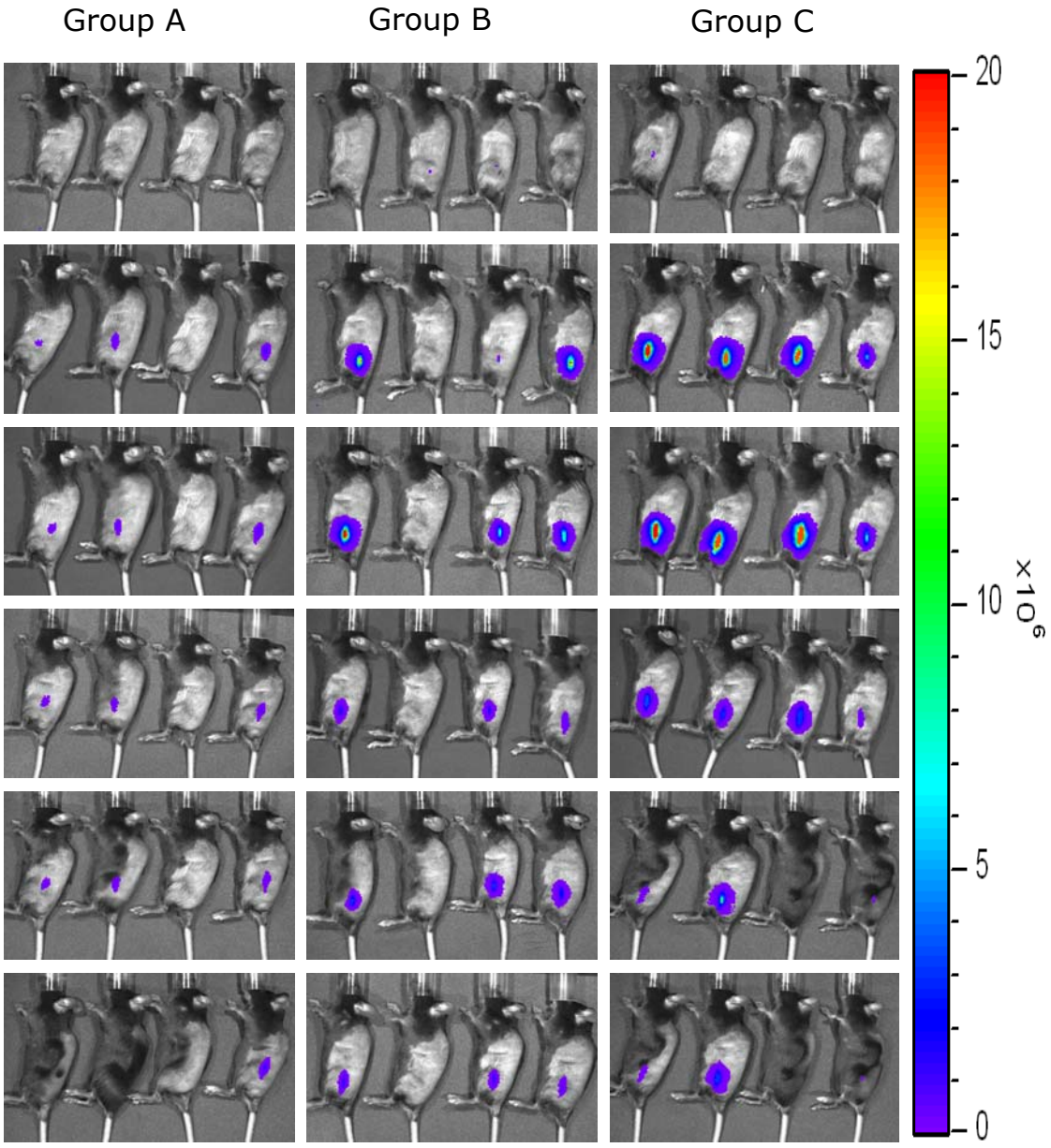

Figure 4.29: Images of mice from the three different groups that were statistically different in the amount of luciferase expressed. The luciferase expressed is measured in terms of a photon flux in photons/sec/cm^2. The figure shows pictures of three Groups A) plasmid injection only B) plasmid injection followed by 30 minutes of positive corona and C) plasmid injection followed by 10 minutes of negative corona on days post treatment. Images taken on days 0, 2, 4,8,16 and 25 are shown.

4.5 Specific Aim 5: To Investigate the Mechanism of Interaction of Corona Ions with Biological Cells

Experimental results from Specific Aims 2, 3 and 4 demonstrated that corona ions could be used to deliver tracer molecules, drugs and genes to biological cells and that these cells close and remain viable following treatment. Therefore, it may be stated that the exposure to corona ions, of both polarities, somehow renders the cell membrane temporarily permeant to extracellular molecules. The main goal of this specific aim was to try to understand the mechanism involved in the permeabilization process induced by corona charge. B16F10 and fibroblast cells were used for these *in vitro* studies. The study was partitioned into three sections. The first section addressed the interaction of these deposited corona ions with the media. The next section addressed how this interaction with the media affected the cells to allow the passage of impermeable molecules to the cytosol. Finally rate of uptake of the dye SYTOX-green was monitored for 35 minutes and a preliminary model for the resealing time constant of B16F10 cells exposed to corona ions was developed.

4.5.1 Interaction of Deposited Corona Ions with the Media *In Vitro*

An attempt was made to shed some light on the interaction of positive and negative corona ions with media surrounding the cells. Fluorescence from SYTOX-green binding was used as an indicator for

molecular delivery and microscopic observations were performed on corona treated samples. Experimental observations made on samples treated with corona ions showed delivery of SYTOX-green in the central area of the culture dish. The growth area of the central culture dish shown in Figure 4.30 where cells were grown was about 225 mm^2 whereas molecular delivery was observed only in the center of this growth area corresponding to 95 mm^2. Based upon experimental observations *in vitro*, uptake of SYTOX-green (Section 3.2.3) was inhomogeneous in the central area of the culture well corresponding to 95 mm^2 and delivery was observed in 40-50% of the cells in this area.

Another important observation was that delivery of SYTOX-green was observed about five to seven minutes after corona ion deposition of either kind started. Two possible alternatives of interaction of corona ions with the media are suggested here. The high conductivity of the phosphate buffered saline covering the cells during treatment could allow the deposited corona ions to spread on the surface of the media and set up a polarization of the fluid extending to the outer surface of the culture dish. The cells and the media surrounding them are contained in an insulating polystyrene culture dish, when corona ions are deposited on the media surface, this situation is analogous to charge spreading on an isolated Gaussian surface, producing a net charge differential at the extremes of the media where the cultured

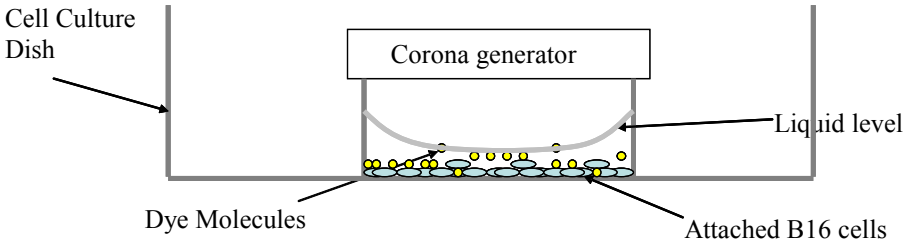

Figure 4.30: Schematic depiction of the corona generator, culture dish, cells, liquid and dye orientation during corona charge mediated delivery.

cells are attached. This charge might produce an electric field that has been suggested to drive the observed delivery similar to that observed when traditional electroporation is used [89-94]. Alternatively, corona ions could diffuse through the media and pass the cells while moving to the outer surface of the conductive media. These ions could inter-act with the cells attached to the bottom of the culture dish and induce delivery via a mechanism that includes charge exchange with the membrane. The current induced due to the ionic charges could also be an alternate driving force for molecular delivery as has been suggested previously [95-97] in electrode simulated delivery.

Figure 4.30 shows that, due to the shape of the liquid meniscus, the thickness of liquid covering the cells was minimum in this central area of the dish. The corona ions that are deposited onto the surface of the media would have undergone approximately million collisions before they reach the surface of liquid and hence would have lost any

excess energy gained in the ionization process. Even though the ions would have lost much of their excess kinetic energy during collisions, they would still have a significant amount of electrostatic and chemical energy. The electrostatic energy would be due to the fact that they are ions and chemical energy would be due to the adhesion between an ion and polarizable water molecules around it. Hence if they affect the cells by diffusing randomly through the liquid (due to this energy that they posses), the area in the center of the dish would present the least amount of liquid volume to move through for the diffusing ions to reach the cells. In addition to the liquid meniscus offering the least amount of resistance, another reason for delivery in the central region of the culture dish could be due the fact that the intensity of the ions was highest over the center of the dish as is typically observed with ions emanating from this kind of a needle source [59]. Alternatively, this observation is consistent with the simulation results from Figure 4.17 which show values of electric fields being highest over the center of the dish.

4.5.2 Mechanism of *In Vitro* Delivery Based on Experimental Observations

Irrespective of the mechanism of how corona ions interact with the media, either by spreading on the surface or diffusing through the media, corona ion deposition does facilitate the uptake of molecules

that are cell impermeant. In this section various experiments were performed to study how the media treated with corona ions responded so as to affect molecular delivery.

4.5.2.1 Temperature and pH Measurements

A change in the microenvironment surrounding the cells was first anticipated due to ion deposition. Temperature and pH measurements were performed to observe whether possible changes in either of these two parameters could be responsible for destabilizing the cell membrane and effect molecular delivery. Temperature measurements of the media surrounding cells that were exposed to either positive or negative corona ions for ten minutes indicated that corona ion exposure with either polarity did not result in an increase or decrease in temperature in the medium close to the cells. Temperature of both the controls and treated samples showed exactly the same value of 22°C. Hence change temperature did not appear to be a factor effecting molecular delivery.

Experiments were next performed to determine if there was a change in pH due to corona ion deposition. Cells were grown in culture dishes and pH was measured using a microelectrode before and after exposure to corona ions of either polarity for ten minutes. Another experiment was also performed where pH was monitored during

the corona ion deposition with chemical strips. The pH indicator strips used were commercially available and commonly used in laboratory experiments. Both experiments did not demonstrate any change in the pH of the medium due to corona ion deposition. Mean pH of six control samples was 6.93 while the six corona treated samples showed a mean pH of around 6.87. The results of these experiments suggest that changes in temperature or pH were minimal and had a remote or no possibility of effecting molecular delivery.

4.5.2.2 Effect of Corona Ions on Resting Membrane Potential

All biological cells are known to exhibit a resting membrane potential. The resting membrane potential is the steady state condition in which the flow of positive or negative ions across the lipid bilayer is balanced. The total resting membrane potential has a value that varies between -20 to -200 mV [98] depending on the cell type. There are three components that contribute to this total resting membrane potential [99, 100], they are: surface potential, membrane dipole potential and the total transmembrane potential difference. Surface potential arises from the net excess of charge present at the membrane aqueous interface and it is the potential difference between the membrane interface and the bulk aqueous. Membrane dipole potential originates from combination of the orientation of the dipolar lipid

groups and the permanent dipoles of water molecules at the membrane water interface and the last one being the total transmembrane potential difference which arises due to the difference in charges in the bulk aqueous mediums outside and inside the cell. Figure 4.31 shows a visual model of the distribution of all three potentials around the plasma membrane. Equation (4.1) shows the expression for the total resting membrane potential $T_{\Delta M}$, with E_s and E_d being the surface and membrane dipole potentials respectively. ΔE_i is the charge differential between the bulk inside and outside of the cell. It is known from previous work that the membrane dipole potential has a positive value [100] and is depicted in Figure 4.31.

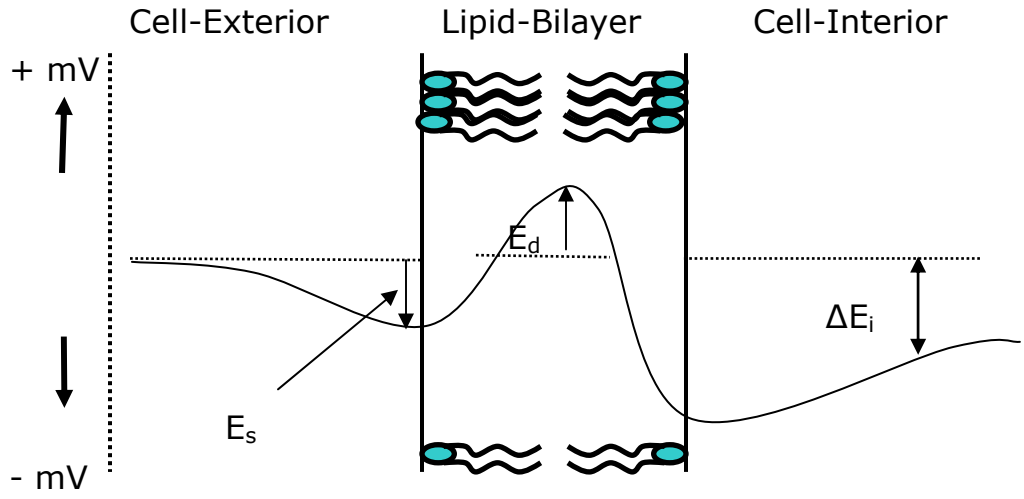

Figure 4.31: Distribution of various potentials existing in a cell with bulk exterior being the reference.

(4.1) $$T_{\Delta M} = E_s + E_d + \Delta E_i$$

An experiment was carried out to see the effect of corona ion exposure on change in total resting membrane potential of two different cell lines. Di-8-ANEPPS, a commercially available dye measuring the change in membrane dipole potential (MDP) was used. The dye increases in fluorescence when there is a change in the strength and packing density of the lipids in the plasma membrane [81-83]. Di-8-ANEPPS is frequently used by neuroscientists to measure the action potential in neurons. Action potentials in neurons are triggered by a sudden depolarization of the plasma membrane and they have a response time which is in milliseconds. Hence Di-8-ANEPPS, a dye with a very fast response time was used. Having a very fast response time, means that the increase in fluorescence is retained for a very short period of time (on the order of milliseconds) and hence observations or quantitative measurements had to be made instantly after treatment. An increase in fluorescence after exposure to corona ions would indicate that the packing of lipids in the bilayer has been affected and also that there was a change in the total resting membrane potential. Figure 4.32 shows pictures of cells stained with Di-8-ANEPPS followed by exposure to positive corona ions for five minutes. The pictures in Figure 4.32 were taken immediately after five minutes of corona exposure and show control and treated samples of B16F10 and fibroblast

cells. There was no visual difference between the positive or negative corona ion treated samples.

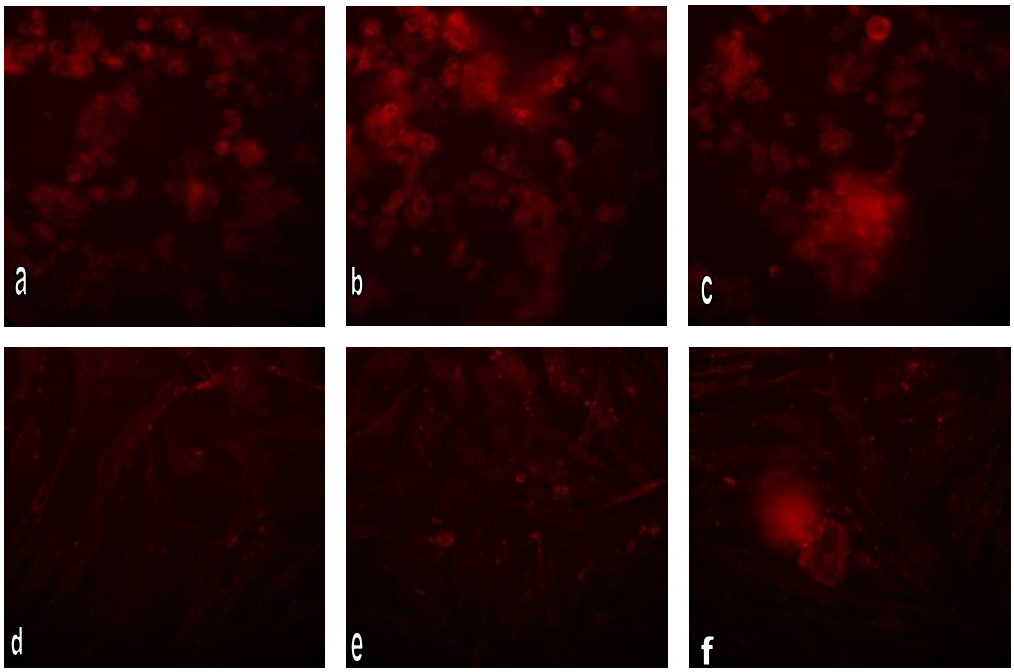

Figure 4.32: B16F10 and fibroblast cells exposed to positive corona ions. a) and d) represents B16F10 and fibroblast cells stained with the dye only that were used as controls. b) and c) represents two different samples of B16F10 cells treated with 5 minutes of positive corona. e) and f) represents two different samples of fibroblasts exposed to 5 minutes of positive corona ions. Negative corona ion exposure (not shown) yielded similar results.

Results from Figure 4.32 were quantified and are shown in Figure 4.33. The pixel values from the images shown in Figure 4.32 were evaluated and the mean light intensities of pictures were recorded using Daime imaging software. The mean intensities show that there is an increase of 7-12% in light intensity, which is what is commonly ob-

served when this dye is used due to its very fast response time. Previous studies carried by Xu and Loew have reported a 9% increase in fluorescence after five seconds that corresponded to a voltage change of 100 mV [101]. The increase in fluorescence was captured five seconds after their treatment condition and it fell drastically and plateaued after 30 seconds. The data shown above indicate that exposure to corona ions does affect the resting membrane potential due to change in packing of the lipids in the bilayer. Studies should be carried out in the future to support this initial work and estimate the values of change in total resting membrane potential due to corona ion exposure.

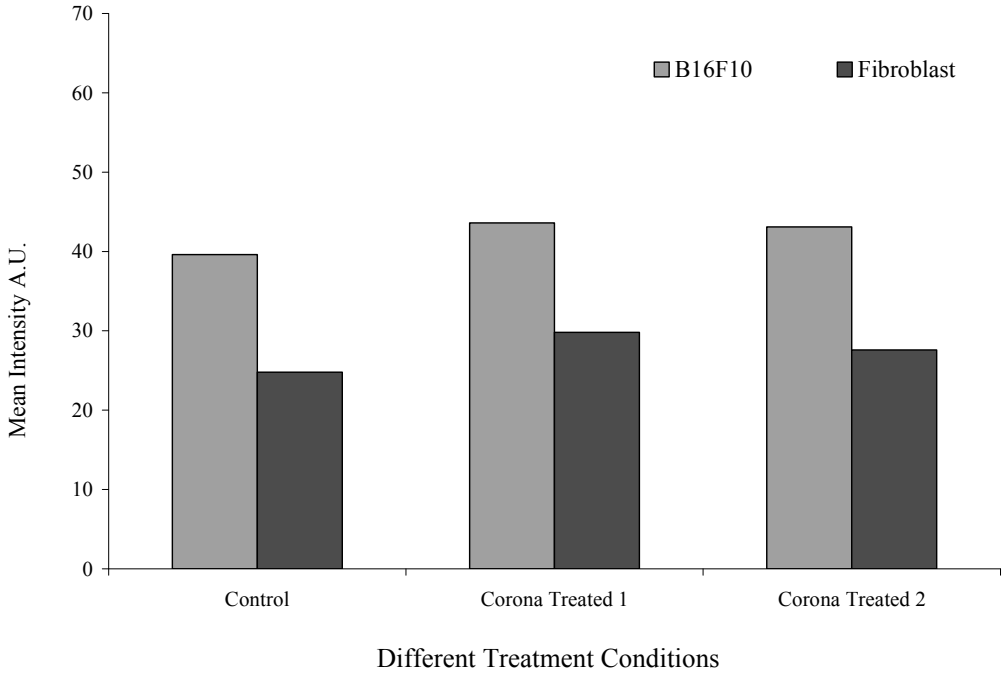

Figure 4.33: Mean light intensities of treated samples from Figure 4.32.

4.5.2.3 Effect of Corona Ions Exposure on Cell Adhesion

This study monitored the cell adhesion characteristics during and after exposure with corona ions. Experiments in section 4.5.1 had noted that delivery of the dye SYTOX-green started after five to seven minutes of corona exposure to either polarity. Also *in vitro* delivery of the drug bleomycin had confirmed the fact that for delivery to occur the exposure time to corona ions had to be at least five minutes. Experiments in this section were designed to see if there was a correlation between cell adhesion and delivery. B16F10 cells were stained with cell permeant fluorescent dye CMFDA to make observations for this study. The stained cells were gown on culture dishes as shown in Figure 4.30 and exposed to corona ions to see the effect on cell adhesion.

For cells to function properly and divide they have to attach to a substrate which in this case is the polystyrene dish. Cells attach to the substrate matrix and to each other through transmembrane proteins. Although there are many kinds of transmembrane proteins the two most important ones are called cadherins and integrins [7]. Cadherins are transmembrane proteins that are calcium channels formed between adjacent cells. Integrins are transmembrane proteins that have receptors on the outer surface of the lipid bilayer and also a cytoplasmic domain. Besides attachment to the extracellular matrix (ECM), in-

tegrins also have functions that relate to cell motility, cell division and cell signaling. Integrin receptors on the cell membrane make decisions on what action to take such as attachment, movement, cell death or differentiation based on the surrounding environment [7]. They also link the ECM to the intracellular actin filamentous system and are important in defining the shape of biological cells [7].

Integrins can only bind to their substrate (or ligands in the ECM) when they exceed a certain minimal number at a certain spot called a focal contact. No attachment occurs when the integrins are distributed over the surface of the cell membrane, but when triggered by a certain signal, integrins will cluster together at a focal point to adhere to the substrate. The combined weak affinities of the integrins at the focal point give enough adhesive capacity for the cell to anchor on a substrate. Attached B16F10 cells stained with CMFDA were exposed to corona ions for ten minutes and their adhesion was monitored during and after exposure to corona ions. Figure 4.34 shows results of this experiment.

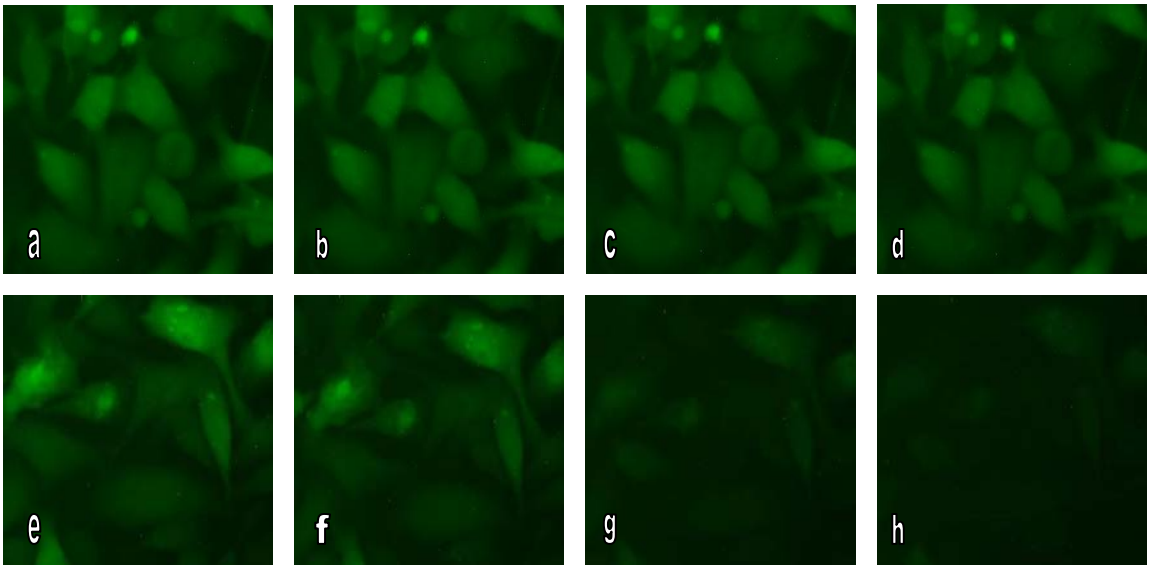

Figure 4.34: Images of control and corona charge treated samples. a), b), c) and d) control samples imaged 0, 5, 10 and 15 minutes. e), f), g) and h) images from samples exposed to corona ions for 0, 5, 10 and 15 minutes during positive corona ion exposure. Negative corona ion exposure yielded similar results (not shown).

All the pictures were taken keeping focus of the microscope the same and without moving the culture dish throughout the time period that images were taken. Hence both the controls and treated samples looked at the same set of cells in the central area of the dish during the complete observation time. Images a) through d) represent pictures taken of cells stained with CMFDA only, whereas images e) through h) show images of cells stained with the dye and exposed to corona ions. As shown in Figure 4.34 g) and h), after exposure to corona ions the cells start to round up and some partially detach from the substrate compared to the controls. The cells start releasing from their substrate and move out of focus somewhere between five and

ten minutes after corona treatment started. This corresponds to the time that the onset of delivery was observed in experiments performed with SYTOX-green and bleomycin. In addition, there were also some cells that were partially detached from the culture dishes that did not have any dye delivered. The exposure of corona ions could probably be affecting the cadherins and integrins or other kinds of membrane proteins in a manner as to create temporary pathways that allow transport of exogenous molecules that do not get in on their own. Future work is suggested to see what particular types of transmembrane proteins are being affected and if there is a correlation between cell detachment and molecular delivery.

4.5.3 Preliminary Model for Resealing Time Constant of B16F10 Cells

The rate of uptake of SYTOX-green was monitored for 35 minutes and a preliminary model was developed for the resealing time constant of B16F10 cells exposed to corona ions. Figures 4.35 and 4.36 show results of the uptake of SYTOX-green beginning immediately after ten minutes of positive and negative corona ion exposure, respectively. The rate of uptake was equated to the increase in fluorescence after binding of SYTOX-green with DNA/RNA inside the cell. Figure 4.35 shows rate of uptake of the dye after ten minutes of positive corona exposure along with controls that had SYTOX-green only.

The controls show increase in fluorescence due to the presence of few dead cells in the culture. Slopes of curves, the controls and positive treated become approximately same by around 20 minutes. Slopes of curves in Figure 4.36 for the negative corona ion treatment showed a similar pattern with the curves having approximately same values of slopes at around 25 minutes. The figure clearly shows that the cell is rendered permeable to extracellular SYTOX-green after corona ion exposure and it takes some time after ion exposure for uptake to cease. For both positive and negative corona ion exposure the rate of uptake ceased at approximately 20-25 minutes.

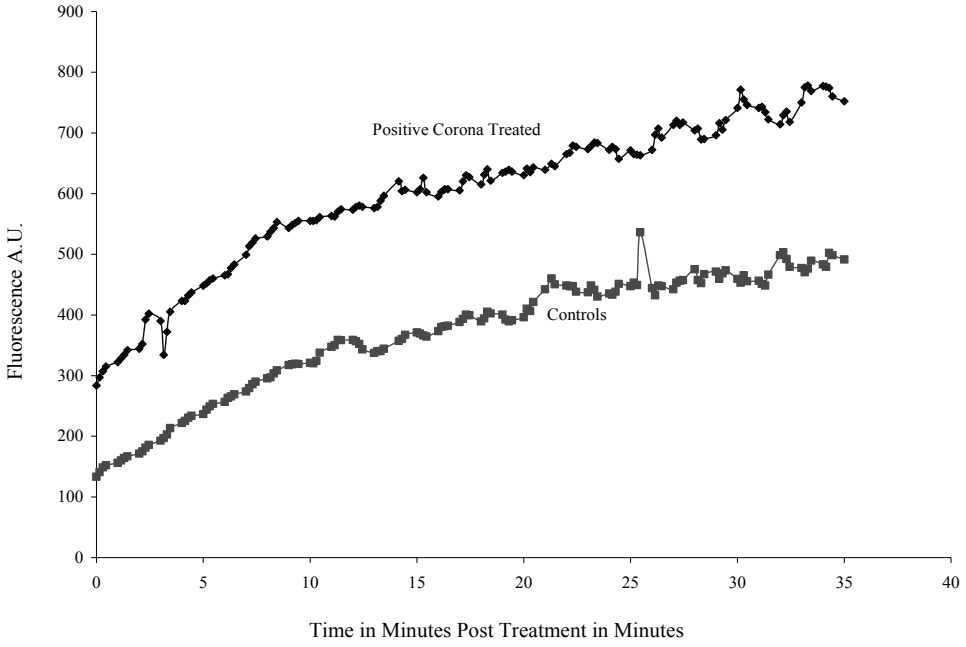

Figure 4.35: Rate of uptake for SYTOX-green in terms of fluorescence of the bound dye measured every 15 seconds following 10 minutes of positive corona ion exposure (n = 9).

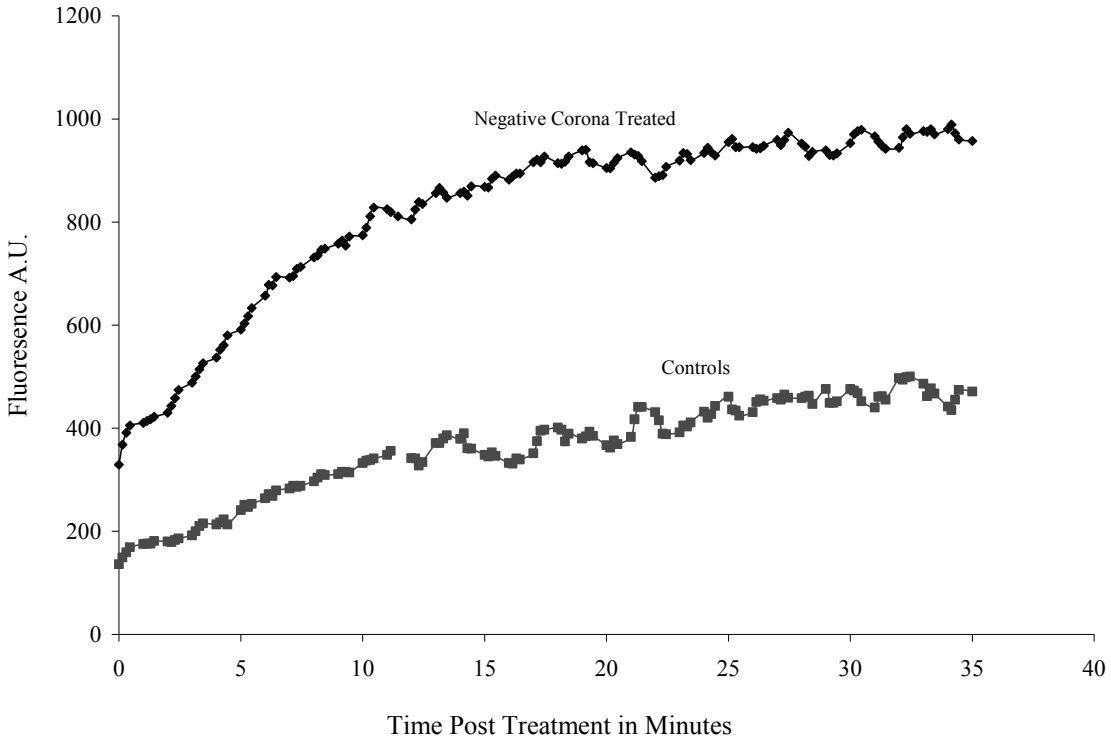

Figure 4.36: Rate of uptake for SYTOX-green in terms of fluorescence of the bound dye measured every 15 seconds following 10 minutes of negative corona ion exposure (n = 9).

It could be concluded from this data that 20 minutes is the time required for permeated B16F10 cells to reseal after corona ion exposure. However, such a conclusion would be biased, as the ability to quantify the resealing time of a cell also depends on the size of the molecule being detected. Assuming that there is some sort of relatively short lived structural defect induced in the lipid bilayer structure by corona charge, the capacity to detect resealing can be a function of the size of the detector molecule because at some point before the membrane has completely resealed, the molecule will be too large to

diffuse through the defects. The size of the molecule can hence influence the resealing time constant based on the method of detection. However, a model was developed to describe the observed behavior.

SYTOX-green is an intercalating dye that binds to any kind of nucleic acid inside the cell and fluoresces. This happens in two stages; first step is the diffusion of SYTOX-green into the permeated cell membrane and second is the attachment of dye to a binding site on DNA or RNA resulting in a strongly fluorescent complex. It is assumed that during the time when the cells start to reseal the permeability of the cells to SYTOX-green (μ in m/s) reduces exponentially with time [102]. Assumption of exponential reduction in permeability is based on previous work done to develop a model for reduction in size of pores formed after exposure to electric fields.

(4.2) $$\mu_1 = \mu_o \exp(-t/\mathrm{T})$$

Equation (4.2) represents the average effective permeability of SYTOX-green inside B16F10 cells through the complete surface area of the cell membrane, where μ_0 is the initial permeability or permeability at time zero which is the moment that the corona ion exposure ceases. The other variables are time (t) in seconds and the resealing time constant (T) also in units of seconds. An equation showing the flux of a

molecule across the permeated cell membrane is proportional to its concentration gradient and is given by

(4.3) $$J_S = \frac{d(C_i V_o)}{S_o dt} = \frac{D_i \phi}{x}(C_o - C_i)$$

where, D_i is the effective diffusivity, ϕ is the partition coefficient of the cell membrane and x is the membrane thickness. C_i and C_o are the intracellular and extracellular concentrations of SYTOX-green (moles/m^3), S_o and V_o are the cell surface area and cell volume respectively. The combined terms, $\frac{D_i \phi}{x}$ may be substituted by the effective permeability from equation (4.2) to obtain

(4.4) $$J_S = \frac{d(C_i V_o)}{S_o dt} = \mu_o \exp(-t/T)(C_o - C_i)$$

and with rearrangement we have

(4.5) $$\frac{dC_i}{(C_o - C_i)} = \frac{S_o \mu_o}{V_o} \exp(-t/T) dt$$

where, S_o and V_o are assumed to be constants in this computation. Integrating both sides of equation (4.5) yields the following time dependant expression in equation (4.6). This equation gives the expression for the concentration of free SYTOX-green inside the cell membrane

during the resealing process after corona ion exposure. See appendix A for more details on deriving equation (4.7) from equation (4.5).

(4.6) $$\ln\left[\frac{C_o - C_i}{C_o}\right] = \frac{S_o T \mu_o}{V_o}\left[\exp(-t/T) - 1\right]$$

(4.7) $$C_i = C_o\left[1 - \exp\left(\frac{S_o T \mu_o}{V_o}\left(\exp(-t/T) - 1\right)\right)\right].$$

If $A = S_o C_o \mu_o / V_o$ and $B = (-t/T)$ we have

(4.8) $$C_i = C_o\left[1 - \exp\left(A\left(\exp B - 1\right)\right)\right].$$

Now equilibrium is assumed when SYTOX-green binds weakly to an intracellular nucleic acid to form a fluorescent complex, i.e. equilibrium is assumed for the binding and dissociation of this complex [103-104]. If SY represents SYTOX-green and NU_B represents a binding site then the equilibrium expression can be given by

(4.9a) $$SY + NU_B \leftrightarrow SY \cdot NU_B .$$

The equilibrium constant in terms of the concentration of bound SYTOX-green is

(4.9b) $$K_E = \frac{[SY \cdot NU_B]}{[SY][NU_B]_{free}} = \frac{SY_b}{C_i(N_o - SY_b)}$$

where K_E is the equilibrium constant of SYTOX-green binding to nucleic acids inside the cell (m^3/mol), SY_b is the amount of SYTOX-green bound to nucleic acid per cell, N_o (mol/cell)is the total number of binding sites in a single cell and NU_B is the intracellular binding site for SYTOX-green. $(N_o - SY_b)$ represents number of unbound sites available. Rearranging equation (4.9b) gives

(4.10) $$SY_b = \frac{K_E N_o C_i}{1 + C_i K_E}.$$

Substituting (4.8) in (4.10) gives an expression for the total time dependant concentration of SYTOX- green that diffused though the plasma membrane and was subsequently bound to nucleic acids after corona ion exposure

(4.11) $$SY_b = \frac{N_o C_o K_E \left[1 - \exp\{A(\exp B - 1)\}\right]}{1 + C_o K_E \left[1 - \exp\{A(\exp B - 1)\}\right]}.$$

This expression can be used in future studies to fit the data from Figures 4.35 and 4.36 and estimate the resealing time constant. To estimate the time constant and the permeability, the equilibrium constant for the cell binding K_E and N_o the total number of binding sites in a cell would need to be determined based upon experimental data or upon calculations. In the absence of values for these parameters, the model equation (4.11) was used to determine if the shape of the

curve generated would fit the experimental data obtained with SYTOX-green.

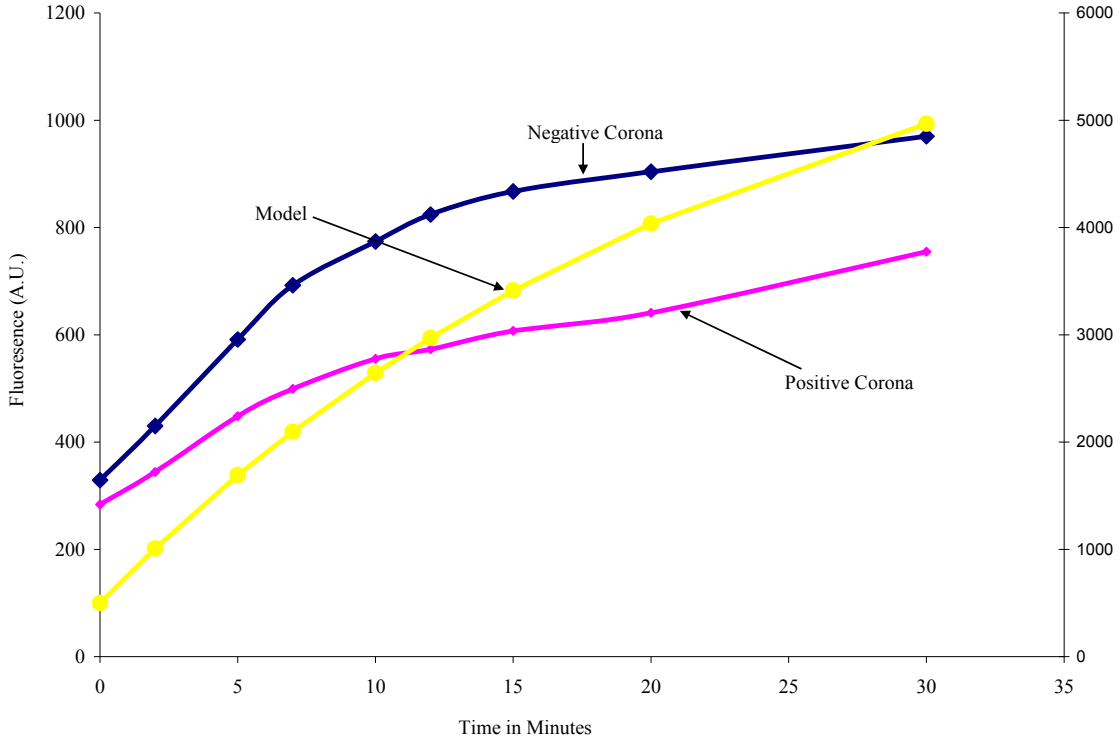

Figure 4.37: Model curve generated with equation (4.11) and a low value for permeability. The model curve is shown along with the experimental data of SYTOX-green uptake obtained in Figures 4.35 and 4.36.

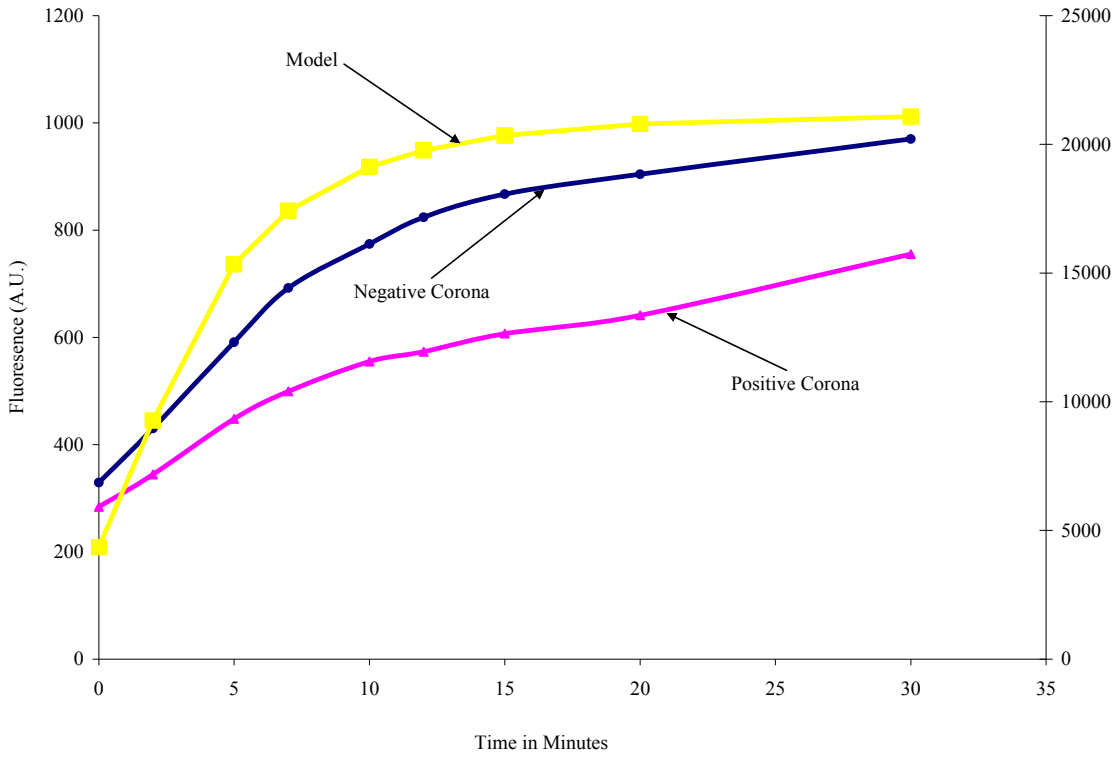

Figure 4.38: Model curve generated with equation (4.11) and a high value for permeability. The model curve is shown along with the experimental data of SYTOX-green uptake obtained in Figures 4.35 and 4.36.

Values for K_E, N_o and μ_o (the permeability) were chosen to generate several curves. A series of values for these variables were used in the model equation (4.11). Figures 4.37 and 4.38 show the results of 2 such curves generated. It was noted that any value chosen for K_E and N_o did not have any effect on the overall shape of the curve, for example the values of K_E were changed by an order of 10^6 and the shape of the curve was not effected. The number of binding sites were also modified by an order of a million and found to have no effect on

the shape of the curve either. Values of all constants chosen for generating the model curves are given in Appendix B. The only parameter that had any effect on the shape of the curve was the permeability and Figures 4.37 and 4.38 show the effect of low and high values of permeability chosen, respectively. In the absence of accepted values from the literature, permeability values of 0.05 and 50 $\frac{\mu m}{\text{sec}}$ were used

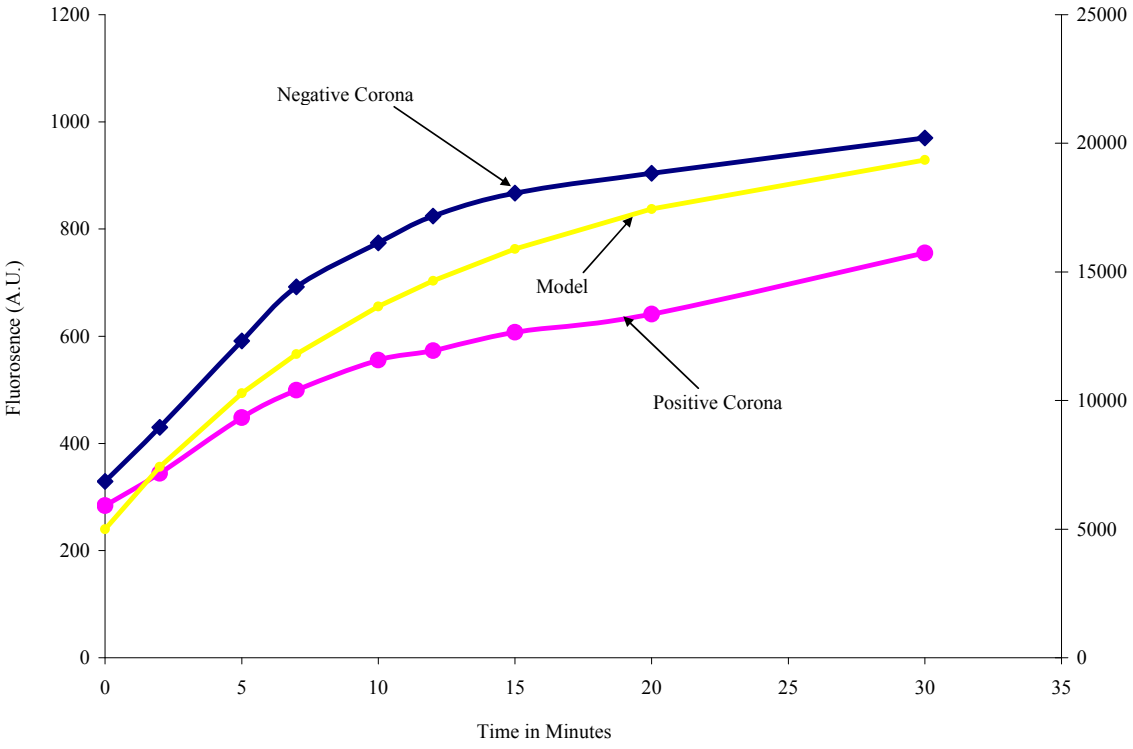

Figure 4.39: Model curve generated with equation (4.11) and a intermediate value for permeability. The model curve is shown along with the experimental data of SYTOX-green uptake obtained in Figures 4.35 and 4.36.

in the model to generate the model curves in Figures 4.37 and 4.38. The values for permeability used here were estimated from the literature from values for diffusion coefficients of the dye SERVA Blue G [105] inside electroporated cells. Figure 4.39 shows data with a value of permeability chosen in between the low and high values chosen in the previous two figures so as to better fit the experimental data obtained from Figures 4.35 and 4.36. The experimental results contain a small number of dead cells that take up SYTOX-green and the model does not account for dead cells, thus the model generated curves were shifted upwards to cross the y axis at about the same point as the experimental curves. Results from the model generated curves, indicate that the model can appropriately describe the experimental results.

5 CONCLUSIONS

5.1 Introduction

The hypothesis of this research was that corona ions can be applied to living systems to deliver drugs and DNA in cell culture and in tissues. The motivation for examining this hypothesis was to progress toward developing a novel physical method for delivering molecules to cells *in vivo* that would not suffer from the known effects of electroporation and would avoid all the drawbacks associated with electrode simulated delivery of drugs and genes. A reproducible system that generated corona charge, at atmospheric temperature and pressure was developed and applied to living systems. Successful application of these charged particles to deliver molecules to cells *in vitro*, established tumors *in vivo* and to cells in skin of mice proved the hypothesis. Specific conclusions from the experimental work are described below.

5.2 *In Vitro* Delivery

Molecular delivery using corona ions was first tested in B16F10 murine melanoma cells with two tracer molecules, calcein and SYTOX-

green. Following delivery of tracer molecules, delivery of the drug bleomycin to B16F10 cells *in vitro* was established. It was noted that to affect molecular delivery *in vitro*, a minimum exposure time of five minutes with corona ions of either polarity was required. Molecular delivery was observed *in vitro* only after about five to seven minutes of exposure to either positive or negative corona ions. Short term and long term viability of cells exposed to corona ions was also investigated leading to the conclusion that neither short term nor long term viability was affected by corona ion exposure of either polarity.

A unique aspect of the method presented in this study *in vitro* is that the cells are contained in conductive media and are attached to an insulated culture dish when the corona ions are deposited, yet they exhibit delivery analogous to direct stimulation with electrodes. One explanation for this could be that applied charges are transported by the media to the outer surface of the culture dish in a manner analogous to charge spreading on an isolated Gaussian surface. The net charge differential produced could create an electric field at the extremes of the media where the cultured cells are attached to the surfaces of the dish. Initially this seemed unlikely based upon the *in vitro* results, as molecular delivery started only after five to seven minutes of ion exposure. As the charges are generated and deposited on the surface, there is a continuous process when charges are neutralized

and deposited, hence the time interval of about five to seven minutes that it takes for delivery to start could be the time it takes for the charges to attain a steady state between charge neutralization and charge deposition. Hence this possibility cannot be completely ruled out.

A second possible mechanism of interaction of deposited corona ions with the cells could be due to diffusion through the liquid covering the cells and interaction due to charge exchange. Delivery of SYTOX-green and cell death due to delivered bleomycin *in vitro* occurred in the central region of the culture dish and not uniformly over the entire growth surface. This 95 mm^2 delivery area, was closest to the corona generating needles and about the same diameter as their circular arrangement, e.g., corresponding to the region of highest applied ion density to the surface of the media containing the cells. The absence of an effect distant from the needles suggests that charge exchange occurs only in close proximity to the charge source as it will have to diffuse though least amount of liquid in the center of the dish due to the shape of the liquid meniscus. In this case it appears that the distance between the corona ion concentration applied to the media surface and the target cells could be a dominant factor for delivery.

5.3 Delivery to Solid Tumors

Delivery of the drug bleomycin to solid tumors as a single treatment and three day series of treatments were successful in slowing down the rate of tumor growth. Considering the aggressive nature of these tumors the 21 day response that was achieved can be considered highly positive. This result also supported the hypothesis as bleomycin does not penetrate cell membranes well without assistance; therefore, decreases in growth rates can be attributed to corona mediated delivery of bleomycin. A possible explanation for achieving reduced growth rates and not complete tumor destruction is based upon the fact that the electric field emanating from the needle sources (described in Section 4.1.1) reduces with distance moving away from it. Since the tumors were raised masses in the skin, the values of electric fields were highest at the highest part of the tumor. It was envisaged that, fields that the sides of the tumor were exposed to were lower as they were farther away from the source. Therefore, corona ions of either polarity probably affected delivery to more cells in the top most layer of the tumor due it proximity to the corona generating needles while the sides and cells in the deep tumor margin had fewer cells that had the bleomycin delivered.

An important and unexpected observation from the tumor data was that for both the single and triple treatment, corona ion exposure

alone of either polarity resulted in increased growth rates over the no treatment controls. These increased growth rates can be observed in Figures 4.25 and 4.26. It appeared that these solid tumors grew faster compared to the no treatment controls, but only measurement on days three and seven of follow up were possible due to a tumor volume exclusion criteria of 1000 mm^3. Hence we cannot make a definite conclusion and more work would be needed that would either start treatment with smaller tumor volumes or that studies could be designed with a larger tumor exclusion size. This would enable making a definite conclusion about increase in growth rates of tumors following corona ion exposure of either polarity.

5.4 Delivery of Plasmid DNA to Cells in Skin

Skin of mice was chosen as the target tissue due to its easy accessibility for testing delivery of plasmid DNA. The group that received a plasmid injection followed by exposure to 30 minutes of positive corona ions showed an average of five fold increase in gene expression in the ten day post treatment follow up period that it was significantly higher than the group that received the plasmid injection alone. The results of negative corona ion exposure were slightly different from the positive corona exposed groups, with only the group that received exposure to corona ions for ten minutes after plasmid injection being

significantly higher than the plasmid only group. No other groups that received the plasmid and negative corona ion exposure had significantly higher gene expression than the group that received the plasmid alone.

An interesting observation was that the group that received exposure to 30 minutes of negative corona after plasmid injection was not significantly different from the plasmid only group. The ten minute negative corona exposed group had an average of six to eight fold increase in gene expression during the 25 day post treatment time. As has been commonly observed in plasmid delivery using electroporation, no involuntary muscle simulation or visual tissue damage or burn was observed. An electrophoretic force is suggested to be involved in driving the DNA into the cells. Since DNA has a net charge it would experience an electrophoretic driving force created by the accumulation of charges deposited on the skin of mice. This is analogous to a static field produced by charge buildup on the surface of the mice forcing the charged DNA molecules in the interior of cells. This net charge differential produced due to ion deposition could create an electric field and this could be the mechanism facilitating the cells in the skin to uptake the injected plasmid DNA. Subsequent gene expression achieved with this unoptimized system could provide an inexpensive and flexible option for gene delivery.

5.5 Interaction of Corona Ions with Biological Cells *In Vitro*

Irrespective of the mechanism of interaction of deposited corona ions with the media, how this interaction led to the uptake of impermeant molecules inside the cell was also discussed in this work. Temperature and pH measurements made did not indicate a change in the microenvironment surrounding the cells and hence these two parameters had either no effect or a minimal effect not strong enough to cause molecular delivery. The interaction of corona ion exposure with the plasma membrane and proteins embedded in it was studied next.

Effect of corona ion exposure on resting membrane potential and cell adhesion were used to propose a mechanism for *in vitro* delivery. Results from experiments indicated a change in the total resting membrane potential of B16F10 and fibroblast cells after exposure to corona ions of either polarity. This change of voltage was determined from increase in fluorescence of Di-8-ANEPPS, a voltage sensitive dye. This increase in fluorescence due to the corona ion deposition is attributed to a change in the packing of the lipids of the plasma membrane. Also exposure for about five to seven minutes with corona ions of either polarity led to partial or complete detachment of cells from their substrate as compared to the controls indicating a possible effect on the transmembrane proteins.

The integrity of the lipid bilayer and the proteins embedded in it is maintained by hydrophobic interactions. These interactions are nothing but failure to form hydrogen bonds with water molecules that repel the lipid molecules and force them to aggregate together. Thermodynamically since matter seeks to be in its lowest possible energy state, this particular aggregation of lipids is energetically favorable. Water molecules have a permanent dipole and play a very important role in maintaining the conformation of transmembrane proteins [106]. In fact it is the set of dipoles inside the cell close to the bilayer and a set of dipoles close the outer membrane that together contribute towards maintaining the structure of the bilayer. The water dipoles around the bilayer on the outside of the membrane are arranged in an ordered structure [107] and each has two free hydrogen bonds available to bond and it uses these to bond with the amphiphilic lipids and/or transmembrane proteins to keep the structure of the bilayer intact.

It is commonly known that the application of an external electric field can change the orientation of the water dipoles [108]. The change in alignment of water dipoles forces all other dipoles in the vicinity to respond by realignment [107, 109]. It is hypothesized that the field created due to the deposition of corona ions on the surface of the media covering the cells probably changes the orientation of the

water dipoles and this could be affecting the structure of the lipid bilayer and/or inserted transmembrane proteins. Alternatively if the ions are diffusing into the liquid to affect the cells, consideration has to be given to the fact that they would first become solvated as they diffuse and would drag along with it a set of oriented water dipoles. Corona ions are deposited on the surface of the media covering the cells for ten minutes and the solvation pressure created due to these diffusing ions could be affecting the bilayer and/or membrane proteins (including cadherins and integrins) which could result in the creation of temporary destabilized membrane regions or pathways that let extracellular molecules inside the cell.

5.6 Resealing Time Constant for Corona Treated B16F10 Cells

The time that a cell takes to recover from exposure to corona ions and return to its normal impermeable state can be very crucial in determining its viability. To study this, rate of uptake of the dye SYTOX-green was monitored for 35 minutes after exposure to either positive or negative corona ions. SYTOX-green is an intercalating dye that diffuses inside the cell and binds to nucleic acids inside the cell to give a strongly fluorescent complex. Results from this experiment showed that the rate of uptake of SYTOX-green continued for about 25 minutes after exposure to ions of either polarity. Using the results of

this uptake data a preliminary model for the resealing time constant of B16F10 cells exposed to corona ions was developed. Increase in fluorescence was equated to the uptake of SYTOX-green. It was assumed that the permeability of the dye SYTOX-green inside the porated cells after corona ion exposure reduced exponentially with time. This developed model was verified with data from the literature. Values for permeability were evaluated from the diffusion coefficient values of the dye SERVA blue inside electroporated cells. The curves generated using permeability values and the model equation were a reasonably good fit to experimental data of SYTOX-green uptake. Based on the data generated using these permeability values, it may be concluded that proper estimation of the permeability is very key to determining the resealing time constant and correct values used with the model developed would fit the experimental data. Future efforts would hence be directed toward proper estimation of the permeability. Estimation of the permeability would first require the estimation of the number binding sites on DNA/RNA and the equilibrium binding constant for B16F10 cells which are also recommended as a part of future studies.

5.7 Future Directions

A novel non-contact system for drug and gene delivery *in vitro* and *in vivo* was successfully developed. Even though results with this

unoptimized method of delivery are very promising, estimating the magnitude of the electric field inside the liquid close to the cells would help in better understanding of the mechanism of delivery and should be amongst the first studies carried out for the future.

Future work should also concentrate on determining and optimizing the parameters that were responsible for enhancing gene expression with the end goal of maximizing expression. Electric field and impedance measurements are recommended in animal models to further assist in characterizing the effects of corona ions on cells/tissues and in optimizing delivery. Other factors including spacing between the generator and target tissue, higher corona ion currents or the effects of ground or counter charge presence may be appropriate in future efforts to maximize the extent of molecular delivery. Experiments should also be carried out to see if corona exposure alone could enhance cell proliferation as indicated by results of increase in tumor growth rates. Corona ions have been used in the past for sterilization of heat sensitive materials and for killing allergens and dust mites hence it might have an important use in the future as a disinfectant or in sterilization of tumor beds.

Studies can also be carried out to improve the efficiency of this method as compared to the other physical gene therapy methods or improving overall gene transfer efficiency by combining corona ion ex-

posure with other methods like ultrasound, electroporation etc.. Future work is also recommended to determine the specific kinds of transmembrane proteins that could have been affected by corona ions. The effect of corona ion deposition on activation of transcription factors should also be investigated. Preliminary model developed here to determine the resealing time constant should be validated and made to fit the data obtained in Figure 4.35 and 4.36. To estimate the permeability of SYTOX-green inside cells treated with corona ions first an estimation of the number of SYTOX-green binding sites is necessary. Following this the equilibrium constant for the binding of SYTOX-green to these binding sites should be estimated and then finally the permeability and resealing time constant.

REFERENCES

1. Agency, FDA CDER data standards manual. 2006.

2. Crandall M. Drug delivery markets. Kalorama information March 2007. www.kaloramainformation.com.

3. Polson AG,.Y FS, Elkins K, Bing Z, Clark S, Ingle GS, Slaga DS, Giere L, Changchun D, Tan C, Hongo J, Gogineni A, Cole JM, Vandlen R, Stephan J, Young J, Chang W, Scales SJ, Ross S, Eaton D. and Ebens A. Antibody-drug conjugates targeted to CD79 for the treatment of non-Hodgkin lymphoma. Blood 2007, 110(2):616-623.

4. Mugabe C, Azghani OA and Omri A. Liposome-mediated gentamicin delivery: development and activity against resistant strains of Pseudomonas aeruginosa isolated from cystic fibrosis patients. J. Antimic. Chemo 2005, 55(2):267-271.

5. Kwon GS. Polymeric micelles for delivery of poorly water-soluble compounds. Crit. Rev. Therap. Drug Car. Sys. 2003, 20(5):47.

6. Muller RH, Mader K and Gohla S. Solid lipid nanoparticles (SLN) for controlled drug delivery - a review of the state of the art. Eu. J. Ph. and Bioph. 2000, 50(1):161-177.

7. Truskey JA, Yuan F and Katz FD. Transport phenomena in biological systems, ed. P.E. Inc. Person Prentice Hall 2004.

8. Cassidy J. and Schätzlein GA. Tumour-targeted drug and gene delivery: principles and concepts. Exp. Rev. Mol. Med. 2004, 6:1-17.

9. Miller DL and Song J. Tumor growth reduction and DNA transfer by cavitation-enhanced high-intensity focused ultra sound *in vivo*. Ultrasound Med. Bio. 2003, 29:887-893.

10. Scherer F, Anton M, Schillinger U, Henke J, Bergemann C, Kruger A, Gansbacker B and Plank C. Magnetofection: enhancing and targeting gene delivery by magnetic force *in vitro* and *in vivo*. Gen. The. 2002, (9):102-109.

11. Jaroszeski MJ, Heller LC, Gilbert R, Heller R. Electrically mediated plasmid DNA delivery to solid tumors *in vivo*. Meth. Mol. Bio. 2004, 245:237-244.

12. Matsuia H, Shibatta M, Browna B, Labellea A, Hegadorna C, Andrewsa C, Hebbelc PR, Galipeaud J, Hougha C and Lillicrapa D. *Ex Vivo* gene therapy for hemophilia a that enhances safe delivery and sustained *in vivo* factor viii expression from lentivirally engineered endothelial progenitors. Stem Cells October 2007, 25(10):2660-2669.

13. Bordignon C, Notarangelo LD, Nobili N, Ferrari G, Casorati G, Paola P, Mazzolari E, Maggioni D, Rossi C, Servida P, Ugazio GA and Mavilio F. Gene therapy in peripheral blood lymphocytes and bone marrow for ADA immunodeficient patients. Science October 1995, 270(5235):470-475.

14. Ferrari S, Geddes MD and Alton E. Barriers to and new approaches for gene therapy and gene delivery in cystic fibrosis. Adv. Dr. Del. Rev. 2002, 54(11):1373-1393.

15. Liu F, Song YK and Liu D. Hydrodynamics-based transfection in animals by systemic administration of plasmid DNA. Gene The. 1999, 6:1258-1266.

16. Cemazar M, Wilson I, Dachs GU, Tozer GM and Sersa G. Direct visualization of electroporation-assisted *in vivo* gene delivery to tumors using intravital microscopy – spatial and time dependent distribution. BMC Can. 2004, 4:81.

17. Grossin L, Hentrionnet CC, Mir LM, Liagre B, Dumas D, Etienne S, Guingamp C, Netter P, Gillet P. Direct gene transfer into rat articular cartilage by *in vivo* electroporation. FASEB J. 2003, 17:829-835.

18. Neumann E, Ridder MS, Wang Y and Hofschneider HP. Gene transfer into mouse lyoma cells by electroporation in high electric fields. EMBO J. 1982, 1(7):841-845.

19. Okino M and Mohri H. Effects of a high voltage electrical impulse and an anticancer drug on *in vivo* growing tumors. Jpn. J. Can. Res. 1987, 78:1319-1321.

20. Mir LM, Orlowski S, Belehradekjr J and Paoletti C. Electrochemotherapy potentiation of antitumor effect of bleomycin by local electric pulses. Eu. J. Can. 1991, 27(1):68-72.

21. Titomirov AV, Sukharev S and Kistanova E. *In vivo* electroporation and stable transformation of skin cells of new born mice by plasmid DNA. Biochim. Biophy. ACTA 1088 1991, 1:131-134.

22. Vanbever R and Preat V. *In vivo* efficacy and safety of skin electroporation. Adv. Drug Del. Rev. 1999, 35(1):77-88.

23. Dujardin and Preat V. Delivery of DNA to skin by electroporation. Meth. Mol. Biol. 2004, 245:215-226.

24. Aihara H and Miyajaski J. Gene transfer into muscle by electroporation *in vivo*. Nat. Biotech. 1998, 16(9):867-870.

25. Hoover F and Magne JK. A double-injection DNA electroporation protocol to enhance *in vivo* gene delivery in skeletal muscle. Anal. Biochem. 2000, 285(1):175-178.

26. Heller R, Jaroszeski M, Atkin A, Moradpour D, Gilbert R, Wands J and Nicolau C. *In vivo* gene electroinjection and expression in rat liver. FEBS Let. 1996, 389(3):225-228.

27. Suzuski T, Shin BS, Fujikura K, Matsuzaki T and Takata K. Direct gene transfer into rat liver cells by *in vivo* electroporation. FEBS Let. 1998, 425(3):436-440.

28. Sersa G, Novakovic S and Miklavcic D. Potentiation of bleomycin antitumor effectiveness by electrochemotherapy. Can. Let. 1993, 69:81-84.

29. Jaroszeski M, Heller L, Gilbert R and Heller R. Electrically mediated plasmid DNA delivery to solid tumors *in vivo*. Meth. Mol. Biol. 2004, 245:237-244.

30. Wells DJ. Gene therapy progress and prospects: Electroporation and other physical methods. Gene The. 2004, 11:1363–1369.

31. Sophie MH and Richard HG. Physical methods for gene transfer: Improving the kinetics of gene delivery into cells. Adv. Dr. Del. Rev. 2005, 57:733-753.

32. Hartikka J, Sukhu L, Buchner C, Hazard D, Bozoukova V, Nishioka KW, Wheeler JC, Manthorp M and Sawdey M. Electroporation-facilitated delivery of plasmid DNA in skeletal muscle: Plasmid dependence of muscle damage and effect of poloxamer 188. Mol. Ther. 2001, 4:407-415.

33. Lefesvre P, Attema J and Bekkum DV. Comparison of efficacy and toxicity between electroporation and adenoviral gene transfer. BMC Mol. Bio. 2002, 3:1-13.

34. R. Hippler, S. Pfau and M. Schmidt. Low temperature plasma physics: fundamental aspects and applications. Wiley VCH 2001, Berlin.

35. Kieft EI. Plasma needle: exploring biomedical applications of non-thermal plasmas. Ph.D. thesis, 28th September 2005, Technical University of Eindhoven.

36. Smirnov MB. Physics of ionized gases. Wiley Interscience publication 2001.

37. Roth JR. Industrial Plasma Engineering, vol 2: Applications to nonthermal plasma processing. IOP Publishing Ltd, Cornwall 2001, UK.

38. Wei Q, Wang Y, Yang Q and Yu L. Functionalization of textile materials by plasma enhanced modification. J. Ind. Text. 2007, 36(4):301-309.

39. Laroussi M. Nonthermal decontamination of biological media by atmospheric pressure plasmas: review, analysis and prospects. IEEE Tran. Pla. Sci. 2002, 30(4):1409-1415.

40. Moisan M, Barbeau J, Moreau S, Pelletier J, Tabrizian M and Yahia HL. Low-temperature sterilization using gas plasmas: A review of the experiments and an analysis of the inactivation mechanisms. Int. J. Pharm. 2001, 226:1-21.

41. MacDonald DE, Betts F, Stranick M, Doty S and Boskey LA. Physicochemical study of plasma-sprayed hydroxyapatite-coated implants in humans. J. Biomed. Mater. Res. 2001, 54:480-490.

42. Gristina R, Sardella E, Detomaso L, Senesi G, Favia P and d'Agostino R. Fibroblast and keratinocyte behaviour on substrates plasma-patterned with fouling and non-fouling domains. Eur. cell. mater.2002, 4(2):94-95.

43. Ohl A, Schroder K, Keller D and Meyer-Plath A. Chemical micropatterning of polymeric cell culture substrates using low-pressure hydrogen gas discharge plasmas. J. Mat. Sci. Med. 1999, 10:747-754.

44. Oprescu B, Giosanu D and Neagu I. The experimental study of corona discharge on yeast (Saccharomyces Cerevisiae). Rom. J. Phys. 2006, 51:131-140.

45. Laroussi M, Alexeff I and Kang WL. Biological decontamination by nonthermal plasmas. IEEE Tran. Pla. Sci. 2000, 28:184-188.

46. Goodman N and Hughes JF. The effect of corona discharge on dust mite and cat allergens. J. Electr. 2004, 60:69-91.

47. Kessler L, Legeay G, West R, belcourt A and Pinget M. Physicochemical and biological studies of corona-treated artificial membranes used for pancreatic islets encapsulation: Mechanism of diffusion and interface modification. J. Bio. Mat. Res. 1997, 34:235-245.

48. Khang G, Choee J, Rhee JM and Lee HB. Interaction of different types of cells on physicochemically treated poly(L-lactide-co-glycolide) surface. J. App. Ply. Sci. 2002, 85:1253-1262.

49. Kieft EI, Darios D, Roks AJM and Stoffels E. Plasma treatment of mammalian vascular cells: A quantitative description. IEEE Trans. Pl. Sci. 2005, 33:771-775.

50. Kieft EI, Broers JLV, Coubet-Hilloutou V, Slaaf DW, Ramakers FCS and Stoffels E. Electric discharge plasmas influence attachment of cultured CHO K1 cells. Bioelectromagnetics 2004, 25:362-368.

51. Stoffels E, Kieft EI and Sladek REJ. Superficial treatment of mammalian cells using plasma needle. J. App. Phy. 2003, 36:2908-2913.

52. Ogawa Y, Morikawa N, Ohkubo-Suzuki A, Miyoshi S, Arakawa H, Yasuhiro K and Nishimura S. An epoch-making application of discharge plasma phenomenon to gene-transfer. Biotech. & Bio-eng. 2005, 92(7): p. 865-870.

53. Palanker D, Chalberg T, Vankov PA, Huie, Molnar FE, Butterwick A, Calos M, Marmor M and Blumenkranz MS. Plasma mediated transfection of RPE. Proc. SPIE, Ophthalmic Technologies XVI. 2006, 6138:1-9.

54. Yamadaa R, Yanomac S, Makoto A, Akira T, Yukio S, Shoji T, Hi-sahiko M, Yasushi R, Yoshinori T and Toshio I. Water-generated negative air ions activate NK cell and inhibit carcinogenesis in mice. Can. Let. 2006, 239(2):190-197.

55. Van Nostrand's Scientific Encyclopedia, Lenard Effect. John Wiley & Sons, Inc., 2005, DOI: 10.1002/0471743984.vse4536.

56. T. Vilaithong, Yua LD, Apavatjrutb P, Phanchaisric B, Sangyuen-yongpipata S, Anuntalabhochaid S and Browne GI. Heavy ion induced DNA transfer in biological cells. Rad. Phy. Che. 2004, 71(3-4):927-935

57. Yu Z. Ion bean application in genetic modification. IEEE Trans. Pl. Sci. 2000, 28:128-132.

58. Junhong C. Direct-current corona enhanced chemical reactions. Ph.D. Thesis, August 2002, University of Minnesota, USA.

59. Chang J, Lawless AP, Yamamoto T. Corona discharge processes. IEEE Trans. Pl. Sci., 1991, 19:1552-1163.

60. Jonassen N. Breakdown. Mr. Static, Compliance Engineering 1999, 16: 24–28. http://www.ce-mag.com/archive/02/01/MrStatic.html.

61. Goldman M, Goldman A and Sigmond SR. The corona discharge and its properties. Pure & Appl. Chem. 1985, 57:1353-1362.

62. Sakata S, Lnoue M, Sato K, Kushima T and Okada T. Formation of clusters from clean room air by corona discharge. Pro. Inst. Env. Sci. 1993, 79-86.

63. Neumann E, Toensing E, Kakorin S, Budde P and Frey J. Mechanism of electroporative dye uptake by mouse B cells. Biophy. J. January 1998, 74:98-108.

64. Weaver JC. Electroporation of cells and tissues. IEEE Tran. Pl. Sci. 2000, 28(1):24-33.

65. Bureau FM, Gehl J, Deleuze V, Mir ML and Scherman D. Importance of association between permeabilization and electrophoretic forces for intramuscular DNA electrotransfer. Biochimica Biophysica Acta. 2000, 1474:353-359.

66. Golzio M and Rols M. Direct visualization at the single-cell level of electrically mediated gene delivery. Biophy. PNAS 2002, 99(3):1292–1297.

67. Beebe JS, Blackmore FB, White J, Joshi PR and Schoenbach HK. Nanosecond pulsed electric fields modulate cell function through intracellular signal transduction mechanisms. Physiol. Meas. 2004, 25:1077–1093.

68. Jaroszeski JM, Coppola D, Pottinger C, Benson K, Gilbert AR and Heller R. Treatment of heptacellular carcinoma in a rat model using electrochemotherapy. Eur. J Can. February 2001, 37(3):422-430.

69. Mir ML, Morsli N, Garbay RJ, Billard V, Robert C and Marty M. Electrochemotherapy: a new treatment of solid tumors. J. Exp. Clin. Can. Res. December 2004, 22(4):145-148.

70. Mir LM, Glass LF, Sersa G, Teissie J, Domenge C, Miklavcic D, Jaroszeski JM, Orlowski S, Reintgen DS, Rudolf Z, Belehradek M, Gilbert R, Rols MP, Belehradek J Jr, Bachaud JM, DeConti R, Stabuc B, Cemazar M, Coninx P and Heller R. Effective treatment of cutaneous and subcutaneous malignant tumors by electrochemotherapy. Br. J. Can. June 1998, 77(12):2336-2342.

71. Heller R, Jaroszeski JM, Glass FL, Messina LJ, Rapaport PD, DeConti CR, Fenske AN, Gilbert AR, Mir ML and Reintgen SD. Phase I/II trial for the treatment of cutaneous and subcutaneous tumors using electrochemotherapy. Can. March 1996, 77(5):964-71.

72. Sersa G, Stabuc B, Cemazar M, Miklavcic D and Rudolf Z. Electrochemotherapy with cisplatin: clinical experience in malignant melanoma patients. Clin. Cancer Res. 2000, 6(3):863-867.

73. Raphael C, Lee DZ and Hannig J. Biophysical injury mechanisms in electrical shock trauma. Annu. Rev. Biomed. Eng. 2000, 4:477–509.

74. Gissel J, Despa F, Collins J, Mustafi D, Rojhan K, Karczmar G and Lee R. Magnetic resonance imaging of changes muscle tissues after membrane trauma. Ann. N.Y. Acad. Sci. 2005, 1066:272–285.

75. Roth BL, Poot M, Yue TS and Millard JP. Bacterial viability and antibiotic susceptibility testing with SYTOX green nucleic acid stain. Appl. Env. Microbio. June 1997, 63(6):2421-2431.

76. Lebaron P, Catala P and Parthuisot N. Effectiveness of SYTOX green stain for bacterial viability assessment. App. Env. Micro. July 1998, 64(7):2697–2700.

77. Altman SA, Randers L and Rao G. Comparison of trypan blue dye exclusion and fluorometric assays for mammalian cell viability determinations. Biotechnol. Prog. 1999, 9(6):671-74.

78. Jaroszeski MJ, Dang V, Potinger C, Hickey J, Gilbert R and Heller R. Enhanced toxicity of anticancer agents mediated by electroporation *in vitro*. Antican. Drugs 2000, 11:201-208.

79. Heller R, Jaroszeski M, Messina J, Perrott R, VanVoorhis N and Gilbert R. Effective treatment of B16 melanoma by direct delivery of bleomycin using electrochemotherapy. Mela. Res. 1997, 7:10-18.

80. Heller R, Jaroszeski JM, Reintgen SD, Puleo AC, DeConti CR, Gilbert R and Glass FL. Treatment Of cutaneous and subcutaneous tumors with electrochemotherapy using intralesional bleomycin. Can. July 1998, 83(1):148-157.

81. Loew LM. Potentiometric dyes:Imaging electrical activity of cell membranes. Pu. & App. Chem. 1996, 68(7):1405-1409.

82. Gross E, Bedlack SR and Loew L. Dual-wavelength ratiometric fluorescence measurement of the membrane dipole potential. Biophys. J. July 1994, 67:208-216.

83. Newell WE and Schlichter Cl. Integration of K+ and Cl– currents regulate steady-state and dynamic membrane potentials in cultured rat microglia. J Physiol 2005, 567(3):869–890.

84. Boleti H, Ojcius DM and Dautry-Varsat A. Fluorescent labelling of intracellular bacteria in living host cells. J Microbiol. Meth. 2000, 40:265-274.

85. Sadiku MNO. Elements of electromagnetics. The Oxford Series in Electrical and Computer Engineering, ed. A.S. Sedra. 2001: Oxford University Press.

86. Bohm W, Thoma S, Leithauser F, Moller P, Schirmbeck R and Reimann J. T cell-mediated, IFN-gamma-facilitated rejection of murine B16 melanomas. J Immunol. 1998, 161(2):897-908.

87. Seliger B, Wollscheid U, Momburg F, Blankenstein T and Huber C. Characterization of the major histocompatibility complex class I deficiencies in B16 melanoma cells. Can. Res. 2001, 61(3):1095-1099.

88. McCray AN. Electrogenetherapy of established B16 murine melanoma by using an expression plasmid for HIV-1 viral protein R. Ph.D. thesis 2006, Department of Molecular. Medicine, University of South Florida, Tampa FL.

89. Teissie J. Time course of electropermeablilization in charge and field effects in biosystems-3. (1992).

90. Miklavcic D, Beravs K, Semrov D, Cemazar M, Demsar F and Sersa G. The importance of electric field distribution for effective *in vivo* electroporation of tissues. Biophy. J. May 1998, 74(5):2152-2158.

91. Turnbull RJ, Neumann E and Rosenheck K. An alternate explanation for the permeability changes induced by electrical impulses in vesicular membranes. J. Mem. Bio. December 1973, 14(2): 193-196.

92. Abidor IG, Arakelyan BV, Chemomordik VL, Chizmadzhev Y, Pastushenko FV and Tarasevich LM. Electric breakdown of bi-layer membranes. I. The main experimental facts and their qualitative discussion. Bioelectrochem. Bioenerg. 1979, 6:37-52.

93. DeBruin AK and Krassowska W. Modeling electroporation in a single cell. I. Effects of field strength & field potential. Biophys J. September 1999, 77(3):1213-1224.

94. Krassowska W and Neu JC. Asymtotic model for electroporation Phy. Rew. March 1999, 59(3):3471-3482.

95. Sugar PI, Forster W and Neumann E. Model of cell electrofusion. membrane electroporation, pore coalescence and percolation. Biophy. Chem. May 1987, 26(2-3):321-335.

96. DeBruin AD and Krassowska W. Modeling electroporation in a single cell. II. Effects of ionic concentrations. Biophys J. September 1999, 77(3):1225-1233.

97. Bilska OA, DeBruin AK and Krassowska W. Theoretical modeling of the effects of shock duration, frequency and strength on the degree of electroporation. Bioelec. June 2000, 51(2):133-143.

98. Alberts B, Hopkin, Johnson, lewis, Raff, Roberts and Walter. Essential cell biology. 2nd ed, G. Science. 2004.

99. Hickey J. Simulating the electric field mediated motion of ions and molecules in diverse matrices, in Chemical engineering. Ph.D. Thesis 2005, Department of chemical engineering, University of south Florida: Tampa.

100. O'Shea P. Intermolecular interactions with/within cell membranes and the trinity of membrane potentials: kinetics and imaging. Biochem. Soc. Tran. October 2003, 31(5):990-996.

101. Xu C and Loew LM. The effect of asymmetric surface potentials on the intramembrane electric field measured with voltage-sensitive dyes. Biophy. J. 2003, 84:2768-2780.

102. Bier M, Hammer MS, Canaday JD and Lee CR. Kinetics of sealing for transient electropores in isolated mammalian skeletal muscle cells. bioelectromag. 1999, 20:194–201.

103. Mookerjee SG. Estimation of binding sites from the adsorption profile of complexed DNA. Int. J. Quan. Chem. 1981, 20: 185-198.

104. Remington: The science and practice of pharmacy. 21 ed, Lippincott Williams & Wilkins. May 1, 2005.

105. Neumann E, Toensing K, Kakorin S, Budde P and Frey J. Mechanism of electroporative dye uptake by mouse B cells. Biophys. J. January 1998, 74(1): 98-108.

106. Vivian TJ and Callis RP. Mechanisms of tryptophan fluorescence shifts in proteins. Bio. Phy. J. 2001, 80:2093-2109.

107. Chandler D. Interfaces and the driving force of hydrophobic assembly. Nature 2005, 437:640-647.

108. Ohaninan CH. Physics. Benjamin Cummings; 2nd ed. 2001.

109. Hubbard PA. Encyclopedia of surface and colloidal science. 2000, Volume 3.

110. Deng J, Schoenbach HK, Buescher ES, Hair SP, Fox MP and Beebe JS. The effects of intense sub microsecond electrical pulses on cells. Biophys. J. 2003, 84:2709-2714.

111. Beebe JS, Fox MP, Rec JL, Somers K, Stark HR and Schoenbach HK. Nanosecond pulsed electric field (nsPEF) effects on cells and tissues: Apoptosis induction and tumor growth inhibition. IEEE Trans. Plasma Sci. 2002, 30(1):286-292.

112. Schoenbach HK, Beebe JB and Buescher SE. Intracellular effect of ultra short electrical pulses. Bioelectromag. 2001, 22:440-448.

113. Joshi PR and Schoenbach HK. Mechanism for membrane electroporation irreversibility under high-intensity, ultrashort electrical pulse conditions. Phys. Rev. E 2002, 66(5):052901.

114. Selby CG, Pertile T, Walsh R and Ulmer J. Enhancement of DNA vaccine potency by electroporation *in vivo*. J. Biotech. 2000, 83:147–152.

115. Khan SA, Pope M and Akli DR. Highly efficient constant-current electroporation increases *in vivo* plasmid expression. DNA & Cell Bio. 2005, 24(12):810-818.

116. Beebe JS, Blackmore FP, Deng Y, Somers K and Schoenbach HK. Diverse effects of nanosecond pulsed electric fields on cells and tissues. DNA & Cell Bio. 2003, 22(12):785-796.

117. Yehia A, Abdel-Salam M and Mizuno A. On assessment of ozone generation in DC coronas. J. Phy. D. App. Phy. 2000, 33:831-835.

118. Laroussi M and Leipold M. Evaluation of the roles of reactive species, heat and UV radiation in the inactivation of bacterial cells by air plasmas at atmospheric pressure. Int, J. M. Spec. April 2004, 233(1-3):81-86.

APPENDICES

Appendix A: Evaluation of Integral in Equation (4.6)

Equation (4.6) is given as $\frac{dC_i}{(C_o - C_i)} = \frac{S_o \mu_o}{V_o} \exp(-t/T)dt$

Now integrating both sides gives

$$\int \frac{dC_i}{(C_o - C_i)} = \frac{S_o \mu_o}{V_o} \int \exp(-t/T)dt$$

Using the following standard integrals

$$\int \frac{dx}{(a-x)} = \ln(a-x), \quad \text{and} \quad \int \exp(-x/a)dx = a\exp(-x/a)$$

$$\ln\left[C_o - C_i\right]_0^{C_i} = \frac{S_o \mu_o T}{V_o}\left[\exp(-t/T)\right]_0^t$$

Evaluating the above definite integral we get

$$\ln(C_o - C_i) - \ln C_o = \frac{S_o \mu_o T}{V_o}\left[\exp(-t/T) - \exp(0)\right]$$

$$\ln\left[\frac{C_o - C_i}{C_o}\right] = \frac{S_o \mu_o T}{V_o}\left[\exp(-t/T) - 1\right]$$

Taking exponential of both sides of the above equation we get

$$\frac{(C_o - C_i)}{C_o} = \exp\left[\frac{S_o \mu_o T}{V_o}\{\exp(-t/T) - 1\}\right]$$

$$1 - \frac{C_i}{C_o} = \exp\left[\frac{S_o \mu_o T}{V_o}\{\exp(-t/T) - 1\}\right]$$

Hence $\frac{C_i}{C_o} = 1 - \exp\left[\frac{S_o \mu_o T}{V_o}\{\exp(-t/T) - 1\}\right]$ and rearrangement gives

$$C_i = C_o\left(1 - \exp\left[\frac{S_o \mu_o T}{V_o}\{\exp(-t/T) - 1\}\right]\right)$$

Appendix B: Values of Constants Used for Generating Model Curves for Figures 4.37-4.39

V_o Volume of a cell $\frac{4}{3}\pi r^3$

S_o Surface area of a cell $4\pi r^2 \ m^2$

$\frac{S_o}{V_o}$ Ratio of surface area to volume, $\frac{3}{r}$

r Radius of a biological cell, assumed to be 10 μm

T Resealing time constant, assumed to be 28 minutes based on shape of the curve obtained from rate of uptake of SYTOX-green data

μ_0 Permeability of SYTOX-green at time zero after corona ion exposure, $\frac{\mu m}{\sec}$. Range of values assumed were 0.05 to 50

K_E Equilibrium constant for SYTOX-green binding to nucleic acids inside the cell, 10^{-11}

N_o Total number of binding sites, 10^{15}

ABOUT THE AUTHOR

Niraj Ramachandran attended TKIET Warananagar, India from July 1992-July 1996 and earned a bachelors in chemical engineering. During his bachelors he was actively involved in various projects in the area of bioremediation and reactor design. He came to the United States of America in the fall 1997 to pursue his higher education. Following his masters he worked as a software consultant for several years before returning to school to earn his Ph.D.

He joined The University of South Florida in fall of 2002 for his Ph.D. with focus on developing drug and gene delivery systems. His main focus has been the application of fundamental science and engineering principles to developing systems and models to be used for drug and gene delivery. He intends to continue doing research in developing novel systems and improving current systems in the areas of oral, pulmonary, buccal, ocular and transdermal delivery.